Dynamic and Reverse Transformation of Ti-6Al-4V Alloy in the Two-Phase Region

Baoqi Guo

Department of Mining and Materials Engineering

McGill University, Montreal, Quebec, Canada

December 2018

A Thesis Submitted to the Faculty of Graduate and Postdoctoral Studies in Partial Fulfilment of the Requirements for the Degree of Doctor of Philosophy

Abstract

The dynamic and reverse transformations were studied in Ti-6Al-4V. Isothermal torsion tests were performed in the two-phase region. Dynamic transformation was observed to occur at 880°C, 940°C, 960°C, 980°C and 1000°C and continuous straining led to an increase in the beta phase fraction. The extent of this type of dynamic transformation increased when the temperature approached the transus temperature. Based on data from the torsion tests, the energy barriers and driving forces associated with dynamic transformation are evaluated. It is shown that the stored energy is less than the forces inhibiting transformation and insufficient to initiate the phenomenon. By contrast, the driving force derived from the net softening is greater than the opposing force and is responsible for initiating the reaction. The hot deformation reduces the transus temperature and leads to the formation of a thermodynamically metastable state.

In order to investigate the reverse transformation, isothermal holding experiments were performed after compression at 940°C, 970°C and 1000°C in the two-phase region. The reverse transformation is controlled by diffusion and its rate is independent of temperature when the holding time is 18s. By contrast, it depends on temperature when the holding time is increased to 180 s and 1800s. The dilatometer results show that the transformation occurs in two stages; the first involves transformation on dislocations; the second growth of the alpha structure.

The effects of dynamic transformation on the flow stress were evaluated using compression testing and self-consistent modeling. Dynamic transformation from alpha to beta was observed in both microstructures (globular and colonies) at different strain rates with temperatures ranging from 815 °C to 950 °C. The extent of dynamic transformation and the associated flow softening in Ti-6Al-4V by transformation were approximately independent of the initial microstructure. However, the measured flow softening in the globular microstructure was much greater than in the colony microstructure. The best strain rates for observing dynamic transformation are in the range: 0.01 s^{-1} - 0.001 s^{-1}. The roles of dynamic and reverse transformation were further studied using multipass torsion testing. Flow softening was observed during the isothermal multipass deformation tests as indicated by the evolution of the

mean flow stress (MFS). The results indicate that the MFS values increase with interpass time from 2s to 32s. The alpha phase transforms into beta during straining, but it retransforms statically into alpha by amounts that increase with interpass time. The flow softening observed is the net result of softening by dynamic transformation and hardening by reverse transformation.

Résumé

Les transformations dynamiques et inverses ont été étudiées pour le Ti-6Al-4V. Des essais de torsion isotherme ont été menés dans la région bi-phasée. La transformation dynamique a été observée à 880°C, 940°C, 960°C, 980°C et 1000°C et la déformation continue a conduit à une augmentation du pourcentage de phase beta. L'ampleur de ce type de transformation dynamique a augmenté quand la température a approché de la température de transus. Grâce aux données des essais de torsion, les barrières énergétiques et les forces motrices associées avec la transformation dynamique ont pu être évaluées. Il a été démontré que l'énergie stockée est plus faible que les forces inhibant la transformation et qu'elle est insuffisante pour initier le phénomène. En revanche, la force motrice dérivée de l'adoucissement net est supérieure à la force opposée et est responsable de l'initiation de la réaction. La déformation à chaud réduit la température de transus et conduit à la formation d'un état thermodynamiquement métastable.

Afin d'étudier la transformation inverse, des essais de maintien isotherme ont été menés après compression à 940°C, 970°C et 1000°C dans la région bi-phasée. La transformation inverse est controlée par la diffusion et sa vitesse est indépendante de la température quand les durées de maintien sont de 18s. En revanche, cette vitesse dépend de la température quand les durées de maintien sont augmentées à 180s et à 1800s. Les résultats de dilatométrie montrent que la transformation se produit en deux étapes; la première implique une transformation au niveau des dislocations; la deuxième, une croissance de la phase alpha.

Les effets de la transformation dynamique sur la contrainte de déformation ont été évalués par des essais en compression et par de la modélisation automne. La transformation dynamique de la phase alpha à beta a été observé dans les deux microstructures (globulaire et colonies) à différentes vitesses de déformation avec des températures allant de 815°C à 950°C. L'ampleur de la transformation dynamique et l'adoucissement de la déformation plastique que l'on y associe, étaient approximativement indépendants de la microstructure initiale. Cependant, l'adoucissement mesuré de la déformation plastique dans la microstructure globulaire était largement supérieur à celui dans la microstructure de colonies. Les vitesses de déformation optimales pour observer la transformation dynamique se situaient entre 0.01 s^{-1} et 0.001 s^{-1}. Les

rôles des transformations dynamiques et inverses ont été approfondis avec des essais de torsion multi-passes. L'adoucissement de la déformation plastique a été observée pendant les multiples essais de déformation isotherme tel qu'indiqué par l'évolution de la contrainte de déformation moyenne (CDM). Les résultats indiquent que les valeurs de CDM augmentent avec la durée entre les passes, de 2s à 32s. La phase alpha se transforme en phase beta pendant la déformation, mais elle se retransforme statiquement en phase alpha, en quantités croissantes avec la durée entre les passes. L'adoucissement de la contrainte de déformation observée est le résultat net de l'adoucissement obtenu par la transformation dynamique et le durcissement obtenu par la transformation inverse.

Contributions of the Authors

The thesis was prepared based on guidelines of Faculty of Graduate and Postdoctoral Studies of McGill University for a manuscript-based thesis. The present thesis includes 6 papers as follows:

1. **Baoqi Guo** *, S. L. Semiatin, John J. Jonas, and Stephen Yue. Dynamic transformation of Ti–6Al–4V during torsion in the two-phase region. Journal of Materials Science, 53(2018): 9305–9315. (Chapter 3)

2. **Baoqi Guo** *, S. L. Semiatin, Jiangtao Liang, Binhan Sun, John J. Jonas. Opposing and Driving Forces Associated with the Dynamic Transformation of Ti-6Al-4V. Metallurgical and Materials Transactions A, 2018, 49(5): 1450-1454. (Chapter 4)

3. **Baoqi Guo** *, Clodualdo Aranas Jr., Binhan Sun, Xiankun Ji, John J. Jonas. Reverse Transformation Behavior of Ti-6Al-4V After Deformation in the Two-Phase Region. Metallurgical and Materials Transactions A, 2018, 49(1): 22-27. (Chapter 5)

4. **Baoqi Guo** *, Ameth Fall, Mohammad Jahazi, John J. Jonas. Kinetics of post-dynamic coarsening and reverse transformation in Ti-6Al-4V. Metallurgical and Materials Transactions A, 2018, 49(12): 5956-5961. (Chapter 6)

5. **Baoqi Guo** *, S. L. Semiatin, John J. Jonas. Role of dynamic transformation in the flow behavior during the hot working of two-phase titanium alloys. To be submitted. 2018. (Chapter 7)

6. **Baoqi Guo** *, Clodualdo Aranas Jr., Anes Foul, Xiankun Ji, Ameth Fall, Mohammad Jahazi, John J. Jonas. Effect of multipass deformation at elevated temperatures on the flow behavior and microstructural evolution in Ti-6Al-4V. Materials Science and Engineering: A, 2018, 729: 119-124. (Chapter 8)

All the manuscripts were co-authored with Prof. John J. Jonas who was my primary supervisor and guided me on the research. Dr. Semiatin was involved in the thermodynamic analyses (Gibbs energy calculation) in Chapter 3 and 4 and flow stress modeling in Chapter 7. Prof. Yue provided me with the access to the torsion machine. Dr. Clodualdo Aranas Jr. and Mr. Xiankun Ji assisted me in the compression and torsion tests in Chapter 5 and 8. Dr. Binhan Sun and Mr. Jiangtao

Liang had fruitful discussions with me in Chapter 4 such as the stored energy calculation. Mr. Anes Foul assisted me in the torsion test in Chapter 8. Prof. Jahazi and Dr. Ameth Fall from École de Technologie Supérieure (ETS) offered me the access to the dilatometer equipped with compression shown in Chapter 6 and useful suggestions on dynamic transformation in Chapter 8. All the experiments and result analyses as well as the paper writing were completed by the author under the supervision of Prof. Jonas and Prof. Steve Yue.

In the meantime, I am co-authored in papers listed as follows. Their abstracts are attached in the Appendix.

1. Clodualdo Aranas Jr., Anes Foul, **Baoqi Guo**, Ameth Fall, Mohammad Jahazi and John J. Jonas. Determination of the critical stress for the initiation of dynamic transformation in commercially pure titanium. Scripta Materialia, 2017, 133: 83-85.

2. Anes Foul, Clodualdo Aranas Jr., **Baoqi Guo**, John J. Jonas. Dynamic transformation of α⟶β titanium at temperatures below the β-transus in commercially pure titanium. Materials Science and Engineering: A, 2018, 722: 156-159.

3. Clodualdo Aranas Jr., **Baoqi Guo**, Samuel Rodrigues, Joonphil Choi, Sanghoon Kim, Binhan Sun, John J. Jonas. Deformation-induced phase transformation in Zircaloy-4 below the beta transus. Materials Letters, 2018, 220: 229-233.

These three papers are associated with the present thesis and the works extended the concept of dynamic transformation to other materials (i.e. pure titanium and zirconium alloy) I am involved in the discussions in article 1 and 3 and the preparation of the metallographic images in article 2 and 3.

Acknowledgements

I would like to express my great gratitude to my supervisor Prof. John J. Jonas. I am grateful that he provided me the opportunity to come to McGill University and embark on the research several years ago. During the study, his professional expertise, patient guidance, thought-provoking discussions, detailed corrections on papers as well as the kindness in life help me a lot and will be precious assets to my future career. I would like to thank my co-supervisor Prof. Steve Yue for the facilities in the laboratory and the useful suggestions on each presentation.

I am grateful to my research group as well as the hot deformation team. The useful discussions with Dr. Clodualdo Aranas, Mr. Xiankun Ji, Dr. Binhan Sun, Mr. Anes Foul, Dr. Samuel Rodrigues and Mr. Jiangtao Liang are helpful to my works. I would like to thank Dr. S. L. Semiatin of Air Force Research Laboratory for the technical discussions about thermodynamics and the flow behaviors in titanium alloys. I would like to thank Prof. Mohammad Jahazi and Dr. Ameth Fall of the École de Technologie Supérieure for their kind suggestions and access to the facilities. The hot deformation laboratory managed by Prof. Jonas and Prof. Yue is the basis of my research. I would like to acknowledge my research colleagues in the hot deformation lab and I am grateful to Mr. André Liberati for the abstract translation. I am thankful to the help by Barbara Hanley and other graduate studies coordinators during my study and research at McGill. I am also grateful to the help from Zhuoran Wang, Ophélie Gourgas, Dhanalakshmi Karthic Ramesh, Kaiwen Hu, Zhimin You, Hongyu Song, Xiang Lu and Huicong Chen in Montreal.

I am grateful to the China Scholarship Council (CSC) and the McGill Engineering Doctoral Award program (MEDA) for the financial support. Finally, I would like to express my sincere gratitude and deep love to my parent for accompanying me throughout the long and unforgettable journey.

Table of Contents

List of Tables

List of Figures

alpha particle radius increase more rapidly with longer interpass annealing times than short times.

145

Chapter 1 Introduction

1.1 Background

The dynamic transformation of austenite to ferrite was first reported to occur in steel in the 1980s [1]. Such transformation was initially explained in terms of the stored energy of the dislocations introduced by straining [2, 3]. However, this approach failed to explain the large difference between the rates of dynamic and reverse transformation. It was later proposed that the applied stress is the driving force for dynamic transformation, consisting of the flow stress difference between the austenite and the ferrite that takes its place [4].

This stress-induced transformation phenomenon was also observed in titanium alloys although it did not receive as much attention as steel at the time. In 1980s, Dutta and Birla [5] reported the occurrence of dynamic transformation in Ti-6.3Al-2.7Mo-1.7Zr alloy at 850 °C during the tensile tests. Later Prada et al. [6] and Yang et al. [7] also found the dynamic transformation in Ti-6Al-4V at the beginning of 1990s. After that the work by Koike et al. [8] reported the same transformation behavior in Ti-Al-Fe alloy. They estimated that an increase of about 500 J/mol in the free energy of the alpha phase was introduced for the experimental and calculated results to be consistent. Furthermore, they found that the transus temperatures were lowered by the hot deformation and the reverse transformation (beta to alpha) took place after unloading. The dynamic transformation was analyzed from the aspect of thermodynamics for the first time, however, the source of driving force for the transformation was still unknown at the time.

In recent years, numerous works have been carried out to reveal the dynamic transformation in titanium alloys using various characterizations. For instance, the occurrence of dynamic transformation in Ti-6Al-4V was described by Matsumoto et al. [9] using the ring patterns of TEM. In the works by Zhang et al. [10], dynamic beta-precipitation was detected in the triple junctions of the grain boundaries via EBSD and similar finding was found by Matsumoto et al. [11] as well through TEM. Later the dynamic transformation was also found in colony microstructure. For example, the work by Matsumoto et al. [12] showed that the beta precipitation in Ti-6Al-4V with an initial microstructure of martensite during hot tensile tests was observed. Wang et al. [13]

found that beta phases were detected around the equiaxed alpha grains in TA15 titanium alloy with an initial colony microstructure and the amount of the transformation was increased with strains. These works indicated that the dynamic transformation serves as an additional stress accommodation mechanism and provides a large superplastic elongation due to the increase in beta phase fraction. More recently, Jonas et al. [14] observed the dynamic transformation from alpha to beta in a near alpha titanium alloy (IMI 834) using hot compression testing. The work by Jing et al. [15] showed that dynamic transformation took place in TC11 alloy during hot compression tests and they concluded that the decrease in flow stress and discontinuous yielding during straining was attributable to the dynamic transformation of alpha into beta, although the critical conditions, such as the critical stress or strain associated with the onset of transformation in Ti-6Al-4V, were not described. The possible softening from the dynamic transformation was mentioned in these works while it was not considered in the modeling of flow behavior in titanium alloys at the time.

The objectives of this work were to examine the characteristics of dynamic transformation in Ti-6Al-4V and determine the conditions governing the phenomenon, such as the critical stress. Subsequently driving force and energy barriers of dynamic transformation will be clarified in detail. The retransformation kinetics will be studied thoroughly by holding for various times after deformation at a range of temperatures as the report of this phenomenon in titanium alloys is very limited. The contribution of dynamic transformation to the flow behavior is explored in present work.

1.2 Thesis layout

Chapter 2 is a literature review on the present topic; the basic concept of titanium alloys and their phases were introduced briefly; the reports of dynamic transformation in various conditions were summarized in detail. The occurrence of dynamic transformation was described in Chapter 3 using torsion tests. According to the phase fraction variation in Chapter 3, the energy barriers and driving force of the dynamic transformation were calculated using the classic solution thermodynamics in Chapter 4. Possible sources of driving force were compared in this chapter and a metastable phase diagram was plotted based on the composition variation associated with

dynamic transformation. In Chapter 5, the reverse transformation was characterized and the kinetics of the transformation behavior were established via compression tests and metallographic measurements. Time-temperature-reverse transformation (TTRT) curves are derived and are used to analyze the kinetics of the reverse transformation. Then a dilatometer equipped with compression was used to detect the reverse transformation in Chapter 6. The in-situ observation is based on the dilatation and contraction associated with reverse transformation behavior. In the end, the role of dynamic transformation in the flow stress is evaluated in Chapter 7 by a combination of experiment and modeling. Two initial microstructures were employed to illustrate their effects on dynamic transformation and flow behavior. The contribution of dynamic transformation to flow stress is compared with other factors such as texture and coarsening. In order to further clarify its role in flow behavior, multi-pass torsion tests were performed in Chapter 8 so as to reveal the effects of dynamic and reverse transformation on flow behavior. Various interpass times were used so that different extents of reverse transformation and coarsening are observed. The main conclusions of the thesis are summarized in Chapter 9. Contributions of the thesis to the original knowledge are presented in Chapter 10.

References

[1] T. Senuma, Massive type transformation induced by hot deformation in low carbon steels, Proc. Int. Conf. on Martensitic Transformations, Nara, 1986, pp. 515-520.

[2] C. Ghosh, V.V. Basabe, J.J. Jonas, Y.-M. Kim, I.-H. Jung, S. Yue, The dynamic transformation of deformed austenite at temperatures above the Ae_3, Acta Materialia 61(7) (2013) 2348-2362.

[3] C. Ghosh, V.V. Basabe, J.J. Jonas, Thermodynamics of dynamic transformation of hot deformed austenite in four steels of increasing carbon contents, Materials Science and Engineering: A 591 (2014) 173-182.

[4] J.J. Jonas, C. Ghosh, Role of mechanical activation in the dynamic transformation of austenite, Acta Materialia 61(16) (2013) 6125-6131.

[5] A. Dutta, N. Birla, Stress induced hydrogen diffusion in a α+β titanium alloy during superplastic deformation, Scripta Metallurgica 21(8) (1987) 1051-1054.

[6] B.H. Prada, J. Mukhopadhyay, A.K. Mukherjee, Effect of strain and temperature in a superplastic Ni-modified Ti–6Al–4V Alloy, Materials Transactions, JIM 31(3) (1990) 200-206.

[7] H. Yang, G. Gurewitz, A. Mukherjee, Mechanical behavior and microstructural evolution during superplastic deformation of Ti–6Al–4V, Materials Transactions, JIM 32(5) (1991) 465-472.

[8] J. Koike, Y. Shimoyama, I. Ohnuma, T. Okamura, R. Kainuma, K. Ishida, K. Maruyama, Stress-induced phase transformation during superplastic deformation in two-phase Ti–Al–Fe alloy, Acta Materialia 48(9) (2000) 2059-2069.

[9] H. Matsumoto, V. Velay, A. Chiba, Flow behavior and microstructure in Ti–6Al–4V alloy with an ultrafine-grained α-single phase microstructure during low-temperature-high-strain-rate superplasticity, Materials & Design 66 (2015) 611-617.

[10] W. Zhang, H. Ding, M. Cai, W. Yang, J. Li, Ultra-grain refinement and enhanced low-temperature superplasticity in a friction stir-processed Ti-6Al-4V alloy, Materials Science and Engineering: A 727 (2018) 90-96.

[11] H. Matsumoto, K. Yoshida, S.-H. Lee, Y. Ono, A. Chiba, Ti–6Al–4V alloy with an ultrafine-grained microstructure exhibiting low-temperature–high-strain-rate superplasticity, Materials Letters 98 (2013) 209-212.

[12] H. Matsumoto, T. Nishihara, Y. Iwagaki, T. Shiraishi, Y. Ono, A. Chiba, Microstructural evolution and deformation mode under high-temperature-tensile-deformation of the Ti-6Al-4V alloy with the metastable α’ martensite starting microstructure, Materials Science and Engineering: A 661 (2016) 68-78.

[13] K. Wang, G. Liu, W. Tao, J. Zhao, K. Huang, Study on the mixed dynamic recrystallization mechanism during the globularization process of laser-welded TA15 Ti-alloy joint under hot tensile deformation, Materials Characterization 126 (2017) 57-63.

[14] J.J. Jonas, C. Aranas Jr, A. Fall, M. Jahazi, Transformation softening in three titanium alloys, Materials & Design 113 (2017) 305-310.

[15] L. Jing, R. Fu, Y. Wang, L. Qiu, B. Yan, Discontinuous yielding behavior and microstructure evolution during hot deformation of TC11 alloy, Materials Science and Engineering: A 704 (2017) 434-439.

Chapter 2. Literature Review

2.1 Titanium alloys and phases

2.1.1 Category of titanium alloys

In general, titanium alloys include alpha titanium alloys, alpha+beta titanium alloys, and beta titanium alloys based on the various amounts of the alpha and beta stabilizers. The below equations (2-1) and (2-2) are used to indicate the alpha and beta stabilities of an alloy [1]. Mo is a typical beta stabilizer for titanium alloys. Fig. 2.1 is a schematic phase component with different amounts of the beta stabilizers including elements such as vanadium and niobium. These alloys can be used in aerospace and biomedical fields due to their high strength and biocompatibility [1-5].

$$Mo(Eq)=1.0Mo+0.67V+0.44W+0.28Nb+0.22Ta+1.6Cr-1.0Al \quad (2\text{-}1)$$

$$Al(Eq)=Al+1/3Sn+1/6Zr+10(O+C+2N) \quad (2\text{-}2)$$

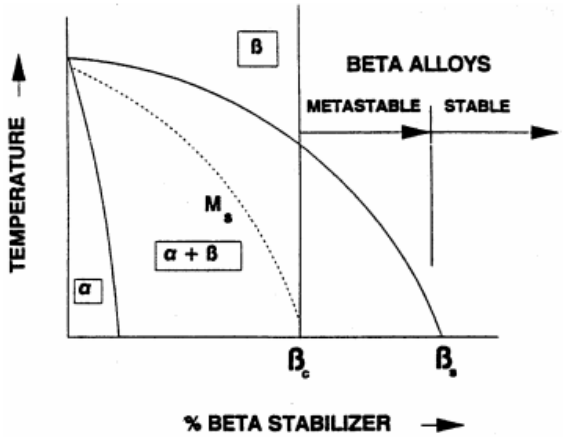

Fig. 2.1 Pseudobinary phase diagram of titanium with various contents of beta stabilizers [5].

Similar to the beta stabilizers, there are alpha stabilizers in titanium alloys as well. Among these elements, Al is a significant alpha stabilizer and is also widely used due to its strong solid solution strengthening contribution and low density. According to the contents of both the alpha and beta stabilizers, typical titanium alloy grades are classified and plotted on the below Fig. 2.2 [1, 6]. The two lines divide the figure into three sections, namely alpha alloys, alpha+beta alloys and beta alloys based on the different contents of the alpha and beta stabilizers.

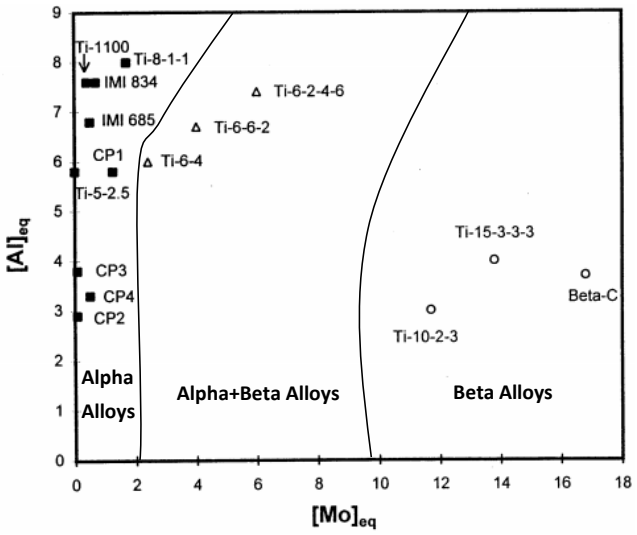

Fig. 2.2 The classification of alpha (■), alpha-beta (△) and beta alloys (○) based on the aluminum equivalent and molybdenum equivalent [1].

The following will introduce more details about the three types of titanium alloy. First, alpha titanium alloys will be summarized and can be subdivided into three groups: unalloyed titanium, alpha alloys, and near-alpha alloys [7]. Unalloyed titanium and alpha alloys with alpha stabilizers such as aluminum, are characterized by a hexagonal close packed (hcp) crystal structure at room temperature. Near-alpha alloys have less than 2% beta stabilizers, and thus can blend small amounts of the beta phase in the titanium alloy, which makes them exhibit better tensile strength compared with unalloyed titanium [1, 8]. For example, the IMI-834 alloy is a typical alpha titanium alloy, and is of medium strength, and has excellent fatigue resistance, while it lacks adequate hardenability due to the limited amounts of the beta stabilizing elements. It is mainly used for rotating components in the compressor part of jet engines, and in some cases can endure up to 650°C [9-11].

Alpha+beta alloys are based on near alpha alloys with increasing amounts of the beta stabilizing elements. The alpha phase is mainly responsible for the mechanical properties of two-phase alloys due to its large volume fraction [12, 13]. For example, the Ti-6Al-4V alloy is a typical two-phase alloy and has been widely deployed in aerospace and occupies about 60% of total titanium production. It has good fatigue and fracture properties and is used in bars and tubing. Due to high strength and good tissue tolerance, the Ti-6A1-4V ELI alloy has been used in knee prostheses and

fixation devices [14-16].

The beta alloys are defined as alloys that retain an all beta structure upon quenching from the beta phase field. This type of titanium alloy features good formability, high hardenability and high density [17, 18]. These alloys contain adequate beta stabilizing elements such as vanadium and molybdenum to lower the martensite start line (M_s), which can therefore avoid the formation of martensite [19]. Based on the content of stabilizers in the alloy, they can be subdivided into metastable or stable beta titanium alloys [18].

2.1.2 Category of the phases in titanium alloys

As for the phases produced during transformation, they can be divided into the alpha phase, beta phase, martensite and omega phase according to the different lattice structures.

The alpha phase is characterized by a hexagonal unit cell shown in Fig. 2.3 (a). It can be calculated that the c/a ratio for pure alpha titanium is 1.587, which is smaller than the ideal ratio of 1.633 for the hexagonal close-packed crystal structure [21]. The alpha phase will transform into the beta phase at a temperature of 882.5 °C in pure titanium. In the meanwhile, there are three categories of most densely packed planes, i.e. the basal plane, prismatic planes, and pyramidal planes [20, 21]. The modulus of elasticity of pure alpha titanium single crystals at room temperature varies with the angle γ between the c-axis of the unit cell and the stress axis. With the increase of temperature, the modulus of elasticity and the shear modulus decrease almost linearly [22, 23].

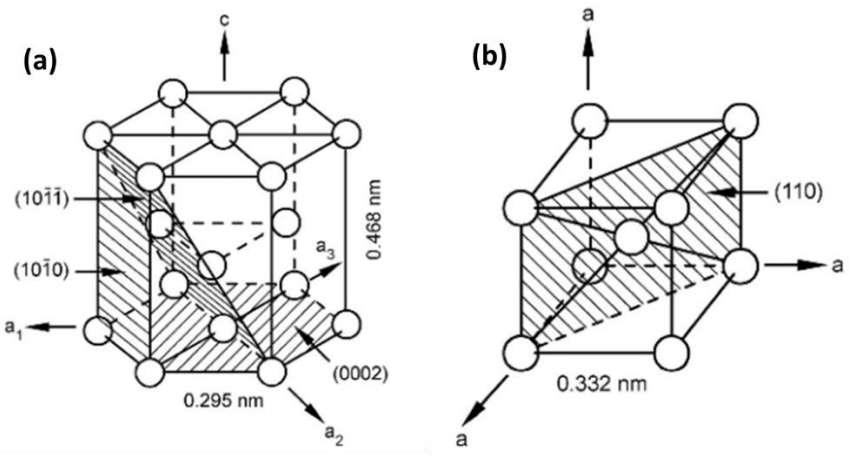

Fig. 2.3 Unit cell of alpha and beta phase [20].

The beta phase is a typical body centered cubic (bcc) structure shown in Fig. 2.3 (b) having six

most densely packed {110} planes. Slip is feasible on {110}<111> and {112}<111> systems [24]. The beta phase in general has a lower modulus of elasticity than the alpha phase, and its value increases with the increasing vanadium content between 20 and 50% vanadium [25]. During the beta transformation, there is a crystallographic orientation relationship between the alpha and beta, and it is the Burgers relationship: (110)beta//(0002)alpha, [111]beta//[1120]alpha. This relationship was determined later for titanium [26], and is applicable in both displacive and diffusional transformations [27].

The martensite in titanium is obtained from transformation of the bcc into the hcp based on the cooperative movement of atoms through shear. The formation of martensite can take place very fast below a certain critical temperature [28]. This hexagonal martensite is usually called alpha prime and has two morphologies. The first type is massive martensite existing in pure titanium, very dilute alloys, and in alloys with a high martensitic transformation temperature. The second type is acicular martensite in alloys with higher solute content and lower martensitic transformation temperatures [20, 29]. Martensite can be decomposed into the alpha and beta phases during aging. At low annealing temperatures the decomposition is incomplete. At temperatures above M_f the decomposition of martensite reaches completion [30, 31].

The omega phase is characterized by its hcp structure. It is formed in titanium alloys with stabilized beta phases through two ways: (1) athermal transformation via rapid quenching and (b) isothermal transformation by diffusional decomposition of beta [32]. The composition of the omega phase produced in quenched material is close to that of the matrix alloy, but many workers have noticed that omega precipitation during ageing is accompanied by an enrichment of the beta phase in the alloying elements [33, 34]. In the second approach, omega phase is a decomposition product of beta and can also result from annealing quenched beta-phase alloys at temperatures from 200-500°C [35, 36]. In addition, deformation at ambient temperature can produce omega phase under some circumstances as well.

2.2 Static transformation in titanium alloys

2.2.1 The static phase transformation

Static phase transformation is associated with annealing and heating/cooling processes in the absence of deformation. By contrast, dynamic transformation is induced by stress and takes place

concurrently with deformation. The static phase transformation during heating is first introduced here. Numerous researches have been conducted to study the phase transformation during cooling process. For example, Ahmed et al. [37] studied the dependence of transformation on cooling rate in Ti–6Al–4V alloy. They found that cooling rates above 410°C s^{-1} can produce a fully martensitic microstructure. Massive transformations took place at cooling rates between 410 and 20°C s^{-1}, as shown in Fig. 2.4. With a further decrease in the cooling rate, the diffusion-like Widmanstatten alpha was formed [37]. The work by Filip et al. [38] illustrated that alpha prime was not produced as the cooling rate was lower than 1.2 °C/s^{-1}. With the cooling rate less than 3.5 °C/s^{-1}, retained beta phases were observed in Ti-6Al-4V alloy. Once the cooling rate was greater than 9 °C/s^{-1}, all the alpha phases were transformed into martensite.

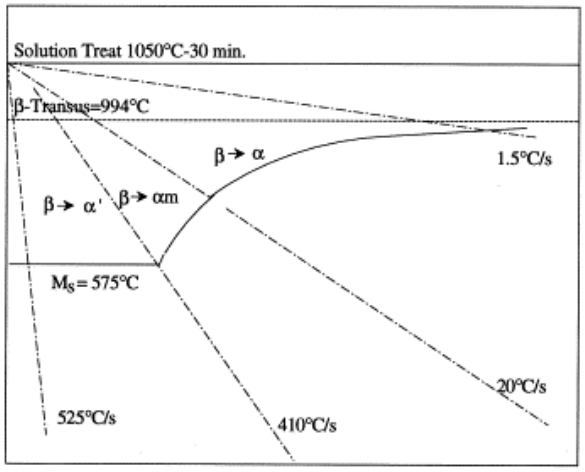

Fig. 2.4 Schematic continuous cooling diagram for Ti–6Al–4V beta-solution treated at 1050°C for 30 min [37].

2.2.2. Categories of phase transformation

Phase transformation can be classified into several types according to different mechanisms and thermodynamics. Here the transformation is divided into diffusional and displacive for simplicity as these two are closely related to the present research topic. For example, it was proposed that the nucleation of dynamic transformation was displacive and its growth was diffusional in steel [39].

The diffusional transformation was characterized by atom movement through a random jump from parent to the product position [32]. The generation of beta/alpha during heating or cooling

pertained to the diffusional transformation. The composition was changed between the parent and product phases due to the atomic diffusion. This behavior was also called civilian transformation representing the random movement of atoms. The transformation from alpha to beta during the heating of two-phase titanium alloys is an example of the diffusional transformation. However, the displacive transformation was completed by lattice distortion accompanied by displacement in a diffusionless way [32]. For instance, the martensite formed in titanium alloys by rapid cooling such as water quenching was produced displacively and its composition was the same as the original beta phase. The displacive transformation was called military transformation as the atomic movement was cooperative instead of random. These distinctions can be differentiated clearly by the schematic graph about the atomic movement during the two types of transformation shown in Fig. 2.5 [32].

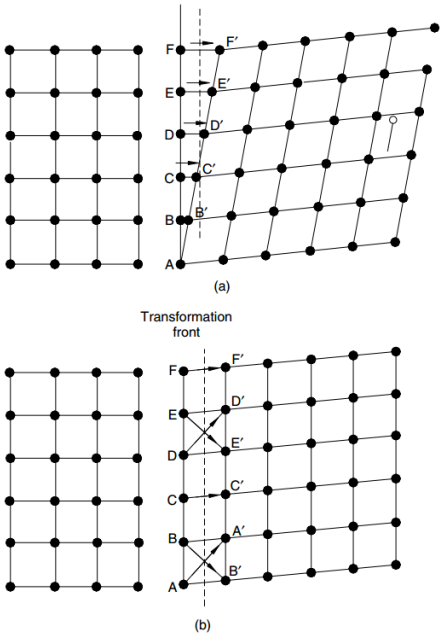

Fig. 2.5 Schematic graph of atomic movements during the (a) displacive transformation and (b) diffusional transformation [32].

2.2.3. Microstructural properties of phase transformation

According to transformation in various heating/cooling conditions, microstructures such as duplex, lamellar, and equiaxed are correspondingly developed in titanium alloys [40].

First of all, duplex microstructure can be obtained by cooling after homogenization in the beta

phase field, as shown in Fig. 2.6. It is important to control the cooling rate from the homogenization temperature above the beta transus temperature, as it affects the morphology of the alpha phase [20]. The typical duplex microstructure is characterized by a low volume fraction of primary alpha grains, which may range from 15% to 30%, and a colony-type lamellar matrix of alternating alpha and beta plates [41].

As for lamellar microstructures, these can be produced by an annealing treatment in the beta phase field after deformation. For example, the size of the alpha lamellae, the alpha colony size, and the thickness of the alpha layers at the beta grain boundaries all decrease with an increase in the cooling rate [42]. Another example of the effect of cooling rate on microstructural evolution was described in the work by Semiatin and Bieler [43]. The microstructures in Fig. 2.7 were obtained by cooling from the 1040 °C in the single beta region via different routes; water quenching, air cooling and furnace cooling were used in Fig. 2.7 (a), (b) and (c), respectively. Correspondingly, the alpha platelet thickness was increased with the reduction in the cooling rates.

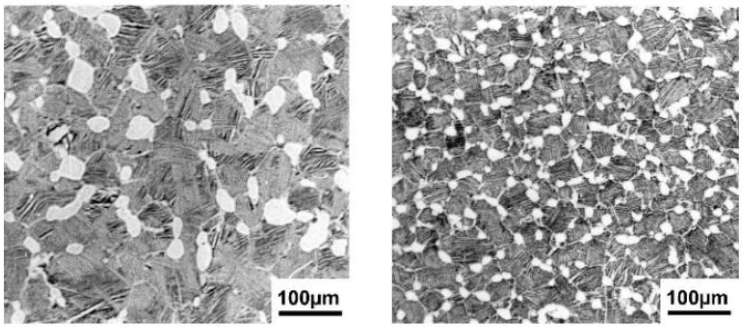

Fig. 2.6 Duplex microstructure (a) slow cooling rate (b) fast cooling rate [20].

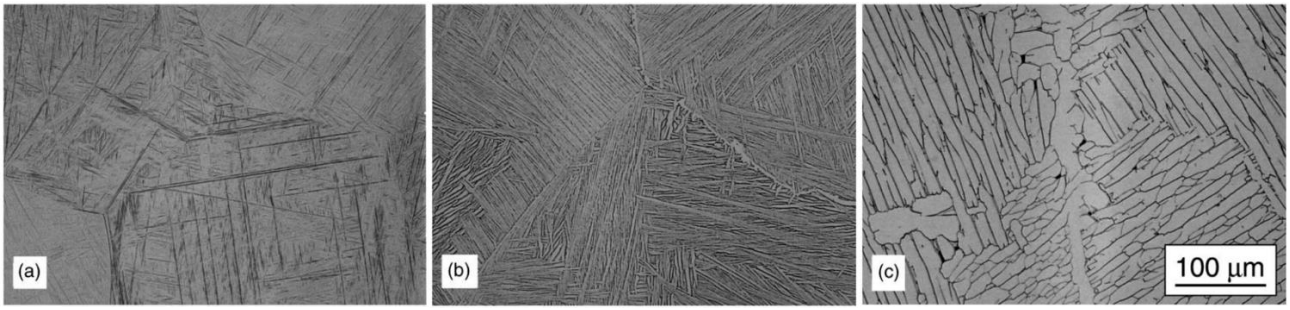

Fig. 2.7 Microstructures of Ti–6Al–4V derived by: (a) water quenching, (b) air cooling and (c) furnace cooling in the beta phase region [43].

Equiaxed microstructures can be produced by employing a very slow cooling rate from the recrystallization annealing temperature. This enables only the alpha grains to grow during the cooling process and no alpha lamellae are formed within the beta grains. Such a procedure results in a fully equiaxed structure with the equilibrium volume fraction of beta phase located at the "triple-points" of the alpha grains, as shown in Fig. 2.8 [20, 44].

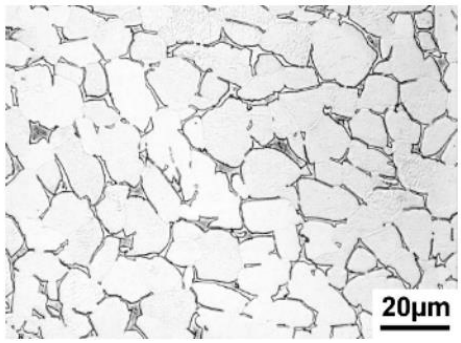

Fig. 2.8 Equiaxed microstructure of the Ti-6242 alloy slowly cooled from the duplex recrystallization annealing temperature [20].

2.3 Dynamic transformation in titanium alloys

Dynamic transformation was described by the transformation from alpha to beta during hot deformation and therefore only alpha and two-phase titanium alloys were studied here. The initiation and development of the transformation can be affected by strain, strain rate, temperature and microstructure in the titanium alloys. As colony and globular microstructures were the typical microstructures in titanium alloys, the introduction here was primarily based on the dynamic transformation in the two microstructures. In the meanwhile, the other factors such as strain and temperature were discussed in the context where related.

2.3.1. Dynamic transformation in the globular microstructure

In 1980s, the work by Dutta and Birla [45] reported the occurrence of dynamic transformation in Ti-6.3Al-2.7Mo-1.7Zr alloy at 850 °C during the deformation. Their tensile results showed that some alpha phases were transformed into beta phases in the less deformed section of the gauge region and almost all the alpha phases were transformed into beta in the neck region where the tensile strain was greater than that in the gauge part, as shown in Fig. 2.9.

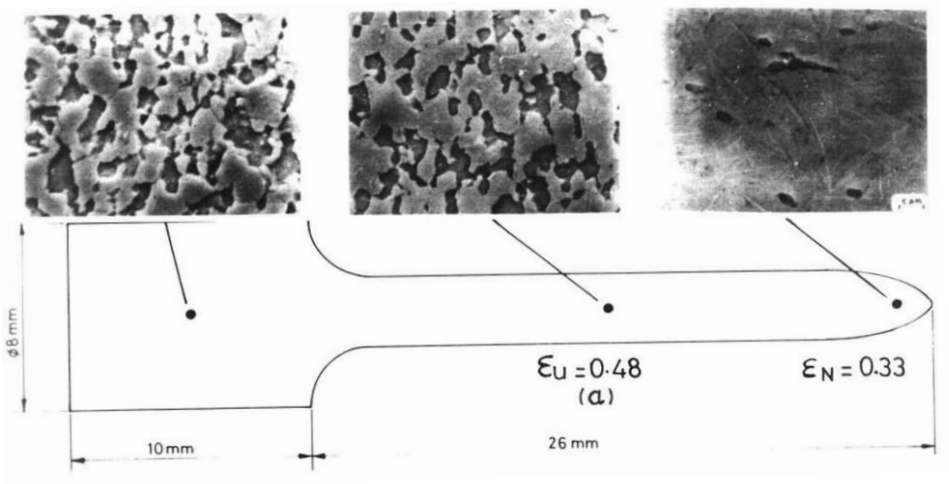

Fig. 2.9 The microstructures of Ti-6.3Al-2.7Mo-1.7Zr alloy at 850 °C at different regions of the tensile sample after deformation. It showed that the volume fraction of beta phases (white parts) was increased by the tests. Here ε_u denotes the uniform strain before the onset of necking and ε_N the strain in the neck by subtracting ε_u from the total strain [45].

Later the work by Prada et al. [46] demonstrated that the beta phase fraction was increased by the straining ranging from 0 to 1.65 at 815 °C in a Ni modified Ti-6Al-4V alloy. As show in Fig. 2.10, the alpha phases were dark and beta phases appeared light. The coarsening behavior of alpha phases can be observed during straining. They extended the tensile tests (ε=1.0, $\dot{\varepsilon}$=2.0x10^{-4} s^{-1}) to different temperatures of 750, 815 and 870 °C using the same material [47]. As shown in Fig. 2.11, the specimen shoulder and gauge length represented undeformed and deformed section, respectively. It can be seen that more alpha phases were transformed into beta phases at the higher temperatures.

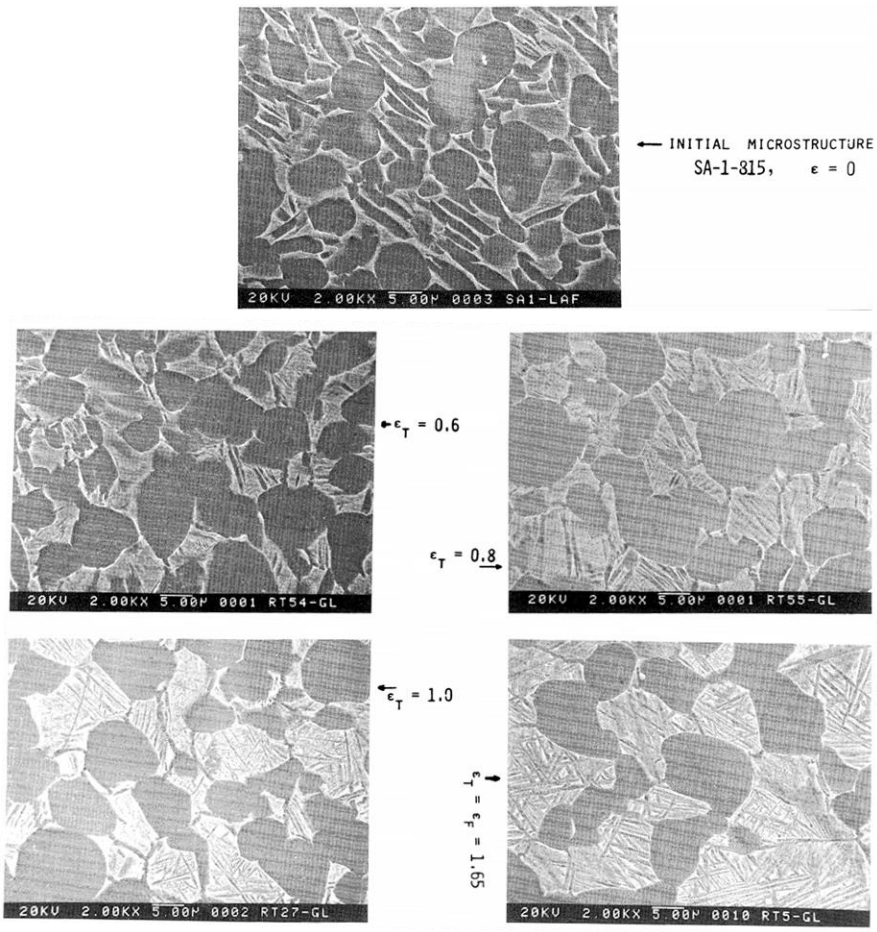

Fig. 2.10 Effects of strain on the phase evolution at 815 °C with a strain rate of $2x10^{-4}$ s^{-1} [46].

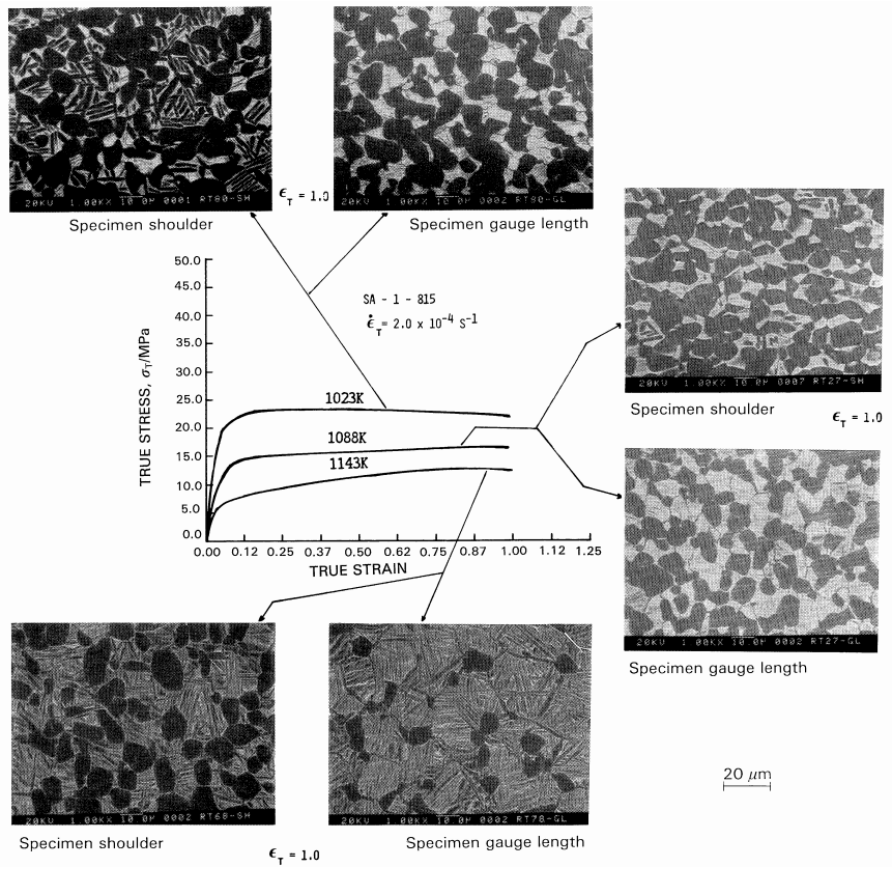

Fig. 2.11 Effect of temperature on the phase evolution deformed to a strain of 1.0 at a strain rate of 2.0×10^{-4} s^{-1} [47].

Similar work on Ti-6Al-4V was undertaken by Yang et al. [48] and showed that the dynamic transformation from alpha to beta was promoted by straining and was dependent on temperatures. For example, the transformation was only evident at 850 °C and was not observed at the lower temperatures. As shown in Fig. 2.12, the increasing volume fraction of beta phase with strain was explained in terms of promoting the diffusion of the beta stabilizing elements into the beta phase [48].

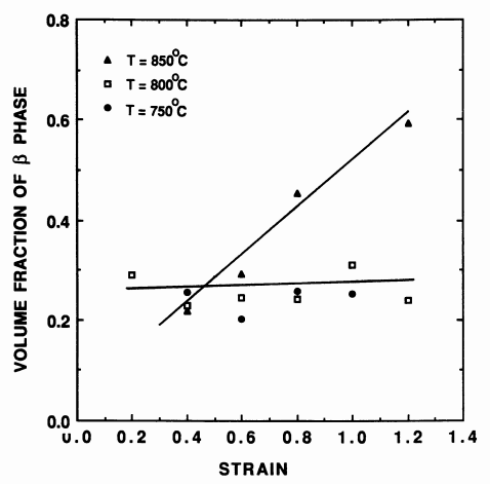

Fig. 2.12 Dependence of volume fraction of beta phase on strain and temperature at a fixed strain rate of 10^{-4} s^{-1} [48].

After that Koike et al. [49] observed a considerable increase in volume fraction of the beta phase during tensile tests in the two-phase region of Ti-Al-Fe alloy. The beta transus temperature of the material was approximately 997 °C. In Fig. 2.13, “grip” referred to the undeformed part, and “gage” represented the deformed part. These researchers estimated that an increase of about 500 J/mol in the free energy of the alpha phase was introduced for the experimental and calculated results to be consistent. As shown in Fig. 2.14, the volume fraction of beta decreased on holding, indicating that there was retransformation in their material [49]. This revealed that the dynamic transformation was induced by the applied stress rather than other factors. In addition, the dynamic transformation from alpha to beta and coarsening of alpha particles took place concurrently.

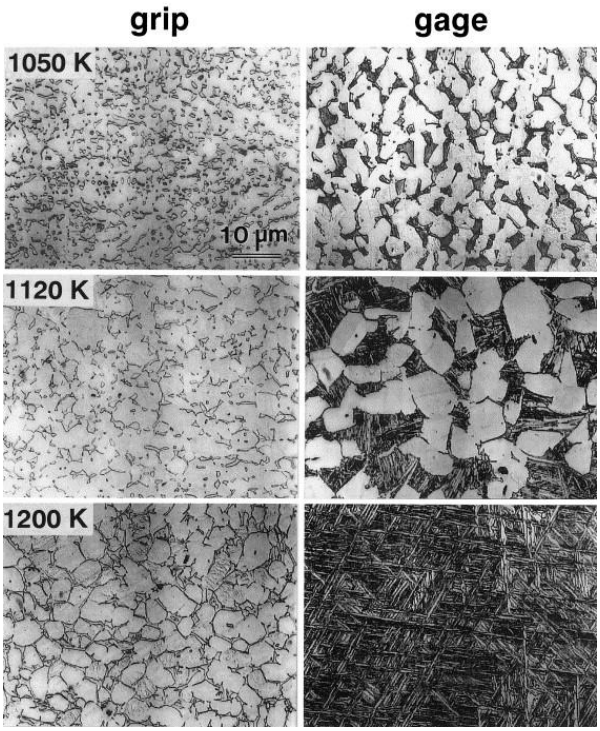

Fig. 2.13 Optical images of samples deformed to failure at various temperatures at a strain rate of 10^{-3} s^{-1} [49].

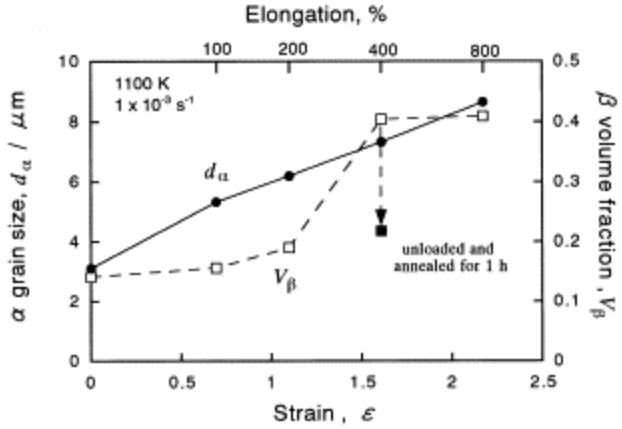

Fig. 2.14 The variation of the alpha grain size and the beta volume fraction with strain [49].

In a similar manner, an increase in the beta phase fraction of TiBw/Ti-6Al-4V composites by hot tensile tests was observed by Lu et al. [50] and its values tended to be stable after reaching 50% in the vicinity of necking, as shown in Fig. 2.15.

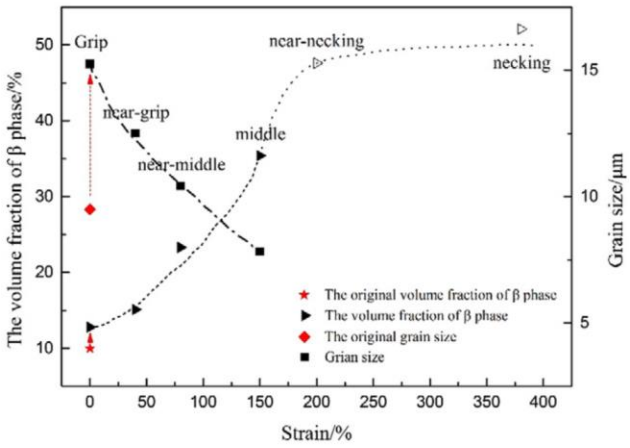

Fig. 2.15 Dependence of volume fraction of beta phase and grain size on strain based on the EBSD analysis [50].

In the meanwhile, Matsumoto et al. [51] observed the dynamic transformation in an ultrafine-grained Ti-6Al-4V (almost single alpha by a certain hot rolling) at a strain rate of 0.01 s^{-1} at 700 °C. As shown in Fig. 2.16, the occurrence of the transformation was characterized using TEM and EBSD; the reflections of beta phase were detected in the ring pattern of the TEM images (a) and (b) and this mirrored the formation of beta during deformation; the beta phases (green sections) were produced on the grain boundaries of the alpha phases (red sections) according to the EBSD results and its amounts were increased with the straining from 0 to 0.69. However, the amounts of transformation were limited due to the low deformation temperatures.

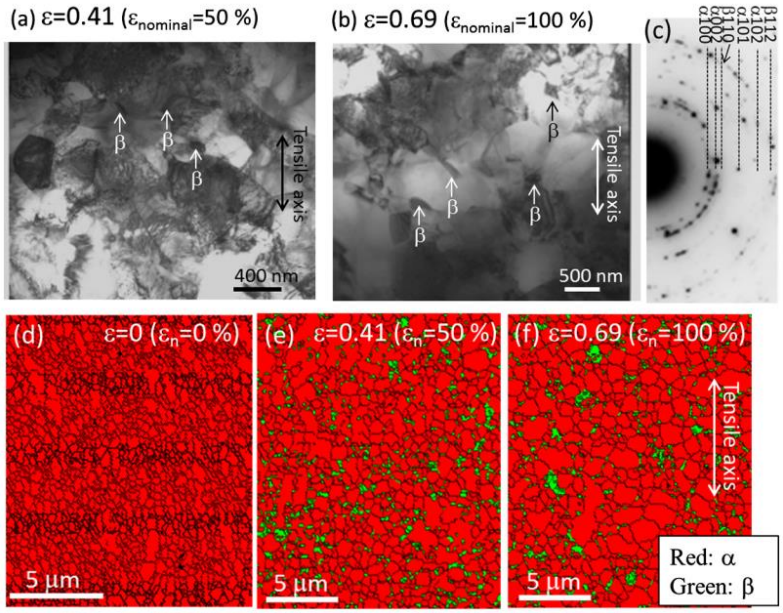

Fig. 2.16 Microstructures of the Ti-6Al-4V alloy subjected to the deformation at a strain rate of 0.01 s^{-1} at 700 °C. Bright field TEM images were displayed in (a) ε = 0.41 and (b) ε= 0.69 and the selected area diffraction pattern of (b) was demonstrated in (c). EBSD-phase maps of tensile specimens corresponded to the strains of (d) 0, (e) 0.41 and (f) 0.69 [51].

Recently, similar tensile tests on Ti-6Al-4V by Zhang et al. [52] showed that the dynamic transformation can be activated at a relatively low temperature although the amount of the transformation was limited. According to the EBSD in Fig. 2.17, the beta phases (blue parts) were detected at the triple junctions of grain boundaries after the sample was deformed to fracture at a strain rate of 3×10^{-4} s^{-1} at 600 °C. The transformation provided the soft beta phases as well as alpha/beta interface boundaries and largely facilitated the hot deformation. This observation was consistent with previous work by Matsumoto et al. [53] shown in Fig. 2.18, in which the dynamic beta-precipitation was detected in the triple junctions of the grain boundaries using TEM. This was associated with the evident stress concentration in the triple junctions during deformation and contributed to the onset of dynamic transformation.

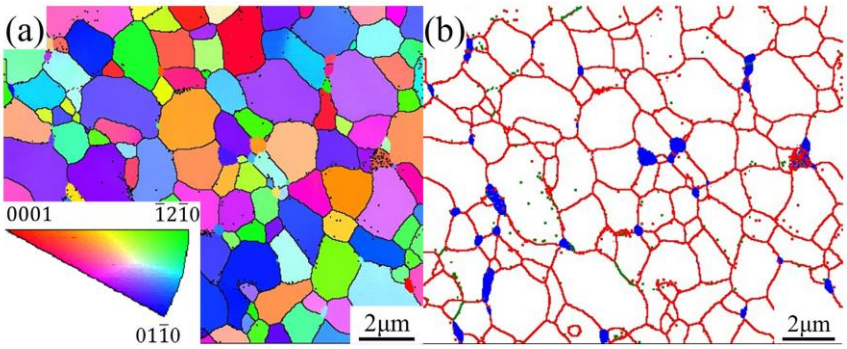

Fig. 2.17 EBSD micrographs of the Ti-6Al-4V alloy subjected to the tensile fracture at a strain rate of 3×10^{-4} s^{-1} at 600 °C (a) orientation map and (b) grain boundary map [52].

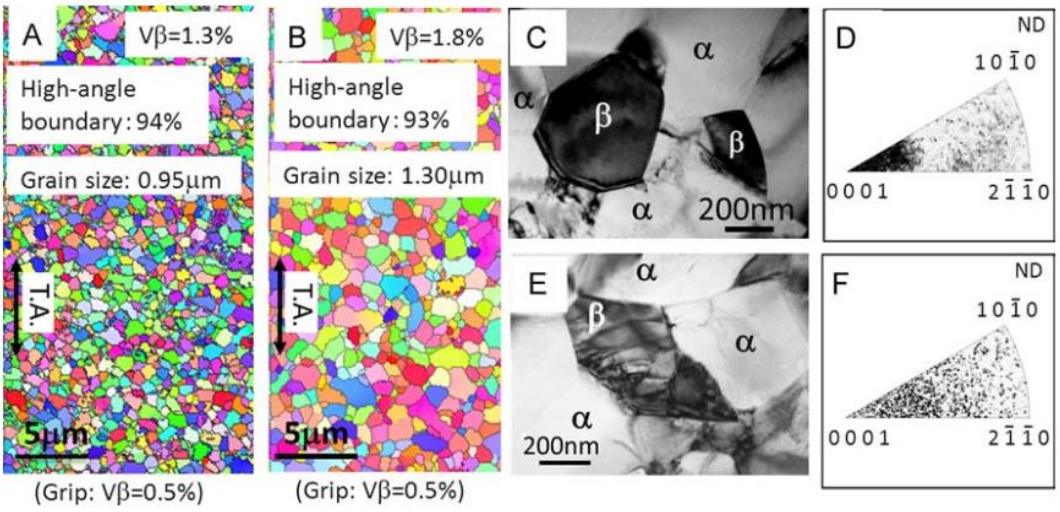

Fig. 2.18 EBSD microstructures of gage region (A) 650 °C and (B) 700 °C and TEM micrographs (C) and (E) corresponding to (A) and (B), respectively. The inverse pole figures described the nominal direction of sample subjected to tensile deformation at 700 °C at a strain rate of 0.01 s^{-1} along the cross-sections of (D) grip and (F) gage sections [53].

2.3.2. Dynamic transformation in the colony microstructure

In recent years, the dynamic transformation was found in colony microstructure during hot deformation. For example, the work by Chen et al. [54] showed that the transformation from alpha to beta took place between adjacent lamellae of the colony microstructure during the hot tensile test of Ti-6Al-4V alloy. Similar tests by Matsumoto et al. [55] proposed that the beta precipitation in Ti-6Al-4V with an initial microstructure of martensite during deformation was derived from dynamic transformation and served as an additional stress-accommodation

mechanism. As shown in Fig. 2.19, the alpha phase appeared dark and the beta phases were white. The beta phase fraction during straining from 73% to 325% at 700 °C was only increased by around 5.5%. However, the value was increased noticeably at 800 and 900 °C. This trend of dynamic transformation with temperature was analogous to the aforementioned works. They can be interpreted by the lower energy barriers and greater strains at the higher temperatures and lower strain rates.

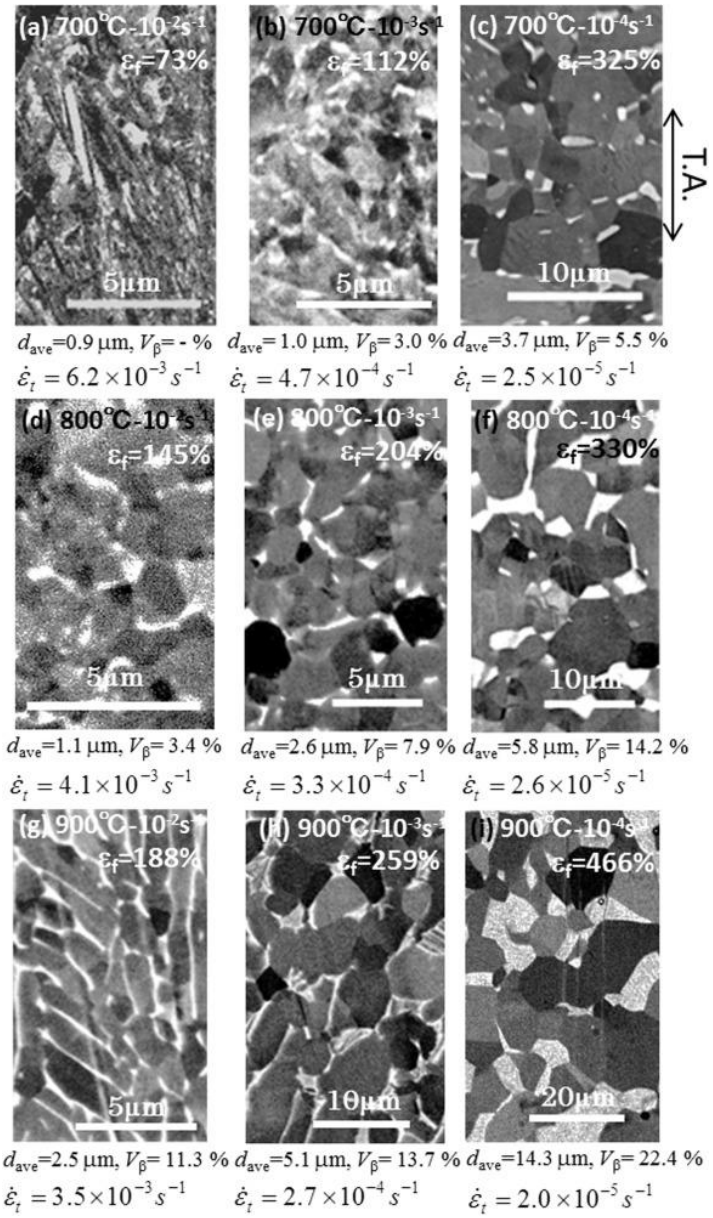

Fig. 2.19 SEM-BSE microstructures and volume fractions of beta phase of the samples with initial colony microstructures after tensile deformation at various temperatures, strains and strain rates,

as marked in the micrographs [55].

The colony microstructure in a near alpha titanium alloy (TA15) was employed by Wang et al. [56] in the tensile tests and the results showed that beta phases were detected around the equiaxed alpha grains and the amount was increased with strains, as marked by the blue parts from Fig. 2.20 (a) to (d). The dynamic globularization was also observed during the straining and was promoted by the dynamic transformation due to the increase in beta phase fraction.

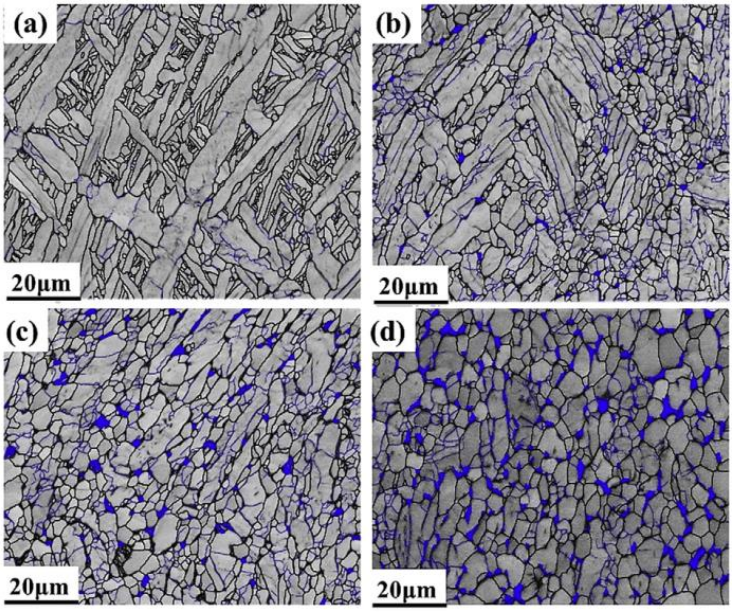

Fig. 2.20 Microstructure of the TA15 alloy with an initial colony microstructure after strains of (a) 0.3 (b) 0.6 (c) 0.9 (d) 1.2 at 900 °C, 0.001 s^{-1} (the grey color denotes the alpha phase and the blue color represents the beta phase) [56].

2.3.3. Dynamic transformation in various deformation ways

The dynamic transformation can occur not only in the aforementioned tensile tests but compression and torsion tests. For example, the isothermal compression by Zong et al. [57] showed that the volume fraction of alpha phase was decreased by deformation. As shown in Fig. 2.21, the number of primary alpha phases (white parts) was reduced by the further compression at 900 °C.

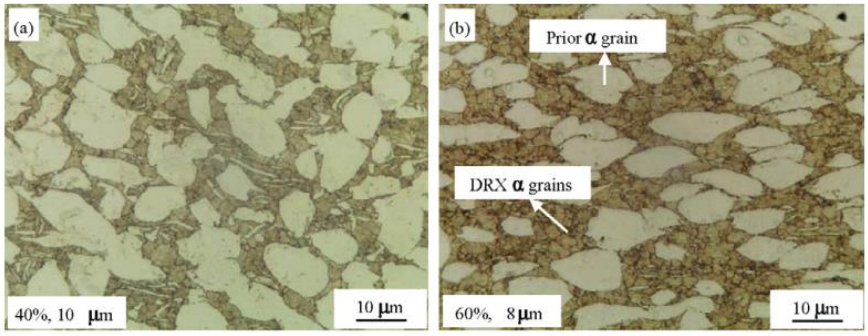

Fig. 2.21 Microstructures of TC11 alloy deformed at 900 °C at a strain rate of 1 s^{-1} to height reductions of (a) 40% and (b) 60% [57].

The compression tests of a two-phase titanium alloy (TC11) were carried out by Jing et al. [58] at 1000 °C and 1050 °C. The increase in beta phase fraction was continuously promoted by straining (0, 17%, 50%). By comparing Fig. 2.22 (a) and (c), it can be found that the beta phase fraction was substantially increased by the compression at 1000 °C. The discontinuous yielding phenomenon in the initial stage of the flow curves was attributable to the dynamic transformation from alpha to beta. Recently, the compression tests were performed in a near isothermal condition (ε=0.7, $\dot{\varepsilon}$=0.1 s^{-1}) by Meng et al. [59] and the results showed that transformation from primary alpha to beta in TA 15 titanium alloy occurred at 810 °C and 870 °C.

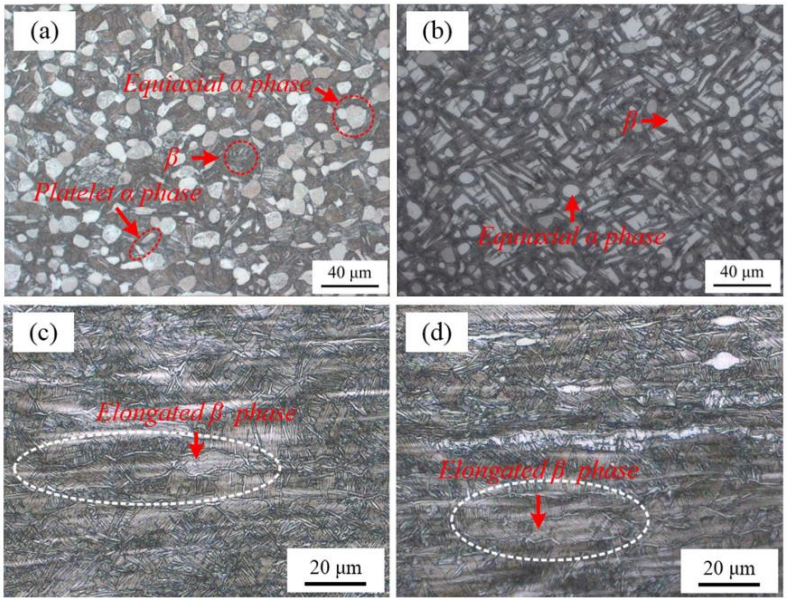

Fig. 2.22 Microstructures of the TC11 alloy of undeformed at (a) 1000 °C and (b) 1050 °C and compressed to a 50% height reduction at a strain rate of 10 s^{-1} at (c) 1000 °C and (d) 1050 °C [58].

It is universally acknowledged that the extent of dynamic transformation is enhanced by the straining through activating more grains in the transformation. The work associate with hot compression by Dong et al. [60] described the effects of strain rate on the dynamic transformation in colony microstructure of a near alpha titanium alloy (Ti-6Al-2Zr-1Mo-1V). As shown in Fig. 2.23, the beta phase fraction was increased by the strain rate. This was particularly evident at the relatively higher temperatures. For instance, the beta phase fraction increased from 65% at a strain rate of 0.001 s^{-1} to 85% at a strain rate of 10 s^{-1}. This behavior was associated with the adiabatic heating and the higher driving force for the dynamic transformation by the greater strain rates.

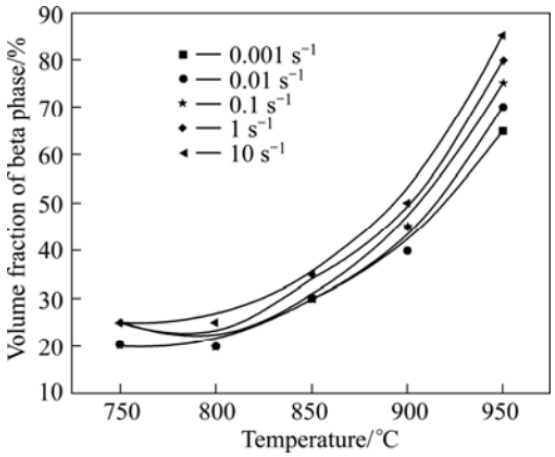

Fig. 2.23 Variation of beta phase fraction in Ti-6Al-2Zr-1Mo-1V alloy with temperature [60].

Recently, Jonas et al. [61] observed the dynamic transformation in a near alpha titanium alloy (IMI 834) using hot compression testing. The fraction of globular alpha phases was noticeably decreased by the deformation to a strain of 1.0 at a strain rate of 0.01 s^{-1} at 1000 °C, as shown in Fig. 2.24. The variation of beta phase fraction was measured at three temperatures and an approximate 20% increase in beta phase fraction was found at these elevated temperatures according to Fig. 2.25. They concluded that the dynamic transformation accounted for the flow softening since the beta was softer than the alpha.

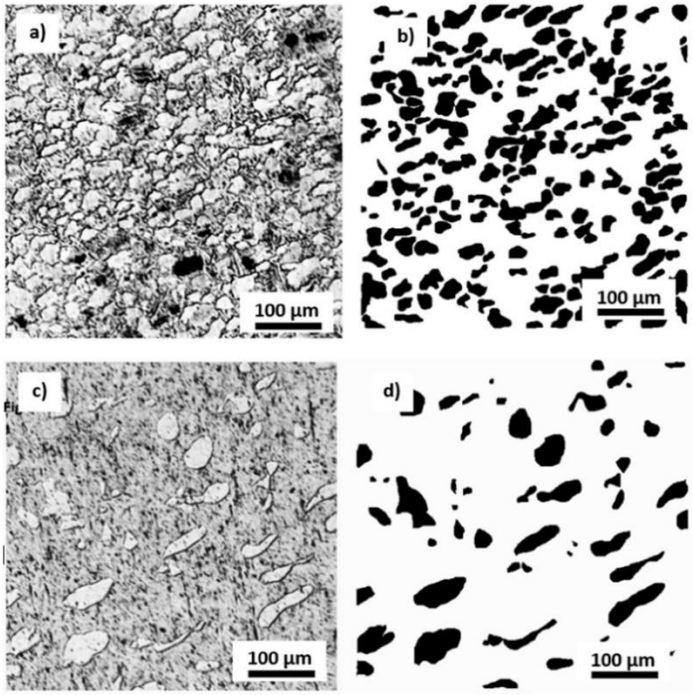

Fig. 2.24 Microstructures of the IMI 834 alloy with (a) and (b) undeformed and (c) and (d) deformed to a strain of 1 at a strain rate of 0.01 s^{-1} at 1000 °C [61].

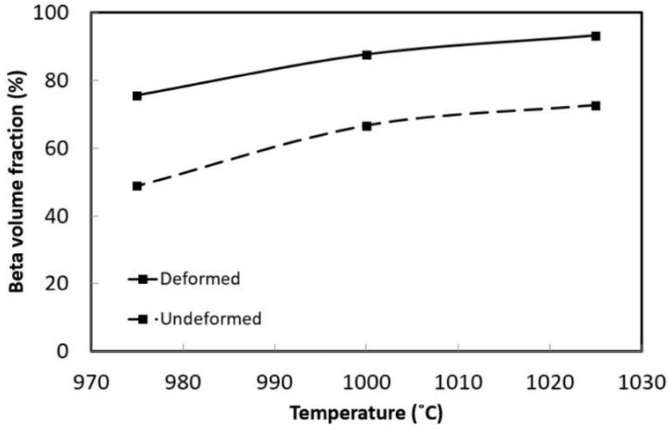

Fig. 2.25 Comparison of volume fraction of the beta phase prior to and after deformation [61].

2.3.4. Comparison of dynamic transformation in titanium alloys and in steels

The above evidences concerning strain-induced transformation are analogous to the observations of dynamic transformation in steel. However, the transformation tendency is reversed compared to the case of steel because the high temperature beta phase is softer than the low temperature alpha phase in titanium alloy, while low temperature ferrite is softer than

high temperature austenite in steel. Nevertheless, the soft phase replaces the hard phase during deformation in both cases.

The second difference is associated with the influence of deformation temperature on transformation. In the paper by Koike et al. [49], more alpha phase is transformed into beta as the deformation temperature is increased. In the experiments by Yang et al. [48], there is an increase in the beta volume fraction at 850°C, whereas there are no changes at the lower temperatures of 750°C and 800°C. The possible reason for this is that the height of the Gibbs energy barrier decreases as the temperature approaches the transus temperature. This makes it easier to transform alpha into beta. The Gibbs energy barriers oppose the dynamic transformation of the alpha into the beta. The driving force for dynamic transformation is derived from the difference between the flow stress of alpha and the yield stress of beta, as shown in Fig. 2.26. The driving forces for the titanium material of Ref. [62] increase from 307 J/mol to 583 J/mol as the crosshead speed is increased. However, steels exhibited a reverse trend with titanium alloys. As shown in Fig. 2.27, the fraction of ferrite produced by dynamic transformation was decreased with temperature [63]. This was associated with the greater energy barrier for transformation (Gibbs energy) as temperature was increased gradually above the Ae_3.

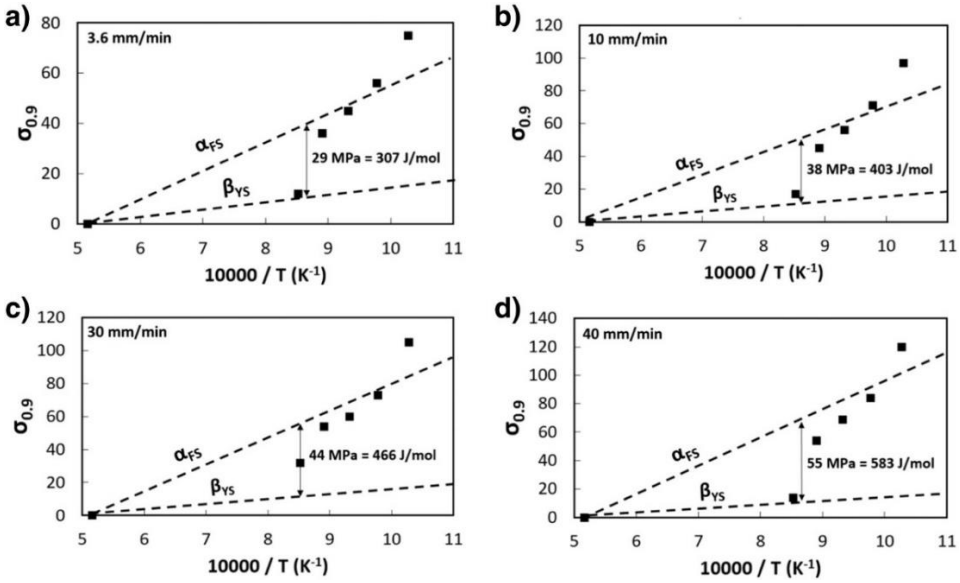

Fig. 2.26 Dependences of the alpha flow stress at ε = 0.9 and the beta yield stress on inverse absolute temperature. Constant crosshead speeds of a) 3.6 mm/min, b) 10 mm/min, c) 30 mm/min, and d) 40 mm/min were employed [61].

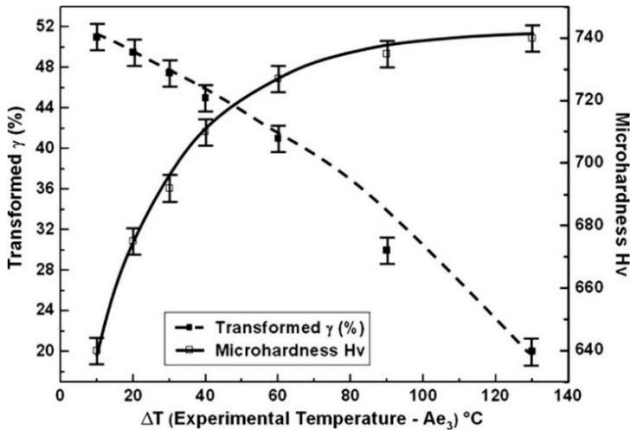

Fig. 2.27 Variation of the ferrite and cementite fraction and microhardness with ΔT (experimental temperature – Ae_3) for steel (0.79C) deformed to a strain of 4.0 at a strain rate of 4.0 s^{-1} [63].

The similarity between the dynamic transformation in titanium alloys and steels is the reverse transformation in the isothermal holding after unloading. In the case of steel, Widmanstatten ferrite can retransform into austenite during holding at the deformation temperature [64]. Similarly, the beta phase in the titanium produced during deformation is metastable and can retransform into the alpha phase after unloading. This has been confirmed in the isothermal holding after tensile testing by Koike et al. [49]. The reverse transformation behavior indicated that the dynamic transformation was derived from the applied stress to some extent. In addition, the reverse transformation in steels and titanium alloys was dependent on time and controlled by diffusion.

The role of strain in the dynamic transformation is identical in both steels and titanium alloys. In the work by Koike et al. [49] and Wang et al. [56], the volume fraction of beta phase in titanium alloys increased with the strain. Increasing the strain introduces more work hardening and increases the driving force for dynamic transformation in this way. This was consistent with the dynamic behavior in steel. Similar tests in a 6Ni–0.1C steel indicated that the fraction of dynamic ferrite transformation deformed above Ae_3 increased with the strain [65] shown in Fig. 2.28. The dependence of dynamic transformation on strain can be described by an Avrami-type equation.

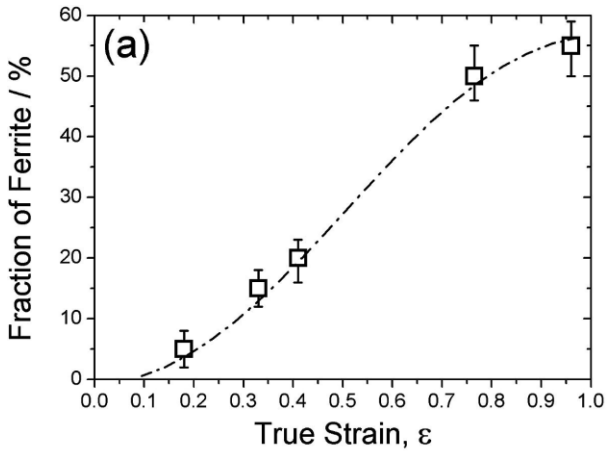

Fig. 2.28 Dependence of the ferrite fraction on strain deformed at 0.1 s^{-1} at 750 °C with an average austenite grain size of 15 μm [65].

2.3.5 Other dynamic phenomena associated with hot deformation in titanium alloys

The dynamic behavior during deformation was not limited to transformation and other phenomena such as dynamic recovery and globularization can take place in titanium alloys as well. Dynamic recovery was found in the hot deformation below the transus temperature (beta → beta+alpha) in both alpha and beta titanium alloys [1, 5]. A steady-state flow behavior was provided by the dynamic recovery and dislocation was annihilated in the process. In colony microstructure, dynamic globularization was a typical softening mechanism. As shown in Fig. 2.29, the globularization fractions of two initial microstructures were increased with strains [66]. However, it was basically initiated at a strain of 0.75-1.0 and completed by strains of the order of 2-2.5. Hence, the globularization was pronounced in torsion or tensile deformation (in superplastic regime) in which greater strains can be achieved.

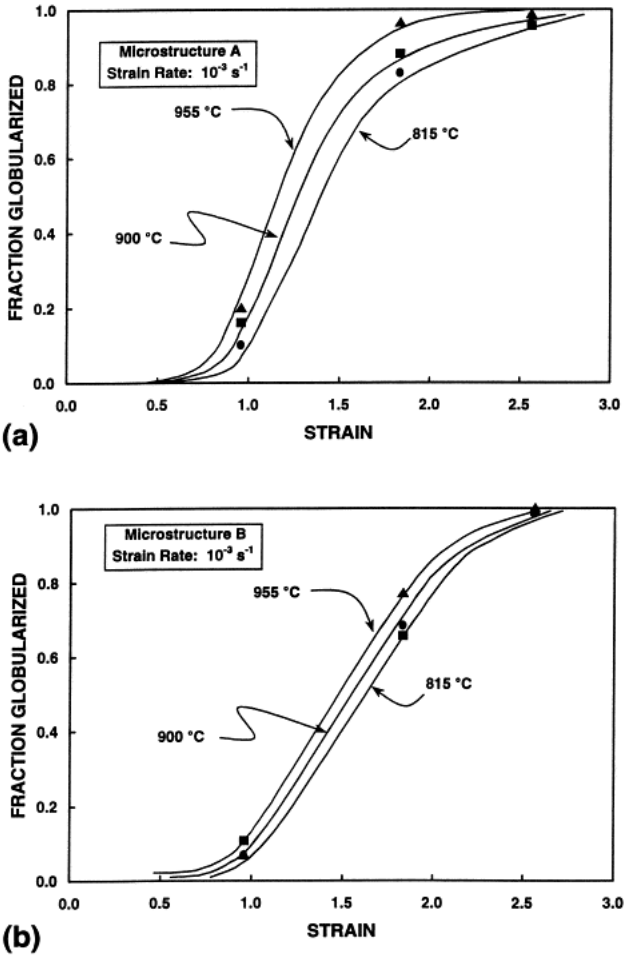

Fig. 2.29 Dependence of globularization fraction on the strain and temperature in Ti–6Al–4V samples deformed at a strain rate of 0.001 s^{-1}: (a) A microstructure (a 100 µm grain size and ≈1 µm thick alpha plates) and (b) B microstructure (a 400 µm grain size and ≈1 µm thick alpha plates) [66].

Dynamic coarsening was observed in an initial globular microstructure at elevated temperatures and relatively low strain rates. The coarsening behavior during hot working provided flow hardening by reducing the amounts of grain boundary which was the source of deformation at the such high temperatures. The work by Semiatin et al. [67] showed that the dynamic coarsening in Ti-6Al-4V took place at 900 °C and 955 °C at a strain rate of 10^{-4} s^{-1} and facilitated by the straining displayed in Fig. 2.30. They found that both the dynamic and static coarsening were controlled by bulk diffusion of solutes through the beta matrix. Similar findings were later reported by Sargent et al. [68] at the lower temperatures and Park et al. [69] in Ti-6Al-2Sn-4Zr-

2Mo-0.1Si alloy.

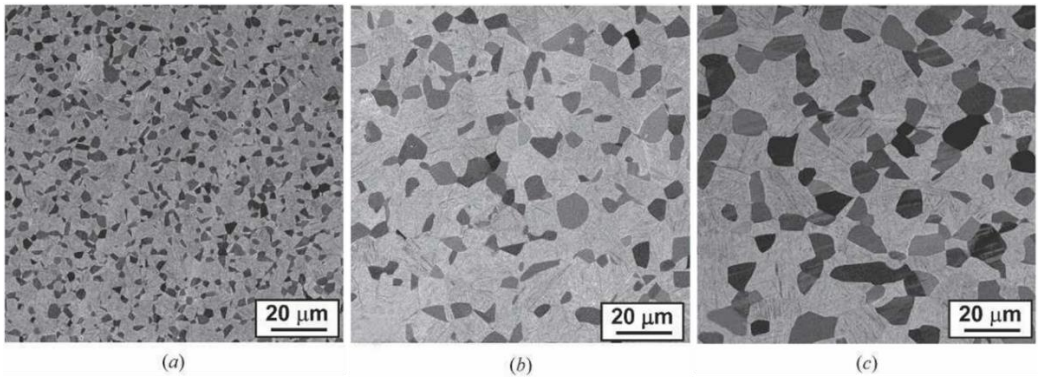

Fig. 2.30 SEM-BSE micrographs of Ti-6Al-4V samples subjected to deformation at 955 °C with strain rate of 10^{-4} s^{-1} to strains of (a) 0, (b) 0.5, and (c) 1.4 [67].

Morphological evolution during hot working in titanium alloy can be observed as well. For example, the platelet kinking in Ti-6Al-4V with colony microstructure acted as a source of flow softening particularly at low strains [70]. Further EBSD characterizations by Mironov et al. [71] revealed that the kinking was continuously developed in the colony microstructure shown in Fig. 2.31 and this behavior was related to the formation of shear bands.

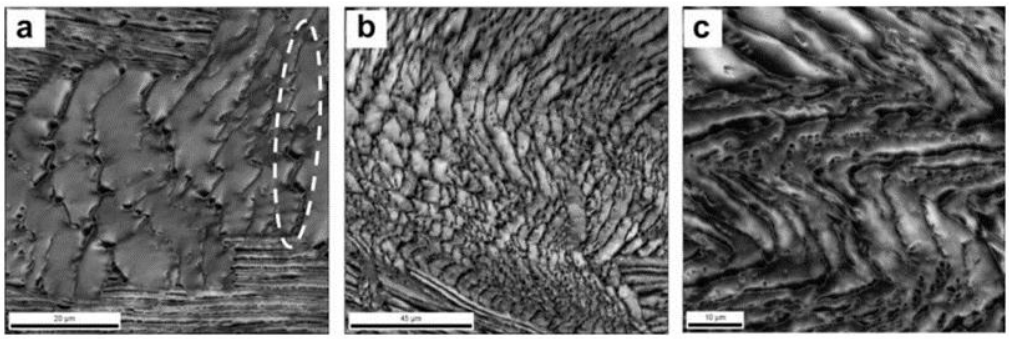

Fig. 2.31 EBSD images of the kinking behavior of alpha lamellae in Ti-6Al-4V alloy during straining. The compression direction is vertical [71].

References

[1] I. Weiss, S.L. Semiatin, Thermomechanical processing of alpha titanium alloys—an overview, Materials Science and Engineering: A 263(2) (1999) 243-256.

[2] H. Rosenberg, Titanium Alloying in Theory and Practice, Titanium Metals Corp. of America, Henderson, Nev., 1970.

[3] E. Eisenbarth, D. Velten, M. Müller, R. Thull, J. Breme, Biocompatibility of β-stabilizing elements of titanium alloys, Biomaterials 25(26) (2004) 5705-5713.

[4] D. Velten, K. Schenk–Meuser, V. Biehl, H. Duschner, J. Breme, Characterization of thermal and anodic oxide layers on β-and on near-β-titanium alloys for biomedical application, Zeitschrift für Metallkunde 94(6) (2003) 667-675.

[5] I. Weiss, S.L. Semiatin, Thermomechanical processing of beta titanium alloys—an overview, Materials Science and Engineering: A 243(1-2) (1998) 46-65.

[6] R. Penelle, Influence of Microstructure on Mechanical Properties and Plasticity of Titanium and Titanium Alloys, Sixth World Conference on Titanium. III, 1988, pp. 1457-1464.

[7] M.J. Donachie, Titanium: a technical guide, ASM international2000.

[8] H.L. Freese, M.G. Volas, J.R. Wood, Metallurgy and technological properties of titanium and titanium alloys, Titanium in Medicine, Springer2001, pp. 25-51.

[9] G. Welsch, R. Boyer, E. Collings, Materials properties handbook: titanium alloys, ASM International 1993.

[10] S. Hardt, H. Maier, H.-J. Christ, High-temperature fatigue damage mechanisms in near-α titanium alloy IMI 834, International Journal of Fatigue 21(8) (1999) 779-789.

[11] B. Geary, V. Bolam, S. Jenkins, D. Davies, High temperature titanium sheet for helicopter exhaust applications, Titanium'95- Science and technology (1996) 1638-1645.

[12] S. Semiatin, B. Kirby, G. Salishchev, Coarsening behavior of an alpha-beta titanium alloy, Metallurgical and Materials Transactions A 35(9) (2004) 2809-2819.

[13] Z. Liu, G. Welsch, Effects of oxygen and heat treatment on the mechanical properties of alpha and beta titanium alloys, Metallurgical Transactions A 19(3) (1988) 527-542.

[14] R. Boyer, An overview on the use of titanium in the aerospace industry, Materials Science and Engineering: A 213(1) (1996) 103-114.

[15] K. Wang, The use of titanium for medical applications in the USA, Materials Science and Engineering: A 213(1) (1996) 134-137.

[16] W. Cui, Z. Jin, A. Guo, L. Zhou, High temperature deformation behavior of α+β-type biomedical titanium alloy Ti–6Al–7Nb, Materials Science and Engineering: A 499(1) (2009) 252-256.

[17] A. Machado, J. Wallbank, Machining of titanium and its alloys—a review, Proceedings of the Institution of Mechanical Engineers, Part B: Journal of Engineering Manufacture 204(1) (1990) 53-60.

[18] S. Ankem, C. Greene, Recent developments in microstructure/property relationships of beta titanium alloys, Materials Science and Engineering: A 263(2) (1999) 127-131.

[19] P.J. Bania, Beta titanium alloys and their role in the titanium industry, Jom 46(7) (1994) 16-19.

[20] G. Lütjering, J.C. Williams, Titanium, Springer2003.

[21] M. McQuillan, Phase transformations in titanium and its alloys, Metallurgical Reviews 8(1) (1963) 41-104.

[22] A. Zarkades, F. Larson, The Science, Technology and Application of Titanium, (1970).

[23] H. Conrad, M. Doner, B. De Meester, Deformation and fracture (controlling mechanisms for titanium plastic flow), Titanium science and technology (1973) 969-1005.

[24] N. Gey, M. Humbert, M. Philippe, Y. Combres, Modeling the transformation texture of Ti-64 sheets after rolling in the β-field, Materials Science and Engineering: A 230(1) (1997) 68-74.

[25] S. Fedotov, Peculiarities of changes in elastic properties of Ti martensite, Titanium Science and Technology 2 (1973).

[26] J. Newkirk, A. Geisler, Crystallographic aspects of the beta to alpha transformation in titanium, Acta Metallurgica 1(3) (1953) 370-374.

[27] W. Burgers, On the process of transition of the cubic-body-centered modification into the hexagonal-close-packed modification of zirconium, Physica 1(7) (1934) 561-586.

[28] D. De Fontaine, N. Paton, J. Williams, The omega phase transformation in titanium alloys as an example of displacement controlled reactions, Acta Metallurgica 19(11) (1971) 1153-1162.

[29] J. Williams, R. Taggart, D. Polonis, The morphology and substructure of Ti-Cu martensite, Metallurgical Transactions 1(8) (1970) 2265-2270.

[30] Y. Mantani, Y. Takemoto, M. Hida, A. Sakakibara, M. Tajima, Phase Transformation of. ALPHA." Martensite Structure by Aging in Ti-8 mass% Mo Alloy, Materials Transactions 45(5) (2004) 1629-1634.

[31] F.G. Mur, D. Rodriguez, J. Planell, Influence of tempering temperature and time on the α'-Ti-6Al-4V martensite, Journal of Alloys and Compounds 234(2) (1996) 287-289.

[32] S. Banerjee, P. Mukhopadhyay, Phase Transformations: Examples from Titanium and Zirconium Alloys, Elsevier, 2010.

[33] P. Frost, W. Parris, L. Hirsch, J. Doig, C. Schwartz, Isothermal transformation of titanium-chromium alloys, Trans. ASM 46 (1954) 231-256.

[34] B. Hickman, Precipitation of the Omega-Phase in Titanium- Vanadium Alloys, J Inst Metals 96(11) (1968) 330-337.

[35] B. Hickman, The formation of omega phase in titanium and zirconium alloys: a review, Journal of Materials Science 4(6) (1969) 554-563.

[36] R. Wood, Martensitic alpha and omega phases as deformation products in a titanium-15% molybdenum alloy, Acta Metallurgica 11(8) (1963) 907-914.

[37] T. Ahmed, H.J. Rack, Phase transformations during cooling in α+β titanium alloys, Materials Science and Engineering: A 243(1) (1998) 206-211.

[38] R. Filip, K. Kubiak, W. Ziaja, J. Sieniawski, The effect of microstructure on the mechanical properties of two-phase titanium alloys, Journal of Materials Processing Technology 133(1) (2003) 84-89.

[39] C. Ghosh, C. Aranas Jr, J.J. Jonas, Dynamic transformation of deformed austenite at temperatures above the Ae_3, Progress in Materials Science 82 (2016) 151-233.

[40] M. Peters, G. Ziegler, G. Lütjering, Control of microstructures of (alpha+ beta)-titanium alloys, Zeitschrift für Metallkunde 74 (1983) 274-282.

[41] R. Nalla, B. Boyce, J. Campbell, J. Peters, R. Ritchie, Influence of microstructure on high-cycle fatigue of Ti-6Al-4V: bimodal vs. lamellar structures, Metallurgical and Materials Transactions A 33(13) (2002) 899-918.

[42] G. Lütjering, Influence of processing on microstructure and mechanical properties of (α+β) titanium alloys, Materials Science and Engineering: A 243(1) (1998) 32-45.

[43] S.L. Semiatin, T. Bieler, The effect of alpha platelet thickness on plastic flow during hot working of Ti–6Al–4V with a transformed microstructure, Acta Materialia 49(17) (2001) 3565-3573.

[44] H. Yoshimura, K.i. Kimura, M. Hayashi, M. Ishii, T. Hanamura, J.-i. Takamura, Ultra-fine equiaxed grain refinement and improvement of mechanical properties of α+β type titanium alloys by hydrogenation, hot working, heat treatment and dehydrogenation, Materials Transactions, JIM 35(4) (1994) 266-272.

[45] A. Dutta, N. Birla, Stress induced hydrogen diffusion in a α+β titanium alloy during superplastic deformation, Scripta Metallurgica 21(8) (1987) 1051-1054.

[46] B.H. Prada, J. Mukhopadhyay, A.K. Mukherjee, Effect of strain and temperature in a superplastic Ni-modified Ti–6Al–4V Alloy, Materials Transactions, JIM 31(3) (1990) 200-206.

[47] B. Hidalgo-Prada, J. Mukhopadhyay, A.K. Mukherjee, Correlation of Mechanical Behavior with Microstructural Aspects of Ni Modified Superplastic Ti–6Al–4V Alloy, Materials Transactions, JIM 31(8) (1990) 689-696.

[48] H. Yang, G. Gurewitz, A. Mukherjee, Mechanical Behavior and Microstructural Evolution during Superplastic Deformation of Ti–6Al–4V, Materials Transactions, JIM 32(5) (1991) 465-472.

[49] J. Koike, Y. Shimoyama, I. Ohnuma, T. Okamura, R. Kainuma, K. Ishida, K. Maruyama, Stress-induced phase transformation during superplastic deformation in two-phase Ti–Al–Fe alloy, Acta Materialia 48(9) (2000) 2059-2069.

[50] C. Lu, L. Huang, L. Geng, B. Kaveendran, Z. Zheng, J. Zhang, Mechanisms behind the superplastic behavior of as-extruded TiBw/Ti6Al4V composites with a network architecture, Materials Characterization 104 (2015) 139-148.

[51] H. Matsumoto, V. Velay, A. Chiba, Flow behavior and microstructure in Ti–6Al–4V alloy with an ultrafine-grained α-single phase microstructure during low-temperature-high-strain-rate superplasticity, Materials & Design 66 (2015) 611-617.

[52] W. Zhang, H. Ding, M. Cai, W. Yang, J. Li, Ultra-grain refinement and enhanced low-temperature superplasticity in a friction stir-processed Ti-6Al-4V alloy, Materials Science and Engineering: A 727 (2018) 90-96.

[53] H. Matsumoto, K. Yoshida, S.-H. Lee, Y. Ono, A. Chiba, Ti–6Al–4V alloy with an ultrafine-grained microstructure exhibiting low-temperature–high-strain-rate superplasticity, Materials Letters 98 (2013) 209-212.

[54] S. Chen, J. Huang, D. Cheng, H. Zhang, X. Zhao, Superplastic deformation mechanism and mechanical behavior of a laser-welded Ti–6Al–4V alloy joint, Materials Science and Engineering: A 541 (2012) 110-119.

[55] H. Matsumoto, T. Nishihara, Y. Iwagaki, T. Shiraishi, Y. Ono, A. Chiba, Microstructural evolution and deformation mode under high-temperature-tensile-deformation of the Ti-6Al-4V alloy with the metastable α’ martensite starting microstructure, Materials Science and Engineering: A 661 (2016) 68-78.

[56] K. Wang, G. Liu, W. Tao, J. Zhao, K. Huang, Study on the mixed dynamic recrystallization mechanism during the globularization process of laser-welded TA15 Ti-alloy joint under hot tensile deformation, Materials Characterization 126 (2017) 57-63.

[57] Y. Zong, D. Shan, M. Xu, Y. Lv, Flow softening and microstructural evolution of TC11 titanium alloy during hot deformation, Journal of Materials Processing Technology 209(4) (2009) 1988-1994.

[58] L. Jing, R. Fu, Y. Wang, L. Qiu, B. Yan, Discontinuous yielding behavior and microstructure evolution during hot deformation of TC11 alloy, Materials Science and Engineering: A 704 (2017) 434-439.

[59] M. Meng, X. Fan, Y. Chen, H. Guo, L. Guo, M. Zhan, Assessment of alpha phase evolution in deformation of two-phase Ti-alloys under the off-equilibrium condition, Materials Science and Engineering: A 738 (2018) 389-398.

[60] X.-j. Dong, S.-q. Lu, H.-z. Zheng, L. Xin, D.-l. Ouyang, Cavity nucleation during hot forging of Ti-6Al-2Zr-1Mo-1V alloy with colony alpha microstructure, Transactions of Nonferrous Metals Society of China 20(12) (2010) 2259-2264.

[61] J.J. Jonas, C. Aranas Jr, A. Fall, M. Jahazi, Transformation softening in three titanium alloys, Materials & Design 113 (2017) 305-310.

[62] X. Chun, W.-F. Zhu, Transformation mechanism and mechanical properties of commercially pure titanium, Transactions of Nonferrous Metals Society of China 20(11) (2010) 2162-2167.

[63] C. Ghosh, V.V. Basabe, J.J. Jonas, Y.-M. Kim, I.-H. Jung, S. Yue, The dynamic transformation of deformed austenite at temperatures above the Ae_3, Acta Materialia 61(7) (2013) 2348-2362.

[64] C. Ghosh, C. Aranas, J.J. Jonas, Dynamic transformation of deformed austenite at temperatures above the Ae_3, Progress in Materials Science 82 (2016) 151-233.

[65] N. Park, S. Khamsuk, A. Shibata, N. Tsuji, Effect of austenite grain size on kinetics of dynamic ferrite transformation in low carbon steel, Scripta Materialia 68(8) (2013) 611-614.

[66] S.L. Semiatin, V. Seetharaman, I. Weiss, Flow behavior and globularization kinetics during hot working of Ti–6Al–4V with a colony alpha microstructure, Materials Science and Engineering: A 263(2) (1999) 257-271.

[67] S.L. Semiatin, M. Corbett, P. Fagin, G. Salishchev, C. Lee, Dynamic-coarsening behavior of an α/β titanium alloy, Metallurgical and Materials Transactions A 37(4) (2006) 1125-1136.

[68] G. Sargent, A. Zane, P. Fagin, A. Ghosh, S.L. Semiatin, Low-temperature coarsening and plastic flow behavior of an alpha/beta titanium billet material with an ultrafine microstructure, Metallurgical and Materials Transactions A 39(12) (2008) 2949.

[69] C.H. Park, B. Lee, S.L. Semiatin, C.S. Lee, Low-temperature superplasticity and coarsening behavior of Ti–6Al–2Sn–4Zr–2Mo–0.1 Si, Materials Science and Engineering: A 527(20) (2010) 5203-5211.

[70] R. Miller, T. Bieler, S. Semiatin, Flow softening during hot working of Ti-6Al-4V with a lamellar colony microstructure, Scripta Materialia 40(12) (1999) 1387-1394.

[71] S. Mironov, M. Murzinova, S. Zherebtsov, G. Salishchev, S. Semiatin, Microstructure evolution during warm working of Ti–6Al–4V with a colony-α microstructure, Acta Materialia 57(8) (2009) 2470-2481.

Chapter 3

Dynamic Transformation of Ti–6Al–4V during Torsion in the Two-Phase Region

This chapter described the dynamic transformation in Ti-6Al-4V using torsion tests at elevated temperatures. Effects of temperature, strain and strain rates on the transformation were discussed. The critical stresses for the initiation of the transformation were calculated based on driving force and energy barriers. This provides a critical condition to determine the occurrence of dynamic transformation associated with the thermodynamics.

- This chapter has been published: **Baoqi Guo** *, S. L. Semiatin, John J. Jonas, and Stephen Yue. Dynamic transformation of Ti–6Al–4V during torsion in the two-phase region. Journal of Materials Science, 53(2018): 9305–9315.

Abstract

Isothermal torsion tests were performed on a Ti-6Al-4V alloy in the two-phase region. The results show that straining leads to an increase in the beta phase fraction, which increases slightly with strain rate. Transformation took place at 880°C, 940°C, 960°C, 980°C and 1000°C. The extent of this type of dynamic transformation (alpha to beta) was increased when the temperature approached the transus temperature. The reverse transformation (beta to alpha) occurred during isothermal holding after torsion and the volume fraction retransformed increased with time. The driving forces promoting dynamic and reverse transformation together with the energy barriers opposing these transformations were derived and compared. The critical stresses required to initiate dynamic transformation are calculated from the flow curves. This analysis confirms that the peak stresses are always higher than the critical stresses at the temperatures employed in the present tests, which makes it possible for the transformation to occur.

3.1 Introduction

The dynamic transformation of austenite to ferrite above Ae_3 was first reported to occur in steel by Yada and co-workers in the 1980's [1, 2]. They performed compression tests at temperatures above the Ae_3 and produced metastable fine-grained ferrite in the austenite region. Later other researchers described the reverse static transformation from ferrite to austenite during isothermal holding after deformation [3-6]. Such dynamic transformation was initially explained in terms of the stored energy of the dislocations introduced by straining. However, this approach failed to explain the large difference between the rates of dynamic and reverse transformation [7-9]. It was later proposed that the applied stress is the driving force for dynamic transformation, consisting of the flow stress difference between the austenite and the ferrite that takes its place [10, 11]. The Widmanstatten ferrite produced by dynamic transformation has been shown to nucleate displacively, while its growth is accompanied by carbon diffusion [12, 13].

Dynamic transformation has also been shown to take place in hexagonal materials, such as the titanium alloys. For example, Koike et al. [14] reported an increase in volume fraction of the beta phase during the deformation of Ti-5.5Al-1.5Fe in the two-phase region. These researchers estimated that the free energy of the alpha phase would have to increase by about 500 J/mol to account for the experimental results. However, the source of this driving force was not known at the time. Yang et al. [15] also described the formation of the beta phase in Ti-6Al-4V in their tensile tests carried out at 850°C and suggested that it was induced by the strain of the deformation. In later work by Prada et al. [16], the beta phase fraction in Ti-6Al-4V was shown to increase with strain, an occurrence that led to a decrease in the flow stress during hot working. More recently, Lu et al. [17] showed that the transformation of alpha to beta during superplastic deformation was promoted by straining. In a similar manner, Matsumoto et al. [18] reported that the amount of beta precipitation in Ti-6Al-4V was greater in the deformed than in the undeformed sections of specimens subjected to tensile testing. Somewhat similar tensile tests were carried out on Ti-6Al-4V by Zhang et al. [19], who showed that the increase in the beta phase fraction contributed to the high observed superplastic elongations. Ding et al. [20] and Zong et al. [21] reported that the transformation of alpha to beta took place concurrently with compression in titanium alloys when these were deformed in the two phase region. More

recently, Jonas et al. [22] observed that a 20% increase in the beta phase fraction in IMI-834 took place during compression testing at 1000°C. They concluded that the decrease in flow stress during straining was attributable to the dynamic transformation of alpha into beta, although the critical conditions, such as the critical stress or strain associated with the onset of transformation in Ti-6Al-4V, were not described.

In the present research, the dynamic transformation of Ti-6Al-4V was investigated under various conditions of temperature, strain and strain rate. Torsion testing was employed as larger strains can be attained than using compression testing.

3.2 Experimental procedure

3.2.1 Thermomechanical Schedule

The present material had a composition (in weight percent) of 6.54 aluminum, 4.14 vanadium, 0.18 iron, 0.17 oxygen, 0.03 carbon, 0.03 nitrogen, the balance being titanium. The transus temperature of this alloy was estimated to be about 1015°C by means of differential thermal analysis (DTA).

The as-received material was characterized by an equiaxed microstructure and was machined into torsion samples with diameters of 6.3 mm and gauge lengths of 22.2 mm. Hot torsion tests were performed on a servohydraulic MTS torsion machine equipped with a horizontal radiation furnace and a temperature controller. A thermocouple was welded to the center of each sample to allow the deformation temperature to be tracked with accuracy. An argon protective atmosphere was used to reduce oxidation during torsion. The samples were heated at 2°C/s to the deformation temperature and then held for 15 min prior to deformation.

The samples were deformed to strains of 2.0 at a strain rate of 0.01 s^{-1} at the following temperatures: 880°C, 940°C, 960°C, 980°C and 1000°C, after which they were water quenched. Strains of 1.0, 2.0 and 4.0 were applied at a strain rate of 0.01 s^{-1} at 980°C to determine the effect of strain on the transformation. Strain rates of 0.1, 0.01. 0.002, 0.001 s^{-1} were also used to investigate the effect of strain rate on the transformation at 980°C. As for the reverse transformation, this was investigated using the holding times of 0s, 10s, 100s and 1000s after deformation to a strain of 2.0 at a strain rate of 0.01 s^{-1} at 980°C.

The stress-strain curves were derived from the torque/twist curves using the Fields and Backofen formula and correspond to the surface of the specimen with maximum strain, as expressed by:

$$\sigma = 3.3\sqrt{3}T/2\pi r^3 \quad (3\text{-}1)$$

$$\varepsilon = r\theta/\sqrt{3}L \quad (3\text{-}2)$$

Here σ denotes the equivalent stress, T is the torque, r the radius of the specimen, ε the equivalent strain, θ the amount of twist in radians and L is the gauge length of the specimen.

In the present experiment, there is a thin oxide layer at the surface of each specimen. The analyzed microstructures here are around 50 µm from the outer surface of the specimen and are considered to be approximately at the same place where the flow curves are calculated. The effect of oxide layer on flow stress is not considered here.

3.2.2 Metallography

Samples were cut transversely for microstructural examination and mounted using a phenolic mounting resin. SiC papers from 400 to 1200 grit were used for grinding. Polishing was carried out with 3 µm and 1 µm diamond suspensions and a colloidal silica suspension was employed for final polishing. The microstructures were examined using backscattered electron imaging (BSEI) in a scanning electron microscope (SEM). In the BSEI micrograghs, beta is white and alpha appears dark. The average phase fractions were evaluated on the basis of five micrographs for each sample. These fractions were determined using the ImageJ software.

3.3 Results

Examples of the true stress-true strain curves determined in this way are reproduced here in Fig. 3.1. The stress levels of the curves increase with decreasing temperature in the usual way. However, marked flow softening is evident in the curves associated with temperatures of 880°C, 940°C and 960°C. Such softening can be attributed to a combination of dynamic recrystallization and dynamic transformation [21, 23].

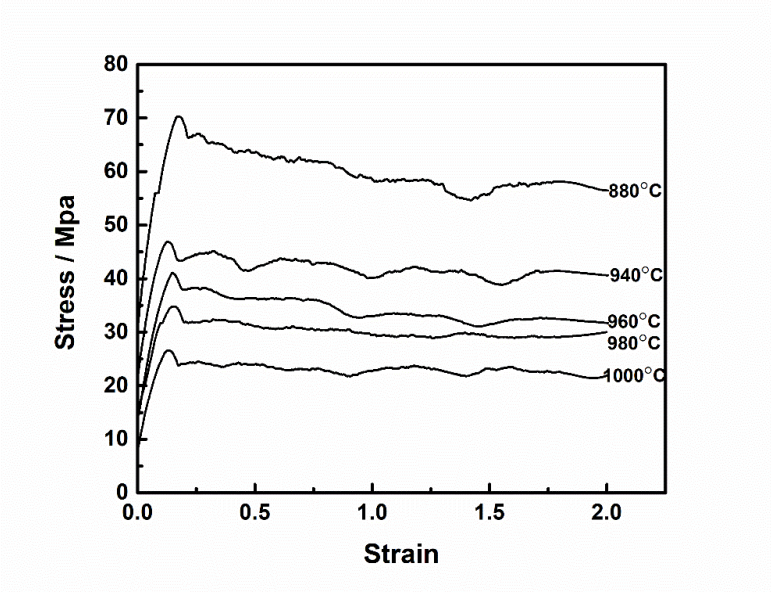

Fig. 3.1 True stress-strain curves at different temperatures determined in torsion at a strain rate of 0.01 s^{-1}.

The microstructures of undeformed and deformed samples tested at different temperatures in the two-phase region are shown in Fig. 3.2. The morphologies of the two phases prior to deformation are similar at various temperatures. For example, the undeformed sample at 940°C is characterized by a duplex microstructure in which the equiaxed dark parts are primary alpha and the light matrix is transformed beta. After deformation, the beta phase fraction has increased at each temperature, indicating that the dynamic transformation (alpha to beta) took place under the present conditions. The effect of deformation temperature on the beta phase fraction is displayed in Fig. 3.3(a). It can be seen that deformation increases the beta fraction from 22% to 34% at 880°C, from 65% to 77% at 960°C, and from 88% to 94% at 1000°C.

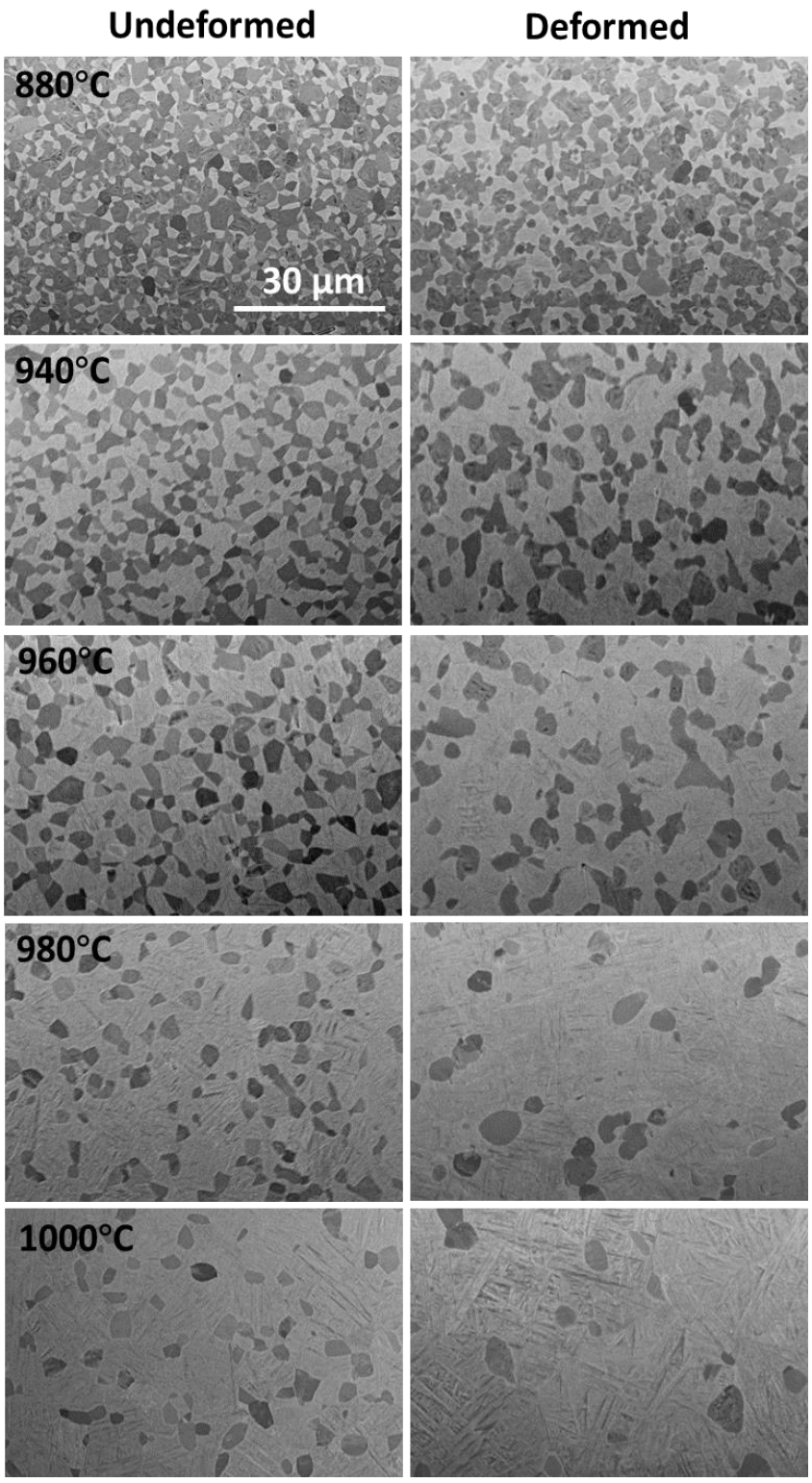

Fig. 3.2 Effect of temperature on the microstructures formed at 880°C, 940°C, 960°C, 980°C and 1000°C on samples deformed to a strain of 2.0 at a strain rate of 0.01 s^{-1}.

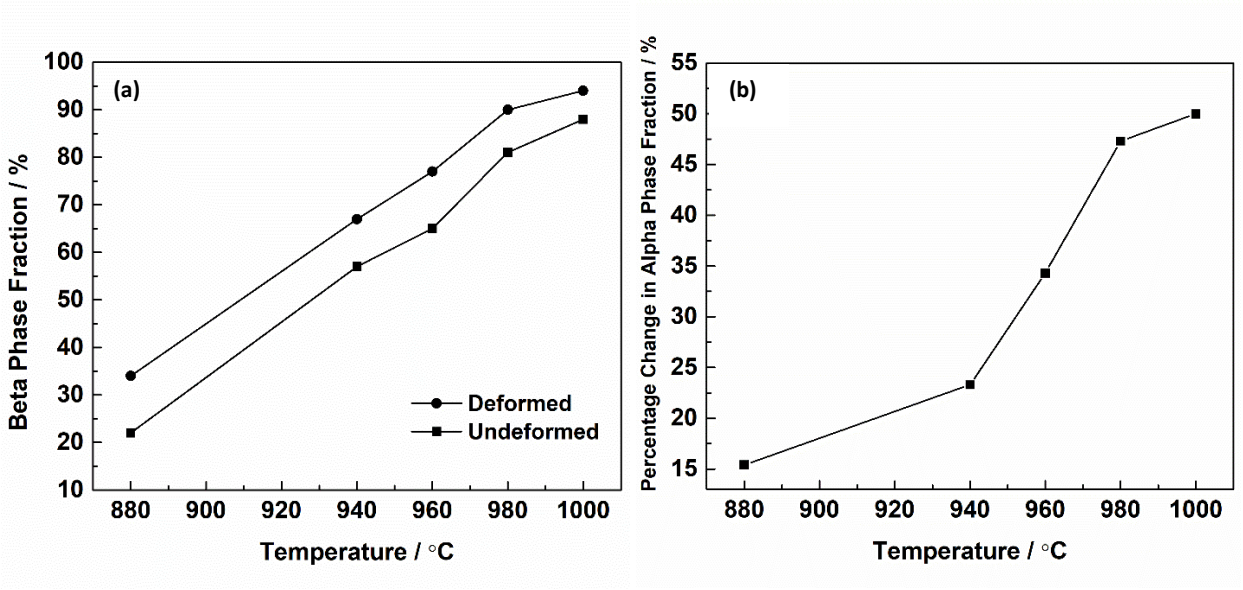

Fig. 3.3 (a) Dependence of the beta phase fraction on temperature in the undeformed and deformed samples and (b) percentage change in the alpha phase fraction in samples deformed to a strain of 2.0 at a strain rate of 0.01 s^{-1}.

As the quantity of equilibrium primary alpha decreases with increasing temperature, the absolute amount of alpha phase alone cannot precisely describe the extent of dynamic transformation. The changes in alpha phase proportions resulting from deformation are thus plotted against temperature in Fig. 3.3(b). The percentage change of alpha fraction was 15.4% at 880°C, which means that only 17.5% of the primary alpha was transformed into beta during straining. At 940°C, 23.3% of the primary alpha was involved in dynamic transformation. When the temperature was increased to 960°C, about 34.3% of the primary alpha was transformed into beta. This percentage increased to 47.4% and 50%, respectively, at 980°C and 1000°C. That is, dynamic transformation occurred more readily as the temperature was progressively increased from 880°C to 1000°C.

The effect of strain, strain rate and holding time on the microstructure is depicted in Fig. 3.4, Fig. 3.5 and Fig. 3.6, respectively. The change in beta phase fraction is displayed in Fig. 3.7(a), where it can be seen that the phase fraction increases with strain. For example, a strain of 1.0 produces a 5% increase in beta fraction compared with the undeformed sample. When the strain was further increased to 4.0, the beta fraction was drastically increased by 13%.

The effect of strain rate on the dynamic transformation is depicted in Fig. 3.7(b), from which it is evident that the beta phase fraction increases slightly with strain rate. The effect of holding time on the reverse transformation is illustrated in Fig. 3.7(c) which shows the rate of formation of the alpha phase. It decreases with holding time, indicating that the reverse transformation (beta to alpha) depends on time.

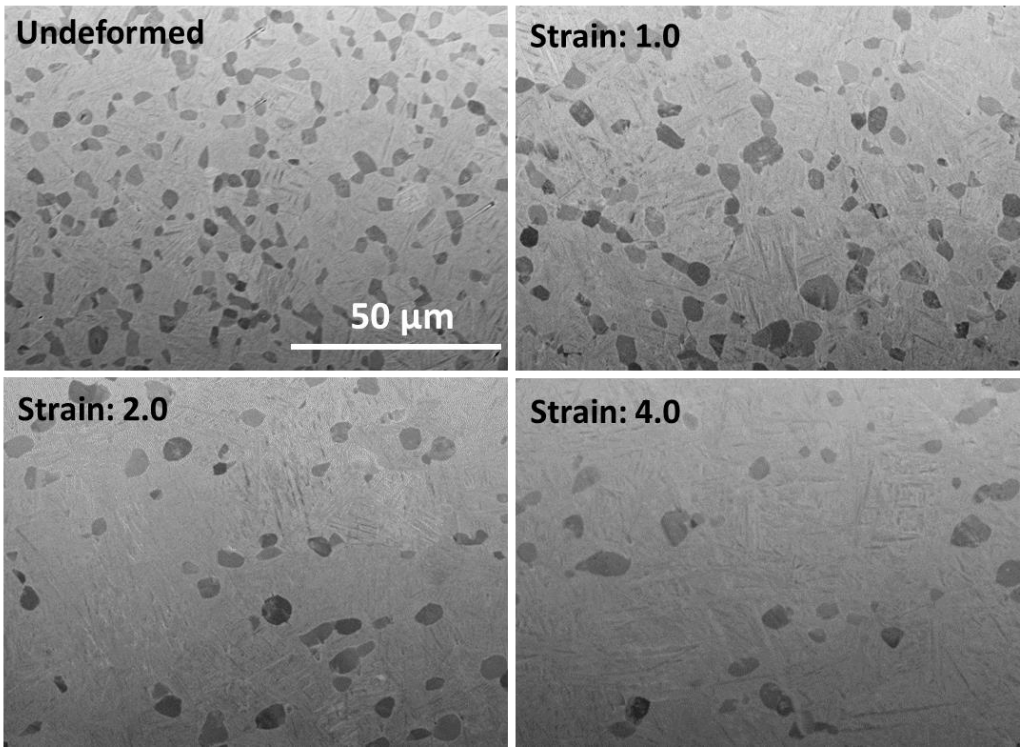

Fig. 3.4 Microstructures of samples deformed to strains of 0, 1, 2 and 4 at a strain rate of 0.01 s^{-1} at 980°C.

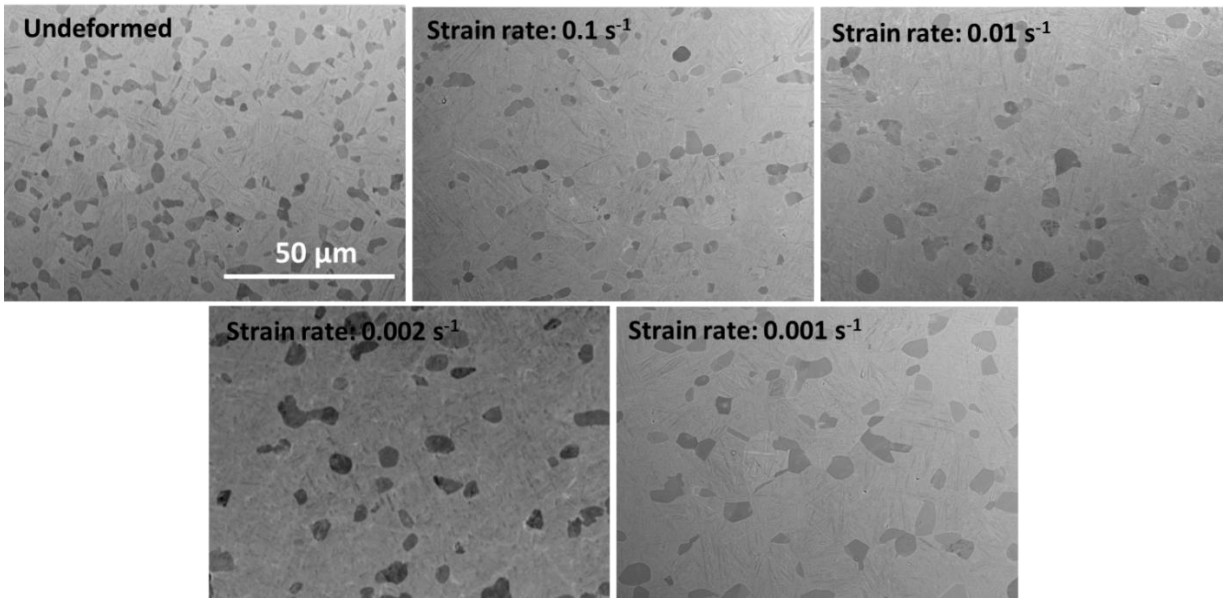

Fig. 3.5 Microstructures of samples deformed to a strain of 2.0 at strain rates of 0 s^{-1}, 0.1 s^{-1}, 0.01 s^{-1}, 0.002 s^{-1} and 0.001 s^{-1}at 980°C.

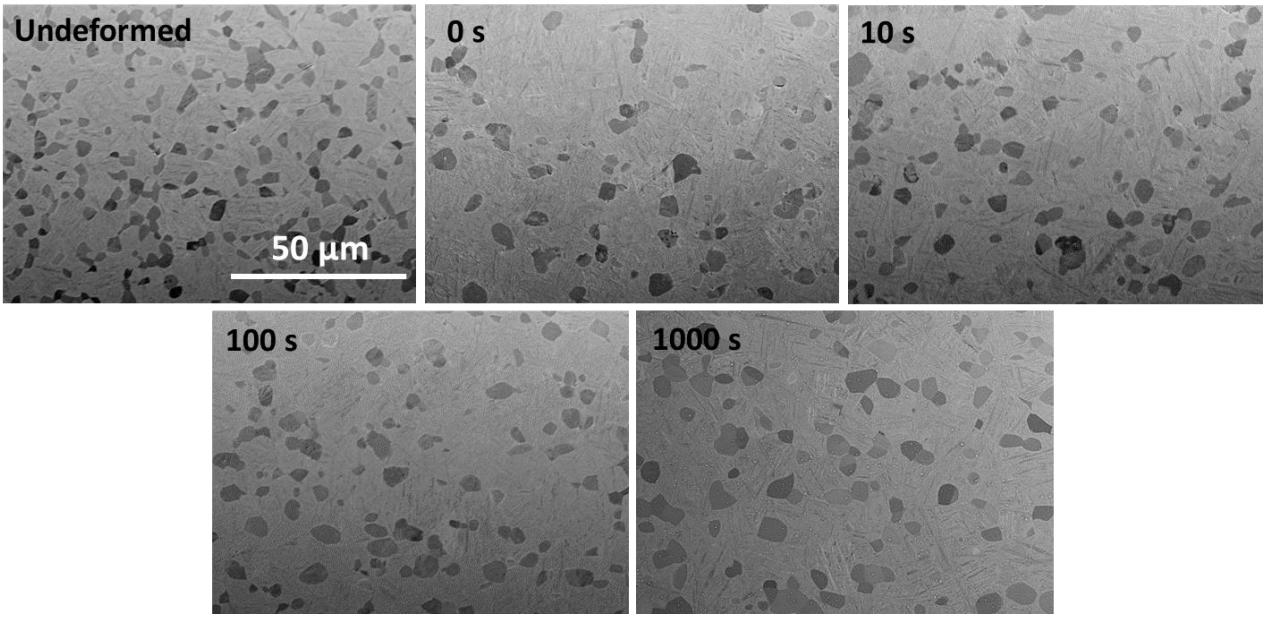

Fig. 3.6 Microstructures of samples subjected to reverse transformation during holding times of 0 s, 10 s, 100 s and 1000 s after deformation to a strain of 2.0 at a strain rate of 0.01 s^{-1} at 980°C.

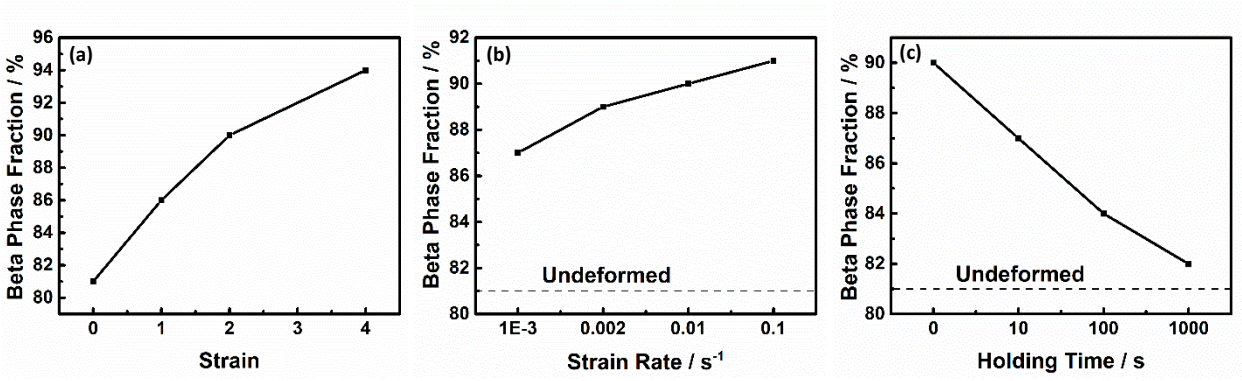

Fig. 3.7 Dependence of the beta phase fraction on (a) strain, (b) strain rate and (c) holding time at 980°C.

3.4 Discussion

As the thermal conductivity of titanium is lower than that of most other metals, deformation heating can lead to increases in temperature as well as to phase transformation. The effect of deformation heating is therefore considered briefly here. The change in temperature attributable to deformation is given by:

$$\Delta T = \frac{0.95\eta}{\rho C_p} \int \sigma d\varepsilon \tag{3-3}$$

Here ΔT refers to the temperature increase, η is the adiabatic correction factor, σ and ε are the stress and strain, respectively, ρ is the density of Ti-6Al-4V, and C_p is the specific heat [24]. The adiabatic correction factor employed here is 0.25 when the strain rate is $0.01s^{-1}$ [24]. The temperature increases at 880°C, 940°C, 960°C, 980°C and 1000°C evaluated in this way are 10.8°C, 7.5°C, 6.1°C, 5.4°C and 4.1°C, respectively. These changes are small as the limited amount of deformation heating is readily dissipated at these temperatures. In what follows, the driving forces and energy barriers of the transformation are discussed.

3.4.1 Thermodynamic evaluation of the dynamic and reverse transformations

The driving force for dynamic transformation is taken as the difference beween the flow stress of the alpha at the critical strain and the yield stress of the fresh beta that takes its place [12]. In this way, the dynamic transformation contributes to the flow softening. This can be expressed as:

$$Driving\ Force = \sigma_{critical-\alpha} - \sigma_{yield-\beta} \quad (3\text{-}4)$$

where $\sigma_{critical\text{-}\alpha}$ is the critical stress of the alpha required to initiate the dynamic transformation and $\sigma_{yield\text{-}\beta}$ is the yield stress of the beta.

The yield stress in the two-phase region was evaluated from the stress-strain curves by employing the 0.2% offset rule. Here it is assumed that the beta phase yields when the overall stress-strain curve reaches the macroscopic yield stress and the alpha/beta flow stress ratio is approximately equal to the alpha/beta hardness ratio at the same temperature. The yield stress of the beta phase ($\sigma_{yield\text{-}\beta}$) in the two-phase region was then estimated using the Law of Mixtures [25] and the high temperature hardness ratio of the two phases [26]:

$$\sigma_{mix} = V_\alpha * \sigma_\alpha + V_\beta * \sigma_\beta = V_\alpha * H_{\alpha/\beta} * \sigma_\beta + V_\beta * \sigma_\beta \quad (3\text{-}5)$$

Here σ_{mix} is the macroscopic stress, V_α and V_β are the volume fractions of alpha and beta, and σ_α and σ_β are the alpha and beta flow stresses. $H_{\alpha/\beta}$ denotes the alpha/beta hardness ratio (1.2) [26]. In this case, σ_{mix} refers to the yield stress evaluated from the stress-strain curves by employing the 0.2% offset rule and σ_β is the corresponding yield stress of the beta phase ($\sigma_{yield\text{-}\beta}$).

The energy barrier opposing the transformation consists of the Gibbs energy difference between the phases as well as the work of shear accommodation and of dilatation [10]. The total energy barrier can therefore be expressed as:

$$Energy\ Barrier = W_{dilatation} + W_{shear\ accommodation} + \Delta G_{\alpha\rightarrow\beta} \quad (3\text{-}6)$$

During phase transformation, dilatation takes place entirely perpendicular to the habit plane. The dilatation work in the present case can be expressed as [12]:

$$W_{dilatation} = \lambda * \sigma_{critical-\alpha} * \varepsilon_{dilatation} \quad (3\text{-}7)$$

where λ is an orientation factor that takes into account the difference between the direction of the applied stress and that of the transformation habit plane normal; the $\varepsilon_{dilatation}$ term refers to the dilatation strain, which has been reported to be around 1.7% [27]. In this case, the Schmid factor is 0.5, which indicates that the active habit plane is the one subject to the maximum resolved shear stress.

The formation of beta from alpha involves shear of the parent lattice by a strain of 0.14 [28]. The shear accommodation work is thus given by [10]:

$$W_{shear\ accommodation} = m * \sigma_{critical-\alpha} * \varepsilon_{shear} \quad (3\text{-}8)$$

Here ε_{shear} is the shear strain associated with the transformation and m is the Schmid factor, which takes into account the difference in orientation between the directions of $\sigma_{critical\text{-}\alpha}$ and that of the resolved stress that produces the transformation shear.

The Gibbs energy difference (ΔG_{chem}) for the transformation from alpha to beta was calculated using classical solution thermodynamics and numerical values taken from the literature [29-31]. As shown in Fig. 3.8, ΔG_{chem} is 185.9 J/mol at 880°C. This value drops to 32.5 J/mol at 940°C and 9.2 J/mol at 1000°C, decreasing as the temperature is increased.

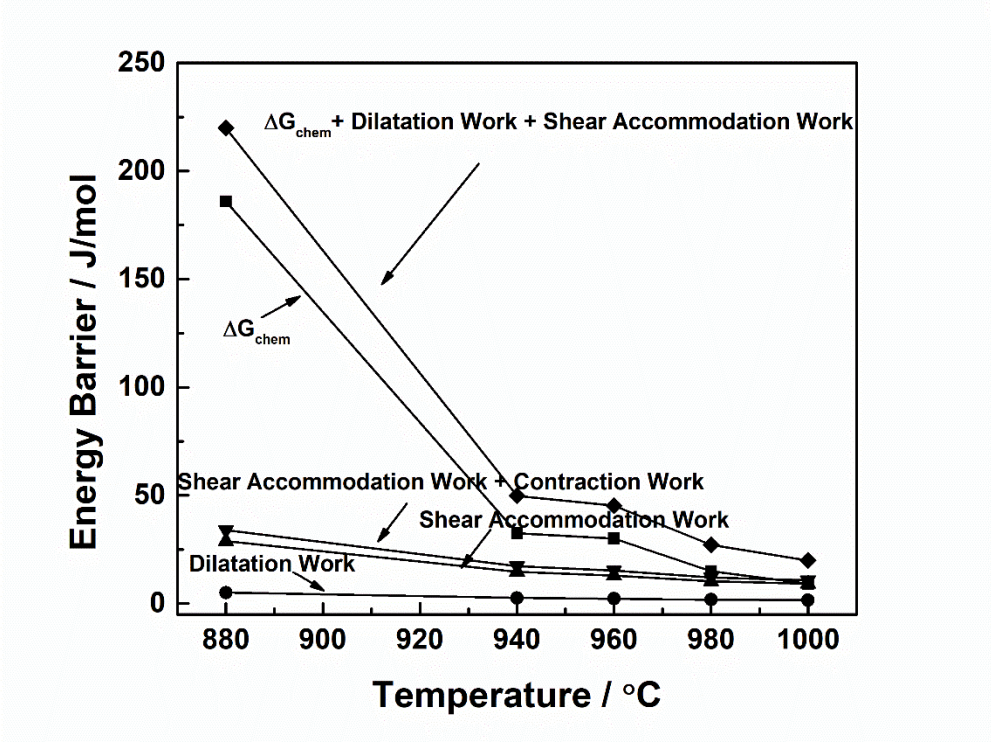

Fig. 3.8 Energy barriers opposing dynamic and reverse transformation.

The behaviors of the other energy barriers are shown in Fig. 3.8. The dilatation work decreases from 5.1 J/mol to 1.6 J/mol when the temperature is increased from 880°C to 1000°C. The shear accommodation work decreases from 28.9 J/mol to 9.1 J/mol over the same temperature range.

It can be seen that the shear accommodation and dilatation work are much less than ΔG_{chem}. The ΔG_{chem} + Dilatation work + Shear accommodation work shown in Fig. 3.8 oppose the dynamic transformation (alpha to beta) and the sum decreases with rising temperature. Thus higher percentages of alpha are transformed into beta when the temperature approaches the transus temperature, as depicted in Fig. 3.3(b).

Once the stress is removed during isothermal holding, the metastable beta transforms back into the thermodynamically more stable alpha phase. The driving force for the reverse transformation (beta to alpha) is ΔG_{chem}, which formerly acted as an energy barrier to the dynamic transformation. The reverse transformation also involves some lattice contraction and accommodation work. Here it is assumed that the absolute values of contraction work and shear work in reverse transformation are same as those of the dilatation and shear work in the dynamic transformation. As shown in Fig. 3.8, at all the temperatures, the driving force, i.e. ΔG_{chem}, is higher than the energy barrier, i.e. the shear accommodation + contraction work, especially when the temperature is lowered. This makes it thermodynamically possible for the reverse transformation to take place during isothermal holding.

The critical stress for dynamic transformation of the alpha phase ($\sigma_{critical-\alpha}$) is considered to be attained when the driving force is equal to the energy barrier [32]:

$$\sigma_{critical-\alpha} - \sigma_{yield-\beta} = 0.7 * \sigma_{critical-\alpha} * 0.017 + 0.5 * \sigma_{critical-\alpha} * 0.14 + \Delta G_{\alpha\rightarrow\beta} \quad (3\text{-}9)$$

Here the yield stress of the beta phase ($\sigma_{yield-\beta}$) was calculated using Eq. (3-5). In steel, dynamic transformation takes place in the single-phase austenite region and so the critical stress corresponds to the flow stress of the austenite phase. However, this transformation takes place in the two-phase region in Ti-6Al-4V, so it cannot be evaluated from the flow stress of the alpha phase alone.

The macroscopic critical stresses ($\sigma_{critical}$) were derived from the calculated values of $\sigma_{critical-\alpha}$ given by Eq. (3-9) and the corresponding beta flow stresses (σ_β) using the Law of Mixtures and the hardness ratio defined in Eq. (3-5). Here σ_{mix} denotes the macroscopic critical stress ($\sigma_{critical}$) in this case so that the beta flow stress (σ_β) can be estimated from the alpha to beta hardness ratio

along with $\sigma_{critical\text{-}\alpha}$. These are plotted against temperature in Fig. 3.9. In this case, $\sigma_{critical}$ is the minimum stress required to initiate dynamic transformation. The critical values of $\sigma_{critical}$ at 880°C, 940°C and 960°C are 39 MPa, 19 MPa and 16 MPa, respectively. These are lower than the corresponding peak stresses of 70 MPa, 46 MPa and 40 MPa on the flow curves of Fig. 3.1. It is thus possible for dynamic transformation to be initiated at these temperatures. The peak stress curve in Fig. 3.9 can be employed to estimate the values of σ_{peak} that correspond to the other temperatures, which can be used to predict whether dynamic transformation will occur or not at a specific temperature by comparing the values of σ_{peak} and $\sigma_{critical}$.

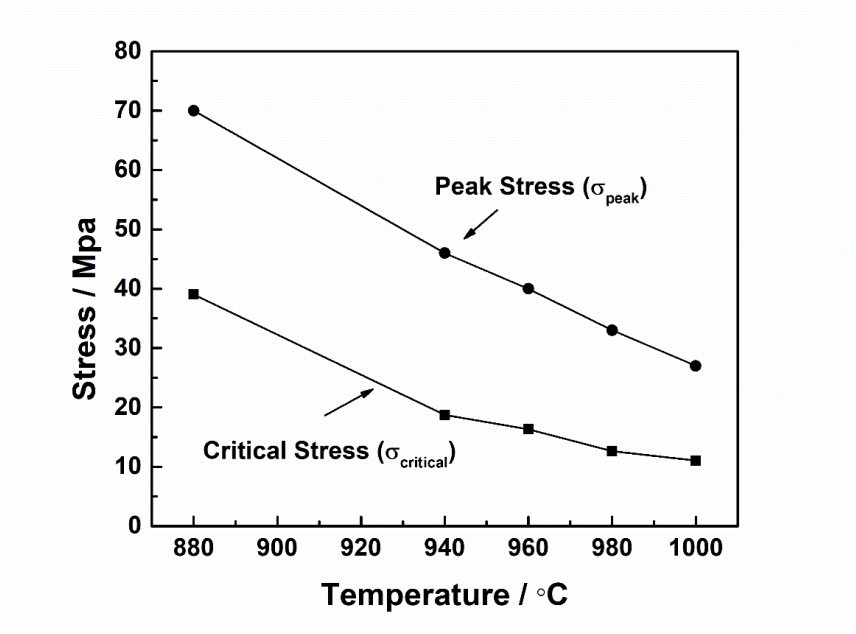

Fig. 3.9 Effect of temperature on the critical and peak stresses.

3.4.2 Effects of strain and strain rate on dynamic transformation

The present results support the view [14, 16, 17] that the beta phase can be produced by straining. As discussed earlier [10, 12], the dynamic transformation is induced by applying a shear stress on the habit plane for the transformation. Although the latter leads to flow softening, grains with favorable orientations continue to be activated as long as the applied stress is greater than the value of $\sigma_{critical}$ shown in Fig. 3.9. For example, $\sigma_{critical}$ at 980°C is 13 MPa in Fig. 3.9 and the corresponding steady state flow stress after the peak is around 30 MPa in Fig. 3.1. As a result, the dynamic transformation continues to be activated during straining.

The present results indicate that more beta phase is produced at higher strain rates because of the associated increase in flow stress. When transformation takes place at a relatively high strain rate, such as 0.1 s^{-1}, the applied stress is able to activate the transformation even in poorly oriented grains, due to the high developed stress. However, when the strain rate is reduced to 0.001 s^{-1}, the developed stress is much lower, so that transformation only takes place in grains with highly favorable orientations, i.e. those with high habit plane Schmid factors.

Such transformation is accompanied by some partitioning of the aluminum and vanadium. The distances over which these elements can diffuse can be estimated from the relation:

$$\bar{X} = \sqrt{Dt} \tag{3-10}$$

where $\bar{X}$ refers to the mean diffusion distance, D is the element diffusion coefficient and t the diffusion time. The diffusion coefficients for aluminum and vanadium employed here were taken from the work of Semiatin et al. [30]. The results show that the diffusion distances for aluminum and vanadium in the beta phase when the strain rate is 0.001 s^{-1} and the testing time is 2000s are 15 μm and 11 μm, respectively. Tests similar to the ones described here were performed by Koike et al. [14]. They found that the aluminum content varied from 8.70% to 9.70% in the alpha phase and from 6.26% to 7.59% in the beta phase during dynamic transformation. This indicates that aluminum diffusion was taking place between the two phases during the transformation.

The diffusion distances for aluminum and vanadium are reduced to 5 μm and 4 μm when the strain rate is increased to 0.01 s^{-1} and the time reduced to 200s. These are further reduced to around 2 μm for the two elements when the strain rate and time are 0.1 $s^{-1}$and 20s, respectively. These short diffusion distances make it difficult for these elements to partition at such relatively high strain rates.

By contrast, lowering the strain rate lengthens the deformation time. Thus more reverse transformation is produced during low strain rate deformation. This also contributes to the decrease in beta phase fraction under these conditions.

3.4.3 Summary of dynamic and reverse transformation results

A schematic model of dynamic and reverse transformation is shown in Fig. 3.10. The dynamic transformation is activated by the applied stress and the flow softening induced by the transformation acts as the driving force. The transformation is opposed by the shear accommodation work and work of dilatation. In steel, the dynamic transformation has been shown to occur displacively accompanied by carbon diffusion. However, the mechanism involved in the dynamic transformation of Ti-6Al-4V has not been conclusively identified. The reverse transformation is diffusion controlled and is driven by the Gibbs energy difference between the phases. The shear accommodation work and contraction work act as its energy barriers [33].

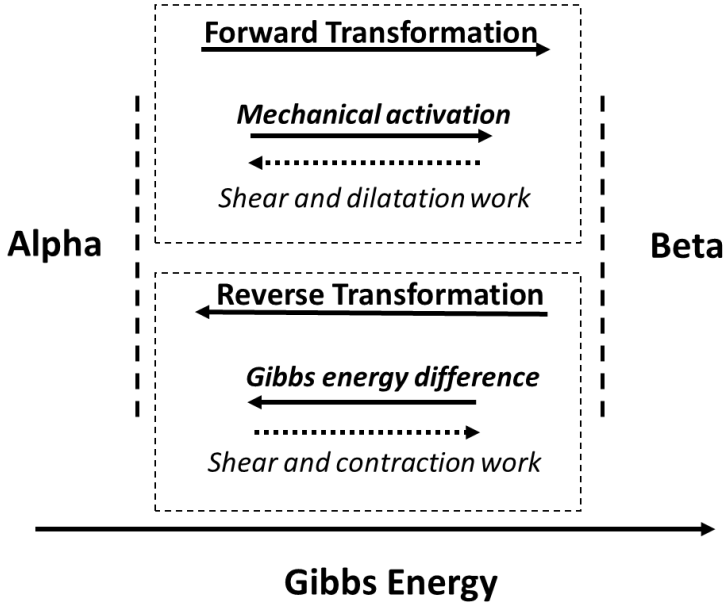

Fig. 3.10 Schematic model of dynamic and reverse transformation.

The dynamic transformation acts as a stress accommodation mechanism and contributes to the superplastic behavior at low strain rates and improves the elongation in the hot deformation of Ti-6Al-4V. In addition, the transformation is also an important source of flow softening and it should be considered in the modeling of the flow behavior during the hot deformation of the Ti-6Al-4V such as rolling and forging in mill in the future.

3.5 Conclusions

The dynamic transformation of Ti-6Al-4V was studied by means of torsion tests carried out in the two-phase region. The present observations can be summarized as follows:

Dynamic transformation takes place at 880°C, 940°C, 960°C, 980°C and 1000°C. Under these conditions, the beta phase fraction increases with strain and also slightly with strain rate. The percentage of primary alpha transformed into beta during deformation increases with temperature in the two phase region since the energy barrier opposing dynamic transformation decreases as the temperature approaches the transus. The reverse transformation takes place during holding after deformation and depends on time. The critical stresses required to initiate dynamic transformation are less than the peak stresses at the temperatures employed here, which makes it thermodynamically possible for the transformation to occur.

References

[1] T. Senuma, Massive type transformation induced by hot deformation in low carbon steels, Proc. Int. Conf. on Martensitic Transformations, Nara, 1986, pp. 515-520.

[2] H. Yada, C.-M. Li, H. Yamagata, Dynamic γ → α transformation during hot deformation in iron-nickel-carbon alloys, ISIJ international 40(2) (2000) 200-206.

[3] C. Ying, C. Qi-an, Dilatometric investigation on isothermal transformation after hot deformation, Journal of Iron and Steel Research International 10 (2003) 46-48.

[4] X. Sun, H. Luo, H. Dong, Q. Liu, Y. Weng, Microstructural evolution and kinetics for post-dynamic transformation in a plain low carbon steel, ISIJ international 48(7) (2008) 994-1000.

[5] C. Aranas Jr, T. Nguyen-Minh, R. Grewal, J.J. Jonas, Flow softening-based formation of Widmanstätten ferrite in a 0.06% C steel deformed above the Ae_3, ISIJ International 55(1) (2015) 300-307.

[6] C. Aranas, S.F. Rodrigues, Y.J. Shen, Z. Zhang, J.J. Jonas, Time – Temperature – Reverse Transformation (TTRT) Behaviors of a C – Mn and a Nb Microalloyed Steel after Dynamic Transformation above the Ae_3, Steel Research International (2017).

[7] C. Ghosh, V.V. Basabe, J.J. Jonas, Y.-M. Kim, I.-H. Jung, S. Yue, The dynamic transformation of deformed austenite at temperatures above the Ae_3, Acta Materialia 61(7) (2013) 2348-2362.

[8] N. Xiao, M. Tong, Y. Lan, D. Li, Y. Li, Coupled simulation of the influence of austenite deformation on the subsequent isothermal austenite–ferrite transformation, Acta Materialia 54(5) (2006) 1265-1278.

[9] C. Ghosh, V.V. Basabe, J.J. Jonas, Thermodynamics of dynamic transformation of hot deformed austenite in four steels of increasing carbon contents, Materials Science and Engineering: A 591 (2014) 173-182.

[10] C. Ghosh, V.V. Basabe, J.J. Jonas, Y.-M. Kim, I.-H. Jung, S. Yue, The dynamic transformation of deformed austenite at temperatures above the Ae_3, Acta Materialia 61(7) (2013) 2348-2362.

[11] C. Aranas, J.J. Jonas, Effect of Mn and Si on the dynamic transformation of austenite above the Ae_3 temperature, Acta Materialia 82 (2015) 1-10.

[12] C. Ghosh, C. Aranas, J.J. Jonas, Dynamic transformation of deformed austenite at temperatures above the Ae_3, Progress in Materials Science 82 (2016) 151-233.

[13] C. Ghosh, V.V. Basabe, J.J. Jonas, S. Yue, X.Y. Xiong, Dynamic transformation behavior of a deformed high carbon steel at temperatures above the Ae_3, ISIJ international 53(5) (2013) 900-908.

[14] J. Koike, Y. Shimoyama, I. Ohnuma, T. Okamura, R. Kainuma, K. Ishida, K. Maruyama, Stress-induced phase transformation during superplastic deformation in two-phase Ti–Al–Fe alloy, Acta Materialia 48(9) (2000) 2059-2069.

[15] H. Yang, G. Gurewitz, A. Mukherjee, Mechanical Behavior and Microstructural Evolution during Superplastic Deformation of Ti–6Al–4V, Materials Transactions, JIM 32(5) (1991) 465-472.

[16] B. Hidalgo-Prada, J. Mukhopadhyay, A.K. Mukherjee, Correlation of Mechanical Behavior with Microstructural Aspects of Ni Modified Superplastic Ti–6Al–4V Alloy, Materials Transactions, JIM 31(8) (1990) 689-696.

[17] C. Lu, L. Huang, L. Geng, B. Kaveendran, Z. Zheng, J. Zhang, Mechanisms behind the superplastic behavior of as-extruded TiBw/Ti6Al4V composites with a network architecture, Materials Characterization 104 (2015) 139-148.

[18] H. Matsumoto, K. Yoshida, S.-H. Lee, Y. Ono, A. Chiba, Ti–6Al–4V alloy with an ultrafine-grained microstructure exhibiting low-temperature–high-strain-rate superplasticity, Materials Letters 98 (2013) 209-212.

[19] T. Zhang, Y. Liu, D.G. Sanders, B. Liu, W. Zhang, C. Zhou, Development of fine-grain size titanium 6Al–4V alloy sheet material for low temperature superplastic forming, Materials Science and Engineering: A 608 (2014) 265-272.

[20] R. Ding, Z. Guo, A. Wilson, Microstructural evolution of a Ti–6Al–4V alloy during thermomechanical processing, Materials Science and Engineering: A 327(2) (2002) 233-245.

[21] Y. Zong, D. Shan, M. Xu, Y. Lv, Flow softening and microstructural evolution of TC11 titanium alloy during hot deformation, Journal of Materials Processing Technology 209(4) (2009) 1988-1994.

[22] J.J. Jonas, C. Aranas, A. Fall, M. Jahazi, Transformation softening in three titanium alloys, Materials & Design 113 (2016) 305-310.

[23] J.J. Jonas, C. Ghosh, X. Quelennec, V.V. Basabe, The critical strain for dynamic transformation in hot deformed austenite, ISIJ international 53(1) (2013) 145-151.

[24] R. Goetz, S. Semiatin, The adiabatic correction factor for deformation heating during the uniaxial compression test, Journal of Materials Engineering and Performance 10(6) (2001) 710-717.

[25] O. Senkov, J. Jonas, Effect of phase composition and hydrogen level on the deformation behavior of titanium-hydrogen alloys, Metallurgical and Materials Transactions A 27(7) (1996) 1869-1876.

[26] H.J. Rack, J. Qazi, L. Allard, R. Valiev, Thermal Stability of Severe Plastically Deformed VT-6 (Ti-6Al-4V), Materials Science Forum, Trans Tech Publ, 2008, pp. 893-898.

[27] G.A. Sargent, K.T. Kinsel, A.L. Pilchak, A.A. Salem, S.L. Semiatin, Variant Selection During Cooling after Beta Annealing of Ti-6Al-4V Ingot Material, Metallurgical and Materials Transactions A 43(10) (2012) 3570-3585.

[28] Y. Ohmori, K. Nakai, H. Ohtsubo, M. Tsunofuri, Formation of Widmanstätten Alpha Structure in a Ti–6Al–4V Alloy, Materials Transactions, JIM 35(4) (1994) 238-246.

[29] S. Semiatin, F. Zhang, R. Larsen, L. Chapman, D. Furrer, Precipitation in powder-metallurgy, nickel-base superalloys: review of modeling approach and formulation of engineering methods to determine input data, Integrating Materials and Manufacturing Innovation 5(1) (2016) 3.

[30] S.L. Semiatin, B. Kirby, G. Salishchev, Coarsening behavior of an alpha-beta titanium alloy, Metallurgical and Materials Transactions A 35(9) (2004) 2809-2819.

[31] S.L. Semiatin, T. Brown, T. Goff, P. Fagin, R. Turner, J. Murry, D. Barker, J. Miller, F. Zhang, Diffusion coefficients for modeling the heat treatment of Ti-6Al-4V, Metallurgical and Materials Transactions A 35(9) (2004) 3015-3018.

[32] C. Aranas, A. Foul, B. Guo, A. Fall, M. Jahazi, J.J. Jonas, Determination of the critical stress for the initiation of dynamic transformation in commercially pure titanium, Scripta Materialia 133 (2017) 83-85.

[33] B. Guo, C. Aranas, B. Sun, X. Ji, J.J. Jonas, Reverse Transformation Behavior of Ti-6Al-4V After Deformation in the Two-Phase Region, Metallurgical and Materials Transactions A 49(1) (2018) 22-27.

Chapter 4

Opposing and Driving Forces Associated with the Dynamic Transformation of Ti-6Al-4V

This chapter described the possible sources of driving force and energy barriers of dynamic transformation in Ti-6Al-4V. The stored energy and mechanical softening were used to interpret the driving force for the transformation. The proportion of energy consumed by dynamic transformation was clarified and a metastable phase diagram was obtained according to the composition variation derived from transformation.

- This chapter has been published: **Baoqi Guo** *, S. L. Semiatin, Jiangtao Liang, Binhan Sun, John J. Jonas. Opposing and Driving Forces Associated with the Dynamic Transformation of Ti-6Al-4V. Metallurgical and Materials Transactions A, 2018, 49(5): 1450-1454.

Abstract

The opposing and driving forces associated with dynamic transformation in Ti-6Al-4V are evaluated. It is shown that the stored energy is less than the opposing forces inhibiting transformation and insufficient to initiate the phenomenon. By contrast, the driving force derived from the net softening is greater than the opposing force and is responsible for initiating the reaction. This approach indicates that deformation reduces the transus temperature and leads to the formation of a thermodynamically metastable state.

4.1 Introduction

The dynamic transformation of austenite to ferrite was first reported to occur in steel by Yada and co-workers in the 1980's [1]. A thermodynamic basis for the occurrence of this phenomenon was later proposed [2-4] and it was shown to take place in titanium alloys as well. For example, Koike et al. found that there was an increase in the beta phase fraction during the tensile testing of Ti-5.5Al-1.5Fe in the two-phase region [5]. They took the view that the energy increase of the alpha phase accounted for the transformation, although the source of the energy increase was unknown at that time. Yang et al. [6] and Prada et al. [7] also observed that the beta phase fraction in Ti-6Al-4V increased with strain. More recently, Matsumoto et al. [8], Zhang et al. [9] and Lu et al. [10] showed that the transformation of alpha to beta takes place during superplastic deformation and is promoted by straining.

4.2 Results and Discussions

Here the opposing forces inhibiting dynamic transformation were derived from torsion tests (Table 4.1). In these experiments, isothermal torsion tests were performed on a Ti-6Al-4V at a strain rate of 0.01 s^{-1} to a strain of 2.0 followed by water quenching. The microstructures were examined using backscattered electron imaging (BSEI) in a scanning electron microscope (SEM). These volume fractions were determined using the ImageJ software. Results showed that the beta phase fraction increased by about 10% during isothermal deformation [11]. In order to illustrate the source of driving force, the stored energy and mechanical driving force are compared in the present work with the opposing forces. Knowledge of the mechanical driving force is employed to derive a metastable phase diagram for Ti-6Al-4V undergoing deformation.

Table 4.1 Effect of deformation on the beta phase fraction during isothermal deformation at a strain rate of 0.01 s^{-1} to a strain of 2.0 [11].

		880°C	940°C	960°C	980°C	1000°C
Beta phase fraction / %	Before deformation	22	57	65	81	88
	After deformation	34	67	77	90	94

4.2.1 Energy Barriers of dynamic transformation

The opposing forces for dynamic transformation comprise those which are chemical in nature, the shear work, and the dilation work associated with the phase transformation. Deformation increases the beta phase fraction, resulting in an increase in the Gibbs energy. This increase can be quantified by the following expression based on solution thermodynamics [12]:

$$\Delta G_{\beta\to\alpha} = -\frac{(C_\beta - C_\alpha)RTln\left[(1-C_\beta)/(1-C_m)\right]}{C_\beta\left[1+\partial lnv/\partial lnC_\beta\right]} \qquad (4-1)$$

Here C_β and C_α denote the equilibrium vanadium concentrations in the beta and alpha phases (vanadium is the rate-limiting solute in the beta matrix), respectively, C_m represents the vanadium concentration of the matrix beta (determined from mass conservation), v is the activity coefficient of the vanadium in the beta, and the term $(1+\partial lnv/\partial lnC_\beta)$ is the thermodynamic factor (TF), evaluated by a linear fit to the values determined previously [13]. The coefficients C_β and C_α were derived from the measurements by Semiatin et al. [14], and C_m was then obtained from Eq. (4-2) below [14]:

$$C_m = (C_0 - f_\alpha C_\alpha)/(1-f_\alpha) \qquad (4-2)$$

Here C_0 and f_α represent the overall vanadium composition and the alpha phase fraction, respectively. The vanadium concentration in the alpha phase (C_α) is considered to be only weakly dependent on temperature and to remain unchanged when dynamic transformation takes place [14]. The Gibbs energy changes (*ΔG*) during dynamic transformation and some related parameters are listed in Table 4.2. It can be seen that dynamic transformation gives rise to an increase in *ΔG*, the value of which increases with decreasing temperature.

Table 4.2 Thermodynamic parameters and Gibbs free energy changes at various temperatures.

Temperature (°C)	C_β (wt. %)	C_α (wt. %)	C_m (wt. %)	TF	ΔG (J/mol)
880	8.4	2.3	6.3	0.87	185.90
940	5.2	2.1	4.7	0.90	32.53
960	4.8	2.0	4.4	0.91	30.05
980	4.2	1.9	4.0	0.91	15.02
1000	4.0	1.8	3.9	0.92	9.22

It is assumed here that dynamic transformation in Ti-6Al-4V occurs via displacive nucleation and diffusion-assisted growth, as in the case of steel. The formation of beta from alpha involves shear of the parent lattice by a (shear) strain of 0.14 [15]. The work associated with shear accommodation can thus be written as [2]:

$$W_{shear\ accommodation} = m * \sigma_{critical-\alpha} * \varepsilon_{shear} \qquad (4-3)$$

Here ε_{shear} is the shear strain associated with the transformation and m is the Schmid factor, which takes into account the difference in orientation between the directions of $\sigma_{critical\text{-}\alpha}$ and that of the resolved stress that produces the transformation shear. In the present study, the Schmid factor is taken as 0.5 on the assumption that the active habit plane is the one subject to the maximum resolved shear stress [2, 4].

During phase transformation, dilatation also occurs and its direction is perpendicular to the habit plane [2]. The dilatation work in the present case can be expressed as [2]:

$$W_{dilatation} = \lambda * \sigma_{critical-\alpha} * \varepsilon_{dilatation} \qquad (4-4)$$

where λ is an orientation factor that takes into account the difference between the direction of the applied stress and that of the transformation habit plane normal and $\varepsilon_{dilatation}$ refers to the dilatation strain, which has been reported to be 1.7% [16]. The mechanical work calculated this way is then converted into J mol^{-1} using the conversion factors 1 MPa = 1 MJ m^{-3} = 10.6 J mol^{-1}.

In Fig. 4.1, the total opposing forces inhibiting dynamic transformation is shown to consist of three obstacles as discussed above. Each of these decreases with increasing temperature; the Gibbs energy is the predominant barrier while the dilatation work accounts for the smallest portion.

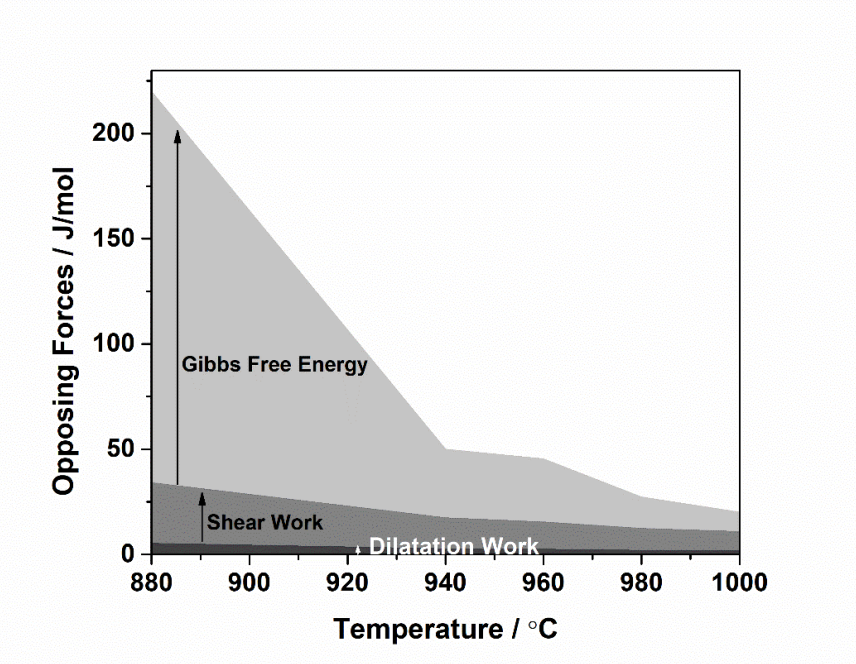

Fig. 4.1 Dependence of the opposing forces on temperature.

4.2.2 Driving forces of dynamic transformation

Some researchers have proposed that the driving force for dynamic transformation is the stored energy of deformation [17-19]. However, the calculations below reveal that this does not apply for Ti-6Al-4V.

The stored energy per unit volume associated with the dislocations introduced by deformation is given by [20]:

$$\Delta G_{Dislocation} = \mu\, b^2\, (\rho - \rho_0)/2 \qquad (4-5)$$

Here b denotes the Burgers vector (2.95×10^{-10} m) and μ refers to the shear modulus which is assumed to be same for both the alpha and beta phases, whose temperature dependence is given by: $\mu = 49.02\text{-}5.821/(\exp(181/T)\text{-}1)$ GPa [20], ρ_0 is the initial dislocation density (10^{12} m^{-2}) [27], ρ refers to the dislocation density per unit volume resulting from deformation and can be estimated from [21]:

$$\rho = \left(\frac{\sigma - \sigma_y}{M\alpha\mu b}\right)^2 \qquad (4-6)$$

Here σ and σ_y denote the flow stress and yield stress, M represents the Taylor factor (approximately 3.1) and α is a constant equal to 0.15 for Ti-6Al-4V [21]. Furthermore, the flow softening caused by dynamic transformation, the morphological evolution of the phases (from an initial equiaxed to a globularized microstructure) as well as the texture changes are not considered. In any event, these factors do not affect the order of magnitude of the stored energy, which is primarily discussed and compared here.

Note that deformation heating can in principle contribute to flow softening as given by $\Delta T=0.95\eta/\rho C_p \int \sigma d\varepsilon$, where ΔT refers to the temperature increase, η is the adiabatic correction factor (0.25), σ and ε are the stress and strain, respectively, ρ is the density of Ti-6Al-4V, and C_p is the specific heat [22]. However, the temperature increase associated with adiabatic heating in the present work is only around 7.5°C and is essentially negligible since it is readily dissipated at the elevated temperature (940°C) employed. Furthermore, it is assumed here for simplicity that the stored energy per unit volume is the same in the two phases. Here the stored energy was calculated by estimating the energies associated with the increases in the grain boundary specific area, the vacancy concentrations and the dislocation density.

The increase in grain boundary stored energy can be evaluated from [23]:

$$\Delta G_{Grain\ boundary} = \left[\left(S_v^{gb} + S_v^{db}\right) - S_v^0\right]\varphi \qquad (4-7)$$

where S_v^{gb} and S_v^{db} are the increases in surface area per unit volume associated with the grain boundaries and deformation bands, respectively. These are taken here as $S_v^{gb} = S_v^0/[2(1 + 1/e^{\varepsilon} + e^{\varepsilon})]$ and $S_v^{db} = 63(\varepsilon - 0.3)$ [23]. Here the initial value of the former is taken to be S_v^0 ($\approx 2/d_{grain}$) which denotes the surface area per unit volume in recrystallization [23], φ represents the grain boundary energy per unit area (0.26 J m^{-2}) in Ti-6Al-4V [24]. It is assumed here that the energy density is the same on alpha-alpha, beta-beta and alpha-beta boundaries.

Deformation also contributes to the formation of excess vacancies leading to the stored energy [23]:

$$\Delta G_{Excess\ vacancy} = C_v Q_f = \left[\left(\frac{\chi\sigma}{Q_f} + \frac{\zeta C_j}{4b^3}\right)\left(\frac{\rho}{\kappa^2} + \frac{1}{L^2}\right)^{-1}\frac{\Omega_0}{D_v}\dot{\varepsilon}\right]Q_f \qquad (4-8)$$

Here C_v denotes the excess vacancy concentration, Q_f represents the vacancy formation energy ($1.9 \cdot 10^{-19}$ J) [25], χ denotes the mechanical production term (≈ 0.1) [26], ζ represents the neutralization effect based on vacancy emitting and absorbing jogs (0.5) [26], C_j is the concentration of jogs expressed by $C_j = exp(-E_j/kT)$ and E_j is given by $E_j = \mu b^3/(4\pi(1-\nu))$ where ν represents Poisson' s ratio (0.342) [27] and κ is a structural parameter equal to 10 in this case [26], L is the grain size of the alpha phase (10 µm), Ω_0 is the atomic volume ($1.76 \cdot 10^{-29}$ m^3) [28], D_v is the vacancy diffusivity expressed by $D_v = D_{v0}\, exp(-Q_m/kT)$, where D_{v0} is $3.3 \cdot 10^{-5}$ $m^2\, s^{-1}$ and Q_m is the vacancy migration energy ($2.49 \cdot 10^{-19}$ J) [23, 28], k is Boltzmann's constant ($1.38 \cdot 10^{-23}$ J K^{-1}), and $\dot{\varepsilon}$ refers to the strain rate.

The stored energies obtained from Eq. (4-5) - (4-8) are compared in Fig. 4.2 for T = 880 °C. The energy stored in dislocations is greater than that associated with grain boundaries and excess vacancies. The excess vacancy energy is approximately unchanged with strain and negligible in the present conditions, because the excess vacancies can be annihilated due to the enhanced vacancy diffusion at elevated temperatures. Fig. 4.3 shows that the total stored energy increases with the decreasing temperature, inasmuch as the dislocation energy (the predominant source of stored energy) is higher at lower temperatures as a result of the higher dislocation density [26, 29].

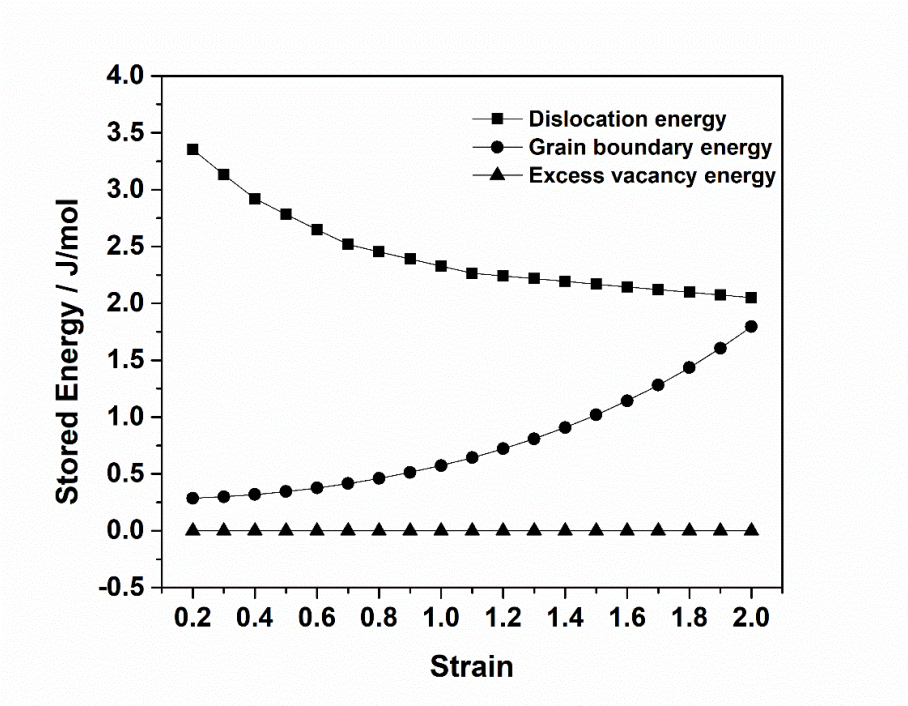

Fig. 4.2 Comparison of the stored energies associated with dislocations, grain boundaries and excess vacancies at 880 °C.

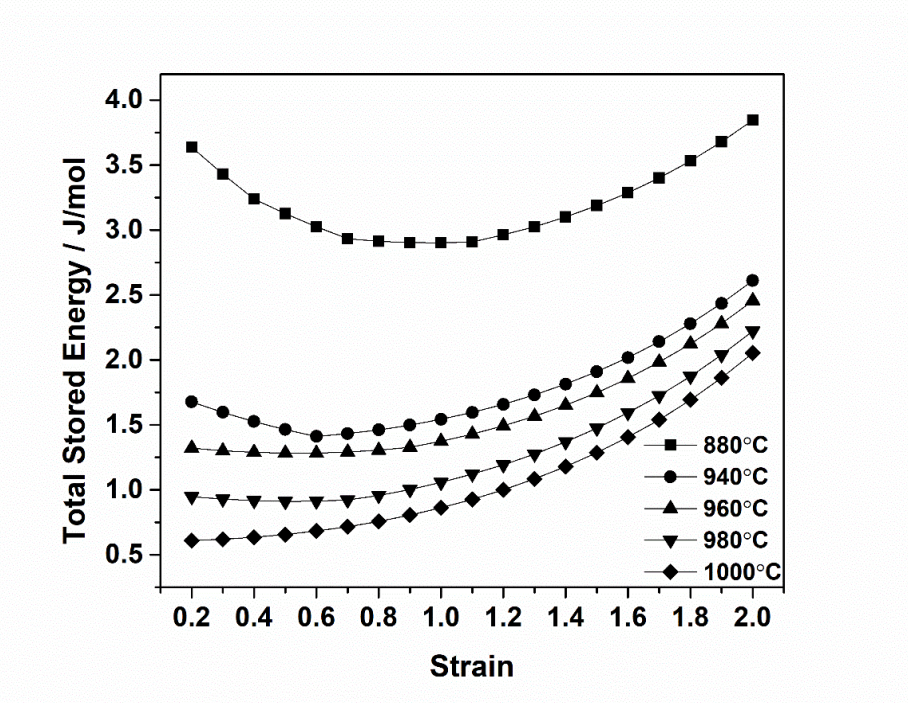

Fig. 4.3 Dependence of the total stored energy on strain at different temperatures.

The mechanical work of deformation is expressed by the integral of the stress with respect to strain, *i.e*. the area under the stress-strain curve, as shown below:

$$Mechanical\ Work = \int_0^{\varepsilon} \sigma\, d\varepsilon \qquad (4-9)$$

Here σ represents the flow stress and ε denotes the final strain (2.0 in this case). As shown in Fig. 4.4, the mechanical work is comprised of three parts. The first is the stored energy in the form of the defects introduced by deformation, as discussed in Eq. (4-5) - (4-8); the second is the energy consumed by the dynamic transformation softening (discussed below), which is largely responsible for overcoming the opposing forces (Gibbs energy, shear accommodation, and dilatation work) which have been analyzed in Eq. (4-1) - (4-4). The dynamic transformation softening accounts for 4-18% of the mechanical work; and the third and predominate portion is associated with heat dissipation.

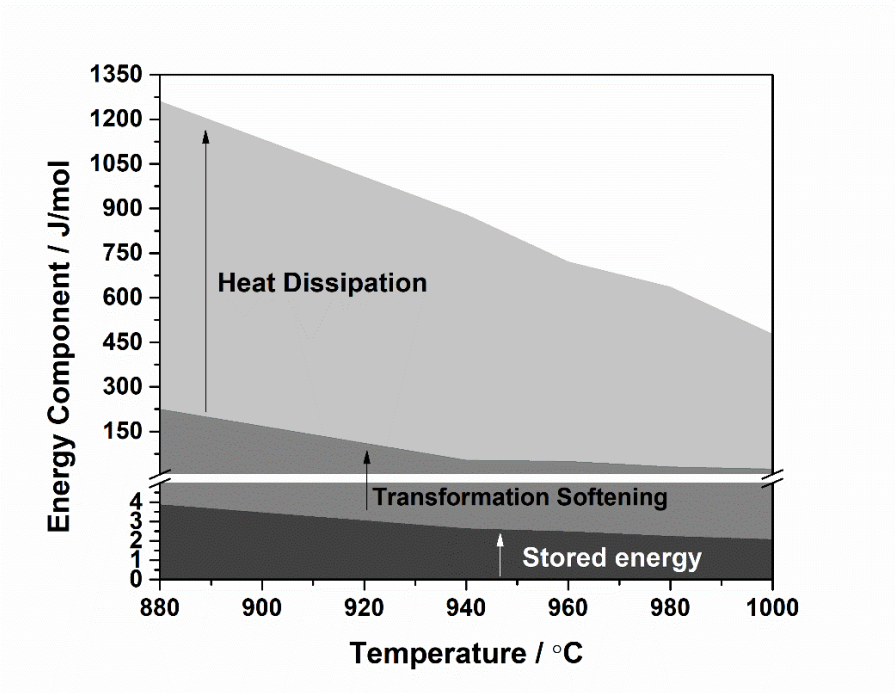

Fig. 4.4 Dependence of the components of the mechanical work on temperature.

Dynamic transformation has been reported to take place displacively and to be driven by the resolved shear stress on the habit plane [2, 3]. The driving force for dynamic transformation is

taken as the net softening associated with the transformation, which is defined as the difference beween the flow stress of the alpha at the critical strain and the yield stress of the fresh beta that takes its place. This can be expressed by [3]:

$$Net\ softening = \sigma_{critical-alpha} - \sigma_{yield-beta} \qquad (4-10)$$

Here $\sigma_{\mathrm{critical-alpha}}$ is the critical stress that initiates the dynamic transformation in the alpha phase, and $\sigma_{\mathrm{yield-beta}}$ is the yield stress of the beta phase. As the $\sigma_{\mathrm{critical-alpha}}$ is difficult to determine, here we employ the alpha peak stress instead. The values of $\sigma_{\mathrm{yield-beta}}$ in the two-phase region were estimated using the hardness ratio and the Law of Mixtures, where it was assumed that the beta phase yields when the overall stress-strain curve reaches the yield stress and that the hardness ratio provides a reasonable approximation of the alpha/beta flow stress ratio at that temperature [30, 31]. Here the alpha peak stress was derived using the Law of Mixtures along with the phase fractions of the two phases when the flow stress reached its peak value.

The mechanical driving force in Eq. (4-10), the total opposing force in Fig. 4.1 and the stored energy in Fig. 4.3 are plotted against temperature in Fig. 4.5. Here it can be seen that the stored energy is much lower than the opposing force and is thus inadequate to activate dynamic transformation. However, the mechanical driving force associated with dynamic transformation is much *higher* than the opposing force, making it thermodynamically possible for the transformation to occur.

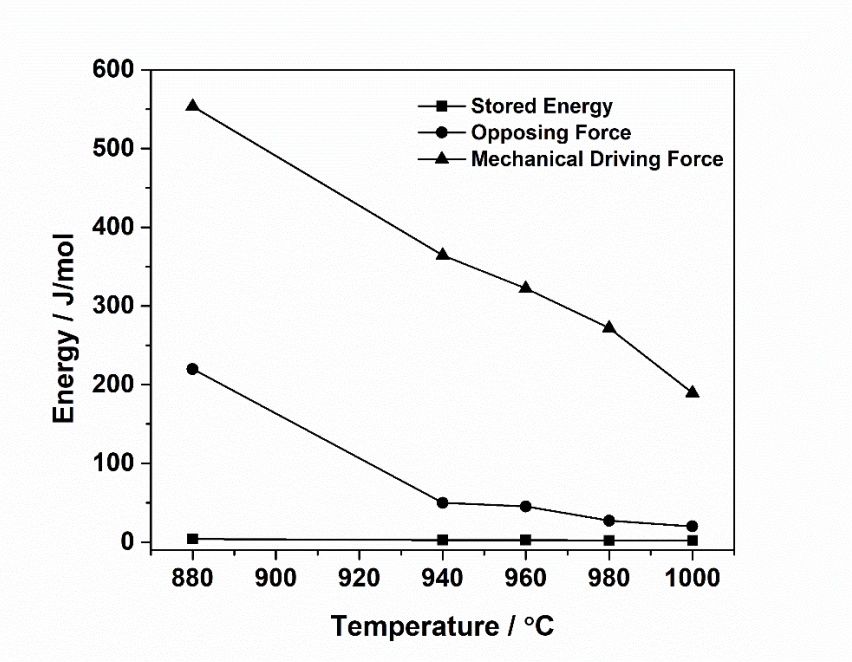

Fig. 4.5 Comparison of the stored energy, opposing forces and mechanical driving force for dynamic transformation at various temperatures.

4.2.3 Metastable phase diagram of dynamic transformation

The above mechanical driving force imposed on the alpha phase decreases its thermodynamic stability and leads to the formation of metastable beta [32]. The change in vanadium concentration in the beta phase is evaluated by comparing C_β and C_m during transformation (C_β and C_m refer to the vanadium contents in the beta prior to and after the transformation, respectively). The titanium-vanadium pseudo-binary phase diagram with a fixed content of aluminum (6%) is shown in Fig. 4.6. The solid lines refer to the equilibrium state without deformation and the dotted lines the metastable state after deformation. The corresponding beta phase fractions are also identified at each temperature. It can be seen that deformation reduces the transus temperatures by amounts that decrease with increasing temperature.

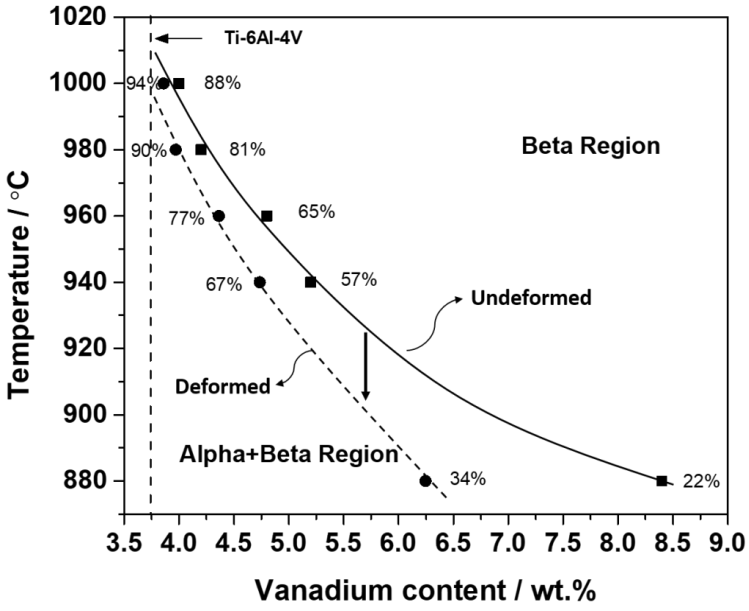

Fig. 4.6 Titanium-vanadium pseudo-binary phase diagram for Ti-6Al-X% V. The solid line is the boundary between the single-phase beta region and the alpha+beta region, while the broken line denotes the boundary in the metastable case. The beta phase fractions in both the undeformed and deformed conditions are provided in the figure, as indicated by the solid squares and circles, respectively.

4.3 Conclusions

Based on the thermodynamic calculations, the present work can be summarized as:

Dislocations are the main source of stored energy; the excess-vacancy energy is negligible for Ti-6Al-4V. The stored energy is lower than the opposing force inhibiting dynamic transformation. By contrast, the driving force derived from the net softening associated with dynamic transformation is much higher than the opposing force and acts as the source of for initiating the transformation. Dynamic transformation consumes 4-18% of the mechanical deformation work, the rest of which is distributed between heatings and stored energy. Hot deformation can reduce the transus temperature and produce a metastable state.

References

[1] Y. Matsumura, H. Yada, Evolution of ultrafine-grained ferrite in hot successive deformation, Transactions of the Iron and Steel Institute of Japan 27(6) (1987) 492-498.

[2] C. Ghosh, V.V. Basabe, J.J. Jonas, Y.-M. Kim, I.-H. Jung, S. Yue, The dynamic transformation of deformed austenite at temperatures above the Ae_3, Acta Materialia 61(7) (2013) 2348-2362.

[3] C. Ghosh, C. Aranas, J.J. Jonas, Dynamic transformation of deformed austenite at temperatures above the Ae_3, Progress in Materials Science 82 (2016) 151-233.

[4] C. Aranas, J.J. Jonas, Effect of Mn and Si on the dynamic transformation of austenite above the Ae_3 temperature, Acta Materialia 82 (2015) 1-10.

[5] J. Koike, Y. Shimoyama, I. Ohnuma, T. Okamura, R. Kainuma, K. Ishida, K. Maruyama, Stress-induced phase transformation during superplastic deformation in two-phase Ti–Al–Fe alloy, Acta Materialia 48(9) (2000) 2059-2069.

[6] H. Yang, G. Gurewitz, A. Mukherjee, Mechanical Behavior and Microstructural Evolution during Superplastic Deformation of Ti–6Al–4V, Materials Transactions, JIM 32(5) (1991) 465-472.

[7] B. Hidalgo-Prada, J. Mukhopadhyay, A.K. Mukherjee, Correlation of Mechanical Behavior with Microstructural Aspects of Ni Modified Superplastic Ti–6Al–4V Alloy, Materials Transactions, JIM 31(8) (1990) 689-696.

[8] H. Matsumoto, K. Yoshida, S.-H. Lee, Y. Ono, A. Chiba, Ti–6Al–4V alloy with an ultrafine-grained microstructure exhibiting low-temperature–high-strain-rate superplasticity, Materials Letters 98 (2013) 209-212.

[9] T. Zhang, Y. Liu, D.G. Sanders, B. Liu, W. Zhang, C. Zhou, Development of fine-grain size titanium 6Al–4V alloy sheet material for low temperature superplastic forming, Materials Science and Engineering: A 608 (2014) 265-272.

[10] C. Lu, L. Huang, L. Geng, B. Kaveendran, Z. Zheng, J. Zhang, Mechanisms behind the superplastic behavior of as-extruded TiBw/Ti6Al4V composites with a network architecture, Materials Characterization 104 (2015) 139-148.

[11] B. Guo, S.L. Semiatin, J.J. Jonas, S. Yue, Dynamic transformation of Ti–6Al–4V during torsion in the two-phase region, Journal of Materials Science 53 (2018) 9305-9315.

[12] R. Doherty, Diffusive phase transformations in the solid state, Physical Metallurgy 2 (1996) 1456-1458.

[13] S.L. Semiatin, T. Brown, T. Goff, P. Fagin, R. Turner, J. Murry, D. Barker, J. Miller, F. Zhang, Diffusion coefficients for modeling the heat treatment of Ti-6Al-4V, Metallurgical and Materials Transactions A 35(9) (2004) 3015-3018.

[14] S. Semiatin, S. Knisley, P. Fagin, D. Barker, F. Zhang, Microstructure evolution during alpha-beta heat treatment of Ti-6Al-4V, Metallurgical and Materials Transactions A 34(10) (2003) 2377-2386.

[15] Y. Ohmori, K. Nakai, H. Ohtsubo, M. Tsunofuri, Formation of Widmanstätten Alpha Structure in a Ti–6Al–4V Alloy, Materials Transactions, JIM 35(4) (1994) 238-246.

[16] G.A. Sargent, K.T. Kinsel, A.L. Pilchak, A.A. Salem, S.L. Semiatin, Variant Selection During Cooling after Beta Annealing of Ti-6Al-4V Ingot Material, Metallurgical and Materials Transactions A 43(10) (2012) 3570-3585.

[17] N. Xiao, M. Tong, Y. Lan, D. Li, Y. Li, Coupled simulation of the influence of austenite deformation on the subsequent isothermal austenite–ferrite transformation, Acta Materialia 54(5) (2006) 1265-1278.

[18] C. Ghosh, V.V. Basabe, J.J. Jonas, Thermodynamics of dynamic transformation of hot deformed austenite in four steels of increasing carbon contents, Materials Science and Engineering: A 591 (2014) 173-182.

[19] D.N. Hanlon, J. Sietsma, S. van der ZWAAG, The effect of plastic deformation of austenite on the kinetics of subsequent ferrite formation, ISIJ International 41(9) (2001) 1028-1036.

[20] X. Fan, H. Yang, Internal-state-variable based self-consistent constitutive modeling for hot working of two-phase titanium alloys coupling microstructure evolution, International Journal of Plasticity 27(11) (2011) 1833-1852.

[21] T. Seshacharyulu, B. Dutta, Influence of prior deformation rate on the mechanism of $\beta \rightarrow \alpha + \beta$ transformation in Ti–6Al–4V, Scripta Materialia 46(9) (2002) 673-678.

[22] R. Goetz, S. Semiatin, The adiabatic correction factor for deformation heating during the uniaxial compression test, Journal of Materials Engineering and Performance 10(6) (2001) 710-717.

[23] C. Ghosh, V.V. Basabe, J.J. Jonas, Y.-M. Kim, I.-H. Jung, S. Yue, The dynamic transformation of deformed austenite at temperatures above the Ae_3, Acta Materialia 61(7) (2013) 2348-2362.

[24] S. Zherebtsov, M. Murzinova, G. Salishchev, S. Semiatin, Spheroidization of the lamellar microstructure in Ti–6Al–4V alloy during warm deformation and annealing, Acta Materialia 59(10) (2011) 4138-4150.

[25] I. Novikov, V. Roshchupkin, N. Semashko, L. Fordeeva, Experimental investigation of vacancy effects in pure metals, Journal of Engineering Physics 39(6) (1980) 1316-1319.

[26] M. Militzer, W. Sun, J. Jonas, Modelling the effect of deformation-induced vacancies on segregation and precipitation, Acta Metallurgica et Materialia 42(1) (1994) 133-141.

[27] B. Babu, L.-E. Lindgren, Dislocation density based model for plastic deformation and globularization of Ti-6Al-4V, International Journal of Plasticity 50 (2013) 94-108.

[28] H.J. Frost, M.F. Ashby, Deformation mechanism maps: the plasticity and creep of metals and ceramics, Pergamon press1982.

[29] H. Mecking, Y. Estrin, The effect of vacancy generation on plastic deformation, Scripta Metallurgica 14(7) (1980) 815-819.

[30] O. Senkov, J. Jonas, Effect of phase composition and hydrogen level on the deformation behavior of titanium-hydrogen alloys, Metallurgical and Materials Transactions A 27(7) (1996) 1869-1876.

[31] H.J. Rack, J. Qazi, L. Allard, R. Valiev, Thermal Stability of Severe Plastically Deformed VT-6 (Ti-6Al-4V), Materials Science Forum, Trans Tech Publ, 2008, pp. 893-898.

[32] B. Guo, C. Aranas, B. Sun, X. Ji, J.J. Jonas, Reverse Transformation Behavior of Ti-6Al-4V After Deformation in the Two-Phase Region, Metallurgical and Materials Transactions A 49(1) (2018) 22-27.

Chapter 5

Reverse Transformation Behavior of Ti-6Al-4V after Deformation in the Two-Phase Region

In this chapter, the reverse transformation was studied using compression tests and characterized by metallographic images. Various holding times were employed after the isothermal compression at different temperatures. The kinetics of the transformation were described by the Time-Temperature-Reverse Transformation (TTRT) curves. The relations between time, temperature and transformation were elucidated.

- This chapter has been published: **Baoqi Guo** *, Clodualdo Aranas Jr., Binhan Sun, Xiankun Ji, John J. Jonas. Reverse Transformation Behavior of Ti-6Al-4V After Deformation in the Two-Phase Region. Metallurgical and Materials Transactions A, 2018, 49(1): 22-27.

Abstract

Isothermal holding experiments were performed on a Ti-6Al-4V alloy after compression in the two-phase region. The forward transformation took place during compression while the reverse transformation was diffusion controlled when the samples were held after unloading at 940°C, 970°C and 1000°C. Time-temperature-reverse transformation (TTRT) curves are derived, which indicate that the rate of reverse transformation is independent of temperature when the holding time is 18s. By contrast, it depends on temperature when the holding time is increased to 180 s and 1800s.

5.1 Introduction

Dynamic transformation was first reported to take place in steel by Yada and co-workers [1]. This phenomenon (i.e. the conversion of alpha into beta) was later observed in titanium alloys [2-7]. For example, an increase in volume fraction of the beta phase during the deformation of Ti-5.5Al-1.5Fe in the two-phase region was described by Koike et al. in 2000 [2] and similar observations of phase transformations have also been published by Yang et al. [3], Zhang et al. [4], Matsumoto et al. [5], Prada et al. [6] and Jonas et al. [7].

The reverse transformation (i.e. beta to alpha) during isothermal holding after hot compression was also described by Koike [2]. This phenomenon has been shown to take place in steel as well and to be diffusion controlled [8, 9]. However, only limited data regarding this phenomenon are available on titanium alloys. The present tests were conducted to fill this gap. In this work, the dependence of phase fraction on holding time after deformation was determined, which enabled the construction of a time–temperature–reverse transformation (TTRT) diagram. The letter describes the microstructural evolution after deformation in Ti-6Al-4V.

5.2 Experiment

The material for the experiments was Ti-6Al-4V with a composition (in weight percent) of 6.53 aluminum, 4.10 vanadium, 0.17 iron, 0.17 oxygen, 0.03 carbon, 0.03 nitrogen, the balance being titanium. Its (alpha + beta) to beta transus temperature is 1015°C according to measurements by differential thermal analysis (DTA). The as-received material was characterized by an equiaxed microstructure and was machined into compression cylinders with heights of 9.6mm and diameters of 6.4mm. Hot compression tests were performed on a 100 kN MTS servohydraulic compression machine equipped with a radiation furnace. As shown in Fig. 5.1, the samples were heated at 2°C/s to the compression temperature and then held for 900 s prior to deformation. A suspension of boron nitride in ethanol was applied to the top and bottom surfaces of the samples for lubrication purposes. An argon protective atmosphere was used to minimize oxidation during compression. Strains of 0.9 were applied at a strain rate of 0.01 s^{-1}. After deformation, the samples were held at temperature to permit reverse transformation of the metastable beta into the thermodynamically stable alpha. The deformation temperatures were 940, 970, and 1000 °C

and the holding times were 0, 18, 180, and 1800s respectively. They were water quenched after holding. Samples were cut along the longitudinal direction and prepared for examination using standard metallographic techniques. The optical microstructures were taken using a magnification of 500 times, at which enough alpha particles can be imaged. The phase fractions were determined based on average values via the ImageJ software.

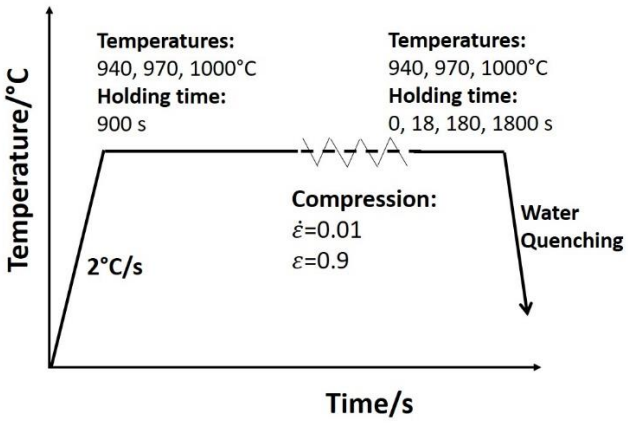

Fig. 5.1 Schematic of thermomechanical deformation and isothermal holding after unloading.

5.3 Results and Discussions

The stress levels of the curves increase with decreasing temperature in the usual way, see Fig. 2. However, marked flow softening is evident in the three curves associated with temperatures below the transus, i.e. those of 940°C, 970°C and 1000°C. Such softening can be attributed to dynamic transformation [7].

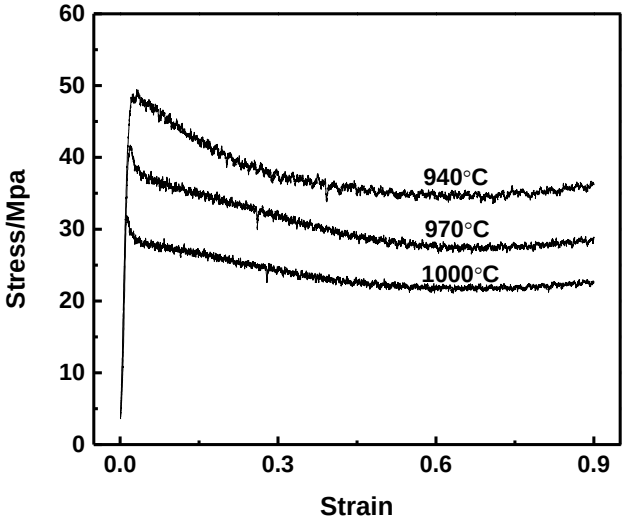

Fig. 5.2 True stress-strain curves at a strain rate of 0.01 s^{-1} at three temperatures.

Some microstructures associated with various testing conditions are shown in Fig. 5.3. The alpha phase appears white and the beta phase is dark. The microstructure prior to deformation is displayed in Fig. 5.3(a). Fig. 5.3(b), Fig. 5.3(c), Fig. 5.3(d), Fig. 5.3(e) correspond to the microstructures observed after deformation and holding for 0s, 18s, 180s, and 1800s, respectively. It can be seen that an increase in the beta phase fraction is produced by deformation, after which there is a gradual decrease with holding time after unloading.

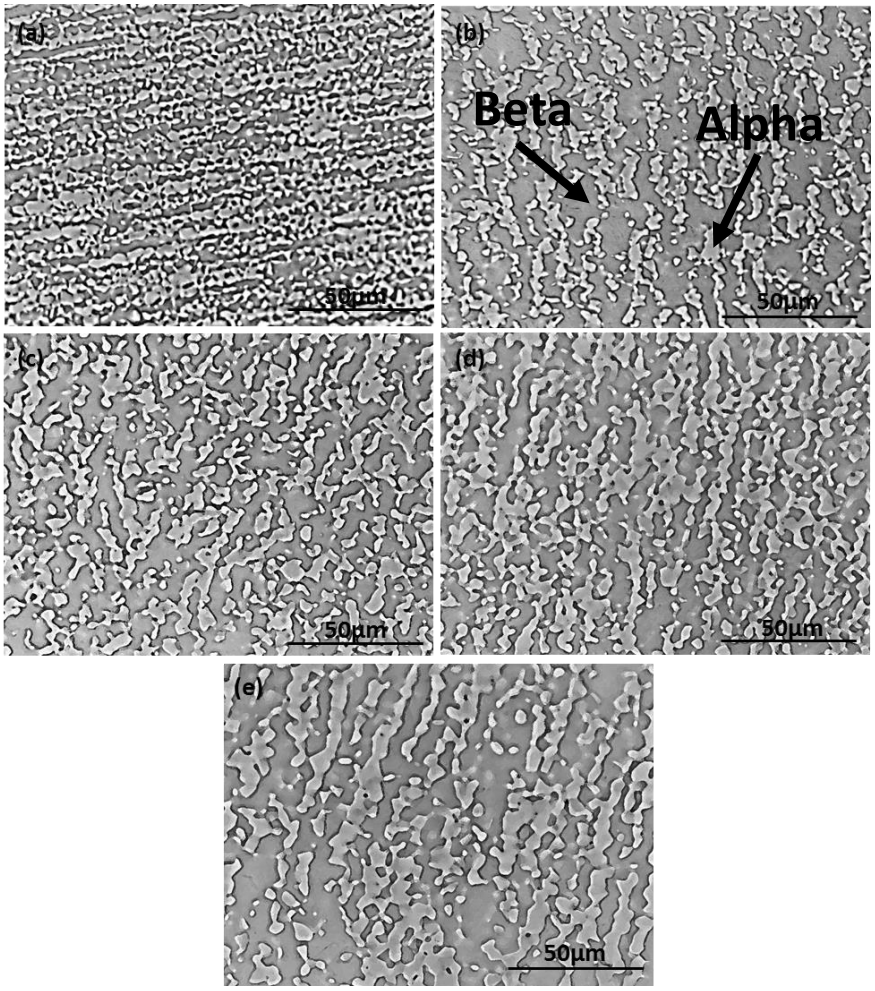

Fig. 5.3 Microstructures at 940°C (a) undeformed; (b), (c), (d) and (e): after deformation with holding times of 0s, 18s, 180s, 1800s, respectively.

The microstructural evolution during holding at 970°C and 1000°C is depicted in Fig. 5.4 and Fig. 5.5. These trends are similar to those observed at 940°C. In addition, there is dynamic coarsening during deformation and static coarsening during isothermal holding after unloading. The latter has been studied by Semiatin et al., who showed that it is controlled by diffusion [10, 11].

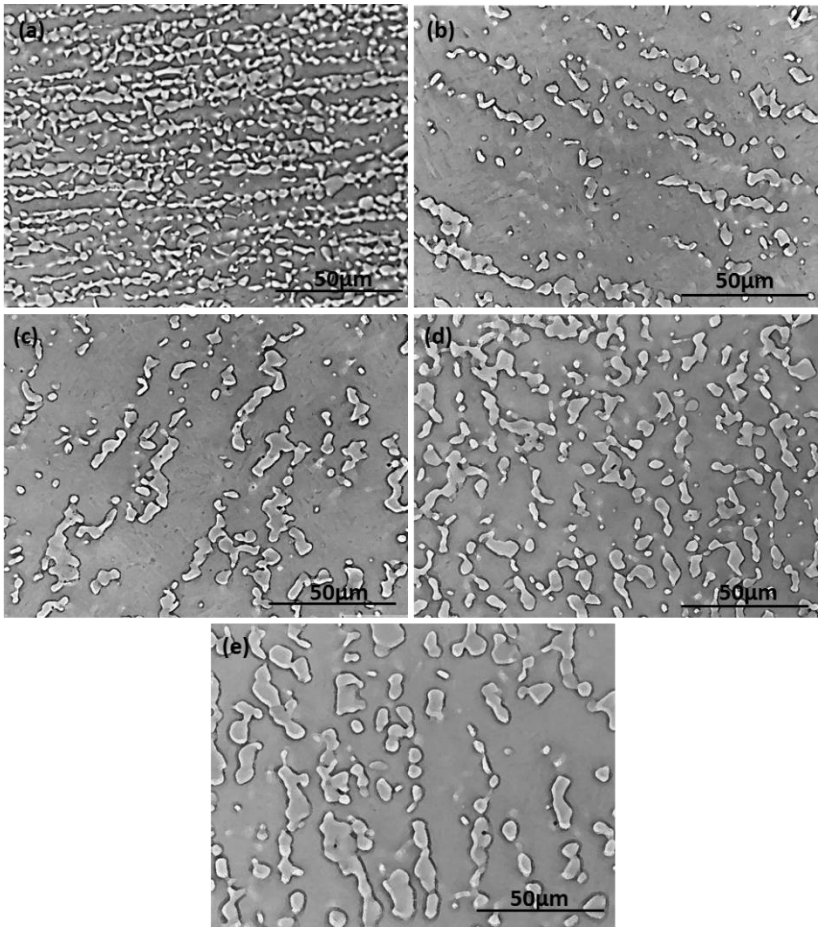

Fig. 5.4 Microstructures at 970°C (a) undeformed; (b), (c), (d) and (e): after deformation with holding times of 0s, 18s, 180s, 1800s, respectively.

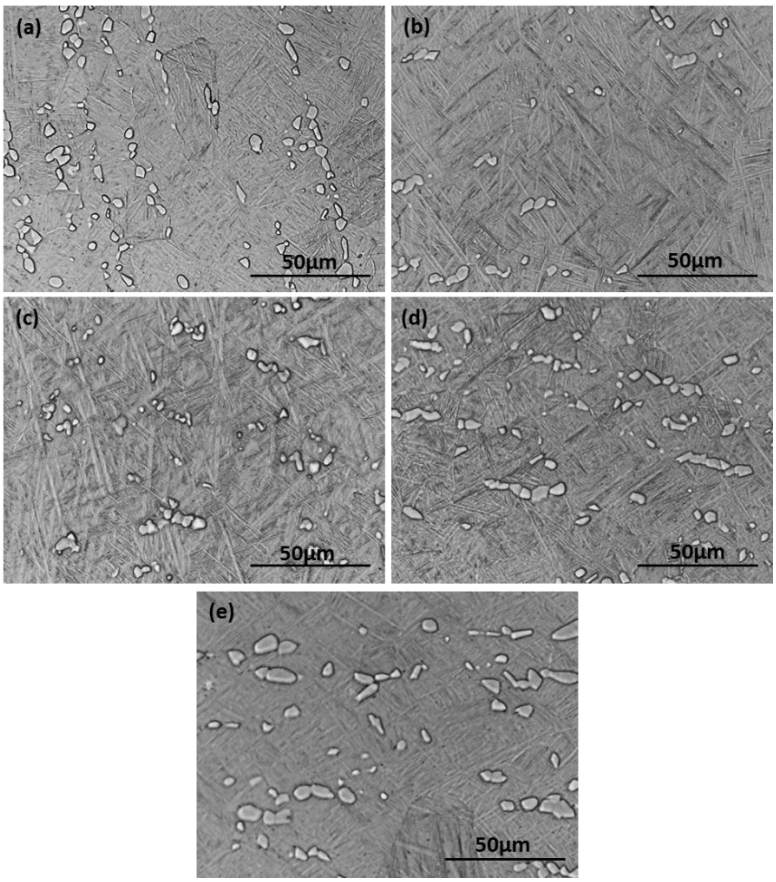

Fig. 5.5 Microstructures at 1000°C (a) undeformed; (b), (c), (d) and (e): after deformation with holding times of 0s, 18s, 180s, 1800s, respectively.

The beta phase fractions were measured and are plotted in Fig. 5.6. The beta phase fractions of the undeformed samples are the equilibrium values associated with long-time annealing of the Ti-6Al-4V. The beta phase fraction behavior is similar at the three temperatures and displays an initial increase (forward transformation). It subsequently decreases with holding time due to reverse transformation (from beta to alpha). For example, the initial beta phase fraction prior to deformation is 73.0% at 970°C. It increases to 91.0% immediately after deformation and then decreases to 86.4%, 79.8%, 78.0%, respectively, when the holding time after unloading is 18s, 180s and 1800s. The forward transformation takes 90s and generates an 18.0% increase in beta fraction. The reverse transformation after unloading decreases the beta fraction by 11.2% when the holding time is 180s. This implies that the forward transformation is considerably more rapid than the reverse.

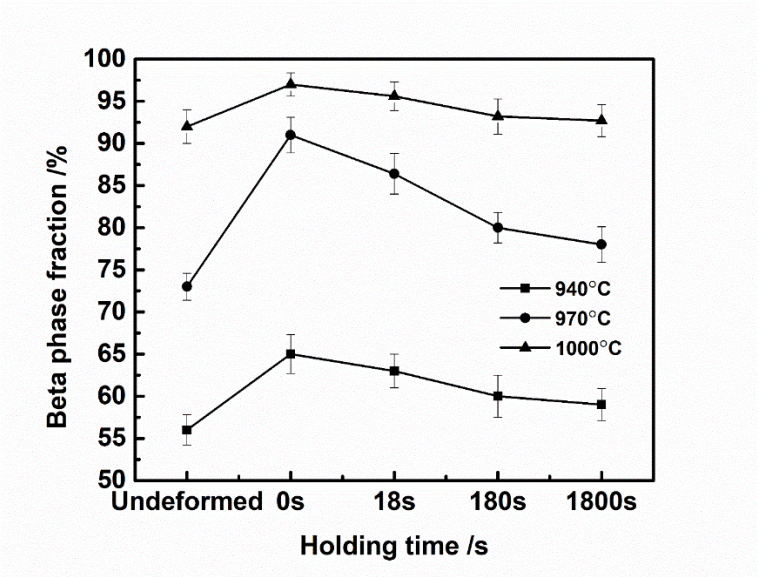

Fig. 5.6 Dependence of beta phase fraction on time at different temperatures.

The amount of reverse transformation can be specified by the relation:

$$\text{Reverse transformation}\% = \frac{\Delta\beta_{\text{reverse}}}{\Delta\beta_{\text{deformation}}}\% \qquad (5-1)$$

Here $\Delta\beta_{deformation}$ refers to the change in the beta fraction caused by the forward transformation during deformation; while $\Delta\beta_{reverse}$ is the change in the beta fraction caused by the reverse transformation during isothermal holding after unloading. The extent of reverse transformation is presented in the form of time-temperature-reverse transformation (TTRT) curves in Fig. 5.7. When the holding time after deformation is 18s, the rate of reverse transformation is similar at the different temperatures. Once the holding time was increased to 180s and 1800s, the reverse transformation rate varied significantly at the three temperatures. For example, the reverse transformation rate is 56% at 940 °C and increases to 76% at 1000°C when the holding times at the two temperatures both increase to 180s. This shows that temperature has a greater effect on the rate after long holding times than during the initial stages of holding.

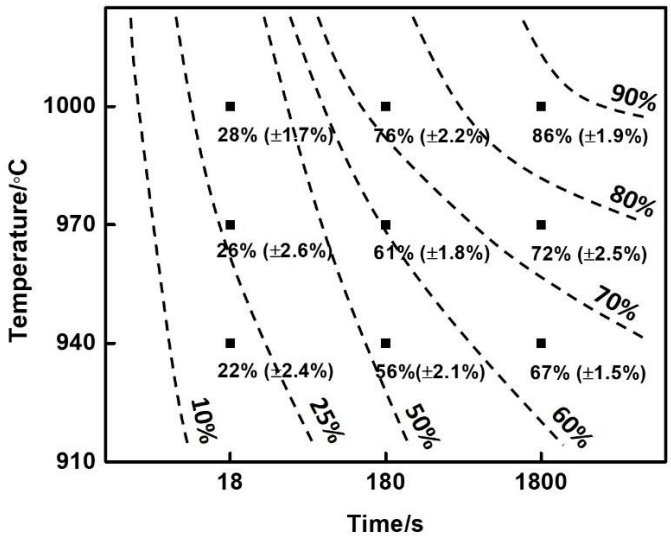

Fig. 5.7 Time-temperature-reverse transformation (TTRT) curves associated with the reverse transformation.

When the holding time was increased from 18s to 180s, the rate of reverse transformation increased by 34% at 940 °C, 35% at 970 °C and 48% at 1000 °C, see Fig. 5.7. However, it only increased by 11% at 940 °C, 11% at 970 °C and 10% at 1000 °C once the holding time was further increased from 180s to 1800s. This shows that the reverse transformation is rapid during the initial stages of holding and becomes sluggish after longer holding times. The stored work such as dislocations and subgrains in the beta matrix immediately after hot deformation is eliminated quickly during reverse transformation, which leads to more sluggish diffusion kinetics. This causes the decrease in the rate of reverse transformation after a certain time.

The driving force for the forward transformation is the difference between the flow stress of the alpha at the critical strain and the yield stress of the fresh beta that takes its place [7, 12]. During reverse transformation, an extra amount of beta phase is produced during dynamic transformation and these are thermodynamically unstable at the same temperature and will transform back into the alpha phase during the subsequent isothermal holding. The driving force for this behavior is the Gibbs energy difference between the two phases. The dilatation work during the phase change also contributes to the energy barrier during forward transformation.

In a similar manner, the contraction work associated with the beta to alpha phase change, the absolute value of which is same as that of the dilatation, acts as an energy barrier to the reverse transformation. The shear work during transformation in titanium is negligible and is thus not considered here [13]. The Gibbs energy derived according to the method of enthalpy and transus temperature [14, 15] and the contraction work derived according to the dilatation work [12, 16] are listed in Table 5.1. It can be seen that the driving force, i.e. the Gibbs energy, is -252.8, -151.7, and -50.6 J/mol at 940°C, 970°C, and 1000°C, respectively, and is higher than the energy barrier, i.e. the contraction work, 7.8, 5.6, 3.6 J/mol at all three temperatures. This makes it thermodynamically possible for the reverse transformation to take place during isothermal holding.

Table 5.1 Driving forces and energy barriers for reverse transformation (from beta to alpha)

Temperature (°C)	940°C	970°C	1000°C
Driving force (J/mol)	-252.8	-151.7	-50.6
Energy barrier (J/mol)	7.8	5.6	3.6

5.4 Conclusions

The present results can be summarized as follows:

(1) The forward transformation takes place during compression testing and the reverse transformation during holding after unloading at 940°C, 970°C and 1000°C.

(2) The reverse transformation is diffusion controlled, the extent of which depends on holding time. The time-temperature-reverse transformation (TTRT) curves associated with the reverse transformation were derived, which indicate that the rates of reverse transformation are similar at different temperatures when the holding time is short (18s) but is dependent on temperature at longer holding times, i.e. 180s and 1800s.

(3) The driving force for reverse transformation is much higher than the work of accommodation at the present three temperatures, which makes it possible for the reverse transformation to occur.

References

[1] Y. Matsumura, H. Yada, Evolution of ultrafine-grained ferrite in hot successive deformation, Transactions of the Iron and Steel Institute of Japan 27(6) (1987) 492-498.

[2] J. Koike, Y. Shimoyama, I. Ohnuma, T. Okamura, R. Kainuma, K. Ishida, K. Maruyama, Stress-induced phase transformation during superplastic deformation in two-phase Ti–Al–Fe alloy, Acta Materialia 48(9) (2000) 2059-2069.

[3] H. Yang, G. Gurewitz, A. Mukherjee, Mechanical Behavior and Microstructural Evolution during Superplastic Deformation of Ti–6Al–4V, Materials Transactions, JIM 32(5) (1991) 465-472.

[4] T. Zhang, Y. Liu, D.G. Sanders, B. Liu, W. Zhang, C. Zhou, Development of fine-grain size titanium 6Al–4V alloy sheet material for low temperature superplastic forming, Materials Science and Engineering: A 608 (2014) 265-272.

[5] H. Matsumoto, K. Yoshida, S.-H. Lee, Y. Ono, A. Chiba, Ti–6Al–4V alloy with an ultrafine-grained microstructure exhibiting low-temperature–high-strain-rate superplasticity, Materials Letters 98 (2013) 209-212.

[6] B. Hidalgo-Prada, J. Mukhopadhyay, A.K. Mukherjee, Correlation of Mechanical Behavior with Microstructural Aspects of Ni Modified Superplastic Ti–6Al–4V Alloy, Materials Transactions, JIM 31(8) (1990) 689-696.

[7] J.J. Jonas, C. Aranas, A. Fall, M. Jahazi, Transformation softening in three titanium alloys, Materials & Design 113 (2016) 305-310.

[8] C. Aranas, S.F. Rodrigues, Y.J. Shen, Z. Zhang, J.J. Jonas, Time - Temperature - Reverse Transformation (TTRT) Behaviors of a C - Mn and a Nb Microalloyed Steel after Dynamic Transformation above the Ae_3, Steel Research International (2017).

[9] C. Ghosh, C. Aranas, J.J. Jonas, Dynamic transformation of deformed austenite at temperatures above the Ae_3, Progress in Materials Science 82 (2016) 151-233.

[10] S. Semiatin, B. Kirby, G. Salishchev, Coarsening behavior of an alpha-beta titanium alloy, Metallurgical and Materials Transactions A 35(9) (2004) 2809-2819.

[11] S. Semiatin, M. Corbett, P. Fagin, G. Salishchev, C. Lee, Dynamic-coarsening behavior of an α/β titanium alloy, Metallurgical and Materials Transactions A 37(4) (2006) 1125-1136.

[12] C. Aranas, J.J. Jonas, Effect of Mn and Si on the dynamic transformation of austenite above the Ae_3 temperature, Acta Materialia 82 (2015) 1-10.

[13] A.A. Kelly, K.M. Knowles, Crystallography and Crystal Defects, John Wiley & Sons2012.

[14] J. Henderson, H. Groot, Technical Report No. TPRL 1284, West Lafayette, IN: Thermophysical Properties Research Laboratory, Purdue University, 1993.

[15] S. Semiatin, F. Zhang, R. Larsen, L. Chapman, D. Furrer, Precipitation in powder-metallurgy, nickel-base superalloys: review of modeling approach and formulation of engineering methods to determine input data, Integrating Materials and Manufacturing Innovation 5(1) (2016) 3.

[16] C. Ghosh, V.V. Basabe, J.J. Jonas, Y.-M. Kim, I.-H. Jung, S. Yue, The dynamic transformation of deformed austenite at temperatures above the Ae_3, Acta Materialia 61(7) (2013) 2348-2362.

Chapter 6

Kinetics of Post-Dynamic Coarsening and Reverse Transformation in Ti-6Al-4V

In this chapter, kinetics of the reverse transformation was further studied using dilatometer equipped with compression tests. Both reverse transformation and post-dynamic coarsening were observed during the isothermal holding after compression. Their kinetics were studied through the dimension variation of the sample and particle evolution of the alpha phases, respectively.

- This chapter has been published: **Baoqi Guo** *, Ameth Fall, Mohammad Jahazi, John J. Jonas. Kinetics of post-dynamic coarsening and reverse transformation in Ti-6Al-4V. Metallurgical and Materials Transactions A, 2018, 49(12): 5956-5961.

Abstract

Experiments were carried out on the post-dynamic coarsening of alpha and reverse transformation of Ti-6Al-4V. The post-dynamic coarsening followed r^n vs time kinetics and the n=3 best fit indicated that it was controlled by bulk diffusion, i.e. by vanadium diffusion through the beta matrix. Its rate was one order of magnitude faster than that applicable to static coarsening. The reverse transformation was characterized using a compression dilatometer and occurred in two stages; the first was transformation on dislocations; the second involved the growth of the alpha structure.

6.1 Introduction

Static coarsening of alpha phase occurs during the annealing of undeformed Ti-6Al-4V while dynamic coarsening takes place during the deformation of this material. These observations have been reported in Refs. [1-5]. The kinetics of these mechanisms have been studied in some detail and it has been concluded that the behavior is bulk diffusion controlled. Post-dynamic coarsening takes place during isothermal holding after deformation, although its kinetics are largely unknown and are discussed here for the first time.

The reverse transformation (beta to alpha) also takes place in two-phase titanium alloys during isothermal holding after deformation [6-10]. For example, Koike et al. found that alpha was transformed dynamically into beta during the tensile testing of Ti-5.5Al-1Fe and then the beta transformed back into the alpha after the deformation [11]. The reverse transformation was quantified recently in Ti-6Al-4V using metallographic observations and its thermodynamics evaluated [12]. However, the kinetics of the reverse transformation in titanium alloys have not been examined in any detail. A novel dilatometer equipped with a compression module was employed in the present work to deal with this issue.

6.2 Experiment and results

The kinetics of the post-dynamic coarsening of alpha are first discussed here. The reverse transformation was investigated by the present authors by holding samples for increasing times after deformation and was characterized using metallographic methods [12]. Based on these results along with another two tests (holding time of 20min and 60min after compression to strains of 0.9 at strain rates of 0.01 s^{-1}), the alpha particle size was measured to study the post-dynamic coarsening. The microstructures were examined using backscattered electron imaging (BSEI) in a scanning electron microscope (SEM). In the BSEI micrograghs, the beta/transformed beta is bright and the alpha appears dark. The alpha particle radius was derived from the average alpha particle size (A_α) according to the circle equivalent area method. Here the average alpha particle size (A_α) was estimated using the equation $A_\alpha = f_\alpha A/N$, where A is the total area of the micrograph, N is the number of alpha particles and f_α denotes the volume fraction of the alpha phase. Particles with “dog-leg” morphologies were treated as being equivalent to 1.5 particles

[1]. Five BSEI photographs were taken in each condition to ensure that 300-600 alpha particles were sampled.

The microstructural evolution during post-dynamic coarsening is displayed in Fig. 6.1. Here the coarsening behavior of the alpha particles and the increase in its phase fraction with holding time are evident. The volume fraction of alpha and the number of alpha particles per unit area (mm^2) have been plotted as a function of time in Fig. 6.2. The number of alpha particle per unit first increased in the initial stage and then decreased with time. For example, it increased from 80 to 110 per unit area when the time increased from 0s to 18s, which was indicative of the occurrence of nucleation at short times. In the second stage, the decreasing number of alpha particle and increasing alpha radius showed that the growth of alpha phase was the predominant behavior. This is consistent with the finding by Xiao and Haasen [13] about the concurrent precipitation and coarsening of gamma prime in nickel-base superalloys. They observed that the process consisted of two stages, i.e. nucleation and Ostwald-ripening. The former involved an increase in volume density and the latter a decrease in volume density as well as increase in particle radius. The average alpha particle radius *r* depends on time as described by the relation $r^n - r_0^n$. As shown in Fig. 6.3, the curvature changes from concave downward to concave upward with increasing values of n at the two temperatures. The best linear fit is attained when n equals 3 at both 940 °C and 970°C. The slopes in Figs. 6.3(e) and (f) represent the coarsening rate and increase from 65.5 $\mu m^3/h$ at 940 °C to 98.6 $\mu m^3/h$ at 970 °C.

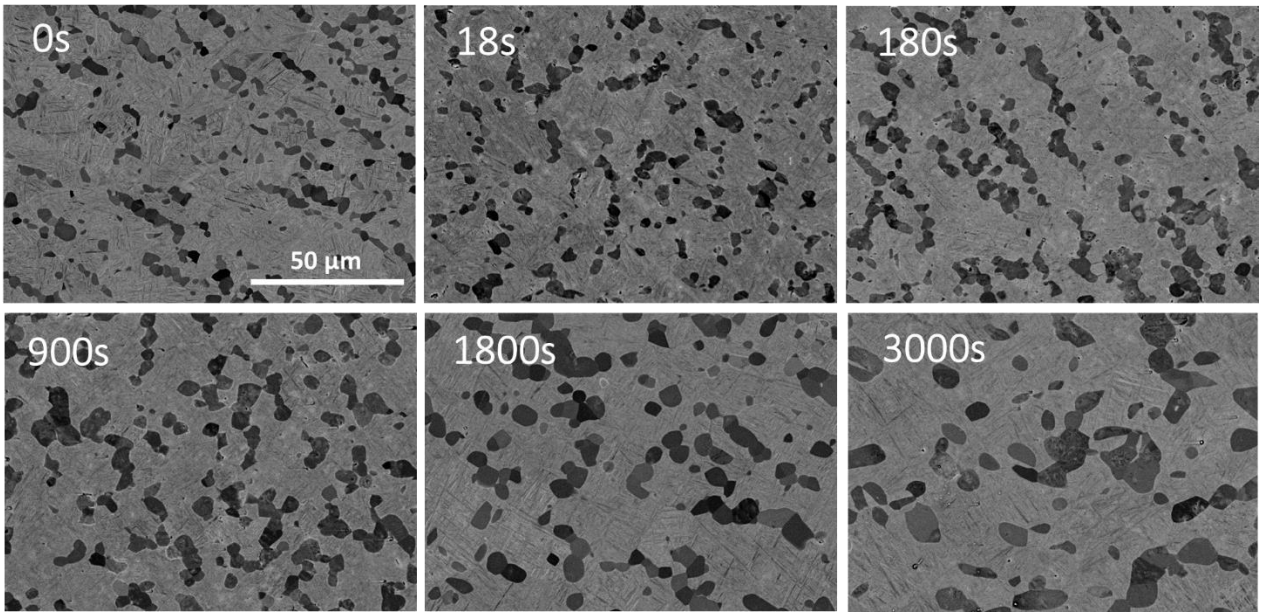

Fig. 6.1 SEM-BSE microstructures of samples subjected to post-dynamic coarsening during holding times of 0, 18, 180, 900, 1800 and 3000 s after deformation to a strain of 0.9 at a strain rate of 0.01 s^{-1} at 970 °C.

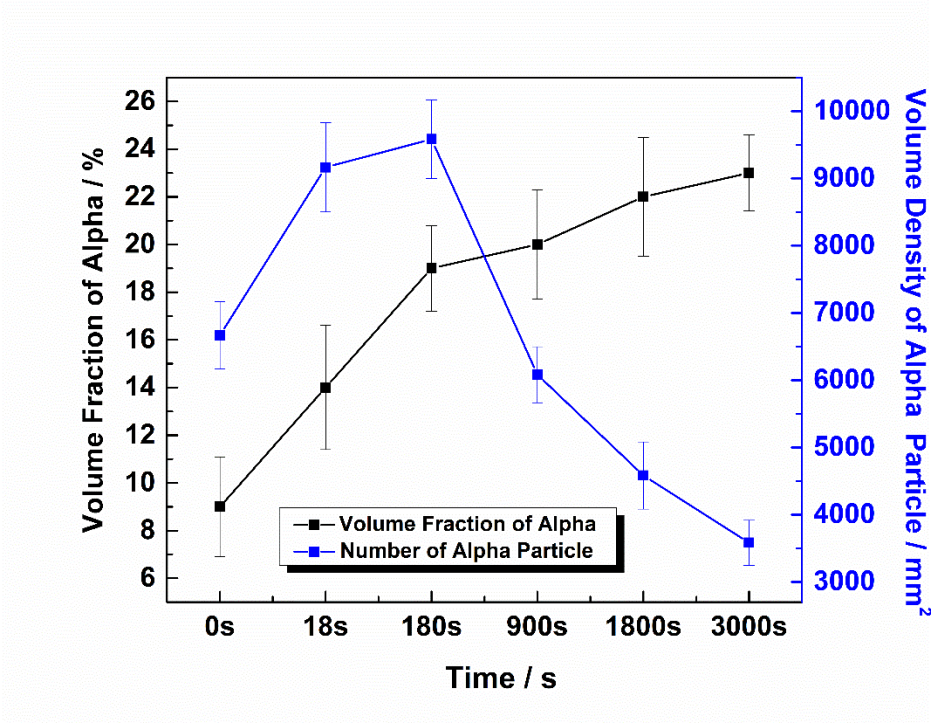

Fig. 6.2 Dependence of volume fraction of alpha and number of alpha particle per unit area on time at 970 °C.

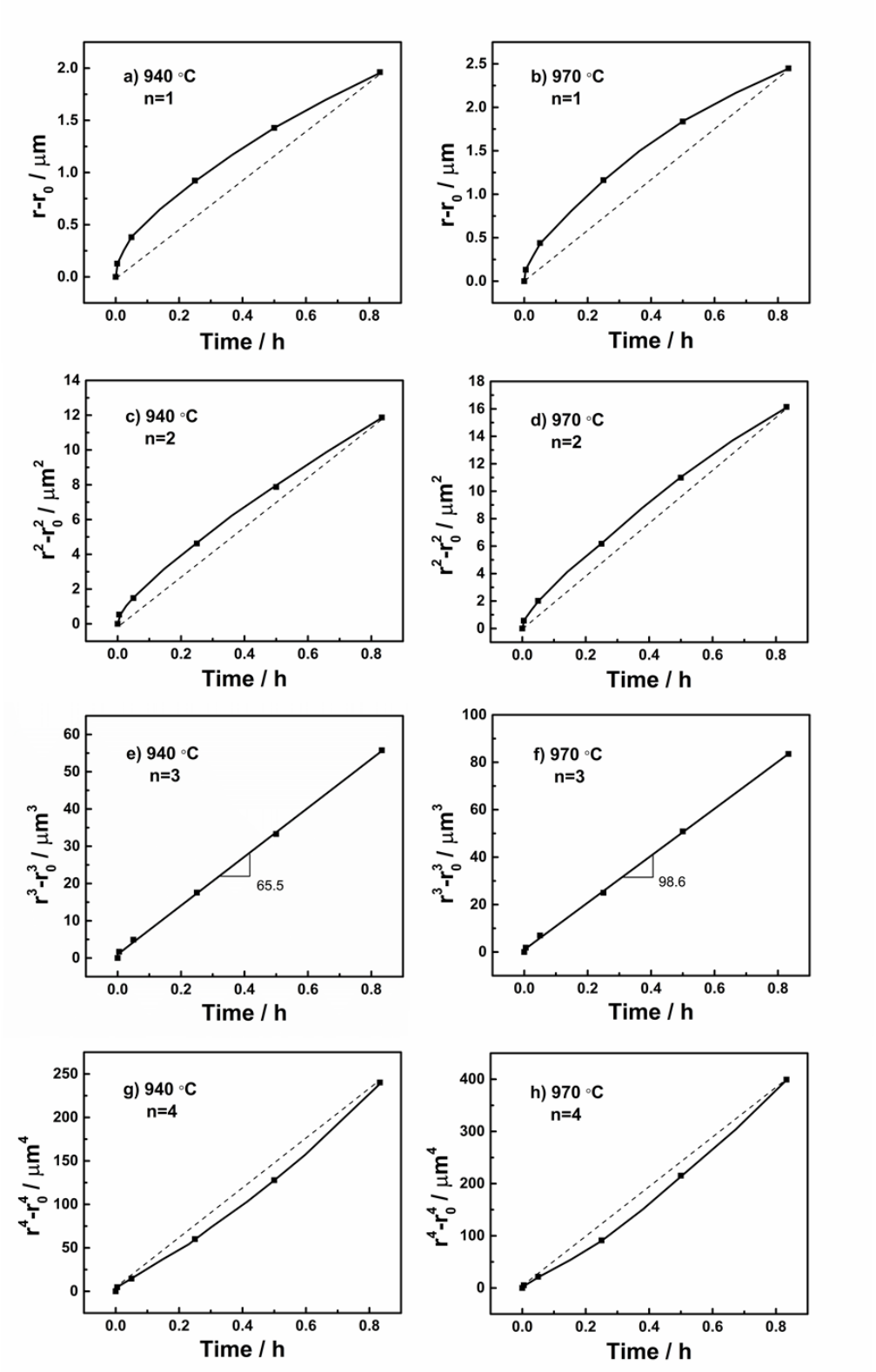

Fig. 6.3 Plots of $r^n - r_0^n$ vs time for isothermal holding after compression of Ti-6Al-4V at 940 °C and 970 °C, assuming values of n of (a) (b) 1, (c) (d) 2, (e) (f) 3, and (g) (h) 4.

6.3 Discussions

The modified Lifshitz-Slyozov-Wagner (MLSW) theory is employed here to interpret the coarsening kinetics [14], as shown in Eq. (6-1).

$$r^n - r_0^n = K_{MLSW}\,(t - t_0) \qquad (6-1)$$

Here r and r_0 denote the average alpha particle radius at time t and initial time t_0, while K_{MLSW} is the coarsening rate. The value of n is related to the mechanism of coarsening (n=2 for interface reaction, n=3 for bulk diffusion, n=4 for grain boundary diffusion and n=5 for pipe dislocation) [15-17]. The n=3 best fit in Fig. 6.2 indicates that post-dynamic coarsening is controlled by bulk diffusion, namely vanadium diffusion through the beta matrix (due to the lower diffusivity of vanadium compared to aluminum). This mechanism is the same as that for static and dynamic coarsening in Ti-6Al-4V.

The static coarsening rate can be evaluated using the following equation [18].

$$K_{MLSW} = \frac{8\{f(\varphi)D\gamma_{\alpha\beta}C_\beta(1-C_\beta)V_M\}}{9\left\{RT\left(C_\alpha - C_\beta\right)^2\left[1+\partial lnr/\partial lnC_\beta\right]\right\}} \qquad (6-2)$$

Here $f(\varphi)$ is the dependence of the rate constant on volume fraction and its dependence on volume fraction is derived from the work by Voorhees and Glicksman [19], D denotes the vanadium diffusivity in the beta matrix, $\gamma_{\alpha\beta}$ is the alpha-beta interfacial energy, V_M represents the molar volume of alpha phase, R is the universal gas constant, the T is the absolute temperature, C_α and C_β are the equilibrium concentrations of vanadium in the alpha and beta phases, $1+\partial lnr/\partial lnC_\beta$ is a thermodynamic factor. Values of these parameters were derived from previous publications on Ti-6Al-4V [1, 2, 5].

The dynamic transformation produced a metastable state via decreasing the alpha phase fraction and the vanadium content in the beta phase. In the reverse transformation, the metastable system was transformed back into a thermodynamic stable state by increasing the alpha phase fraction as well the vanadium content in the beta phase which (determined from mass conservation) is expressed by C_m.

$$C_m = (C_0 - f_\alpha C_\alpha)/(1-f_\alpha) \qquad (6-3)$$

Here C_0 and f_α represent the overall vanadium composition and the alpha phase fraction, respectively. The vanadium concentration in the alpha phase (C_α) is considered to remain unchanged when dynamic transformation takes place. The results at 970 °C are listed in Table 6.1. The vanadium content in beta phase increased with time and gradually approached the equilibrium content (4.6%) in the reverse transformation. The coarsening rate ranged from 9.07-9.80 $\mu m^3/h$.

Table 6.1 Variations of composition and coarsening rate with holding time at 970 °C

Holding time (s)	18	180	900	1800	3000
C_β (wt. %)	3.98	4.09	4.13	4.18	4.21
K_{MLSW} ($\mu m^3/h$)	9.38	9.07	9.39	9.52	9.80

According to Eq. (6-2), the observed values of K_{MLSW} at 940 °C and 970 °C varied in the range of 7.25-7.61 and 9.07-9.80 $\mu m^3/h$, respectively. These static coarsening rates are approximately one order of magnitude lower than those of post-dynamic coarsening. Similar results obtained by Weiss and Jonas [20] showed that the precipitation kinetics in steel increase by around one order of magnitude during isothermal holding after a prestrain of 5% at a strain rate of 0.05 s^{-1}. In these post-dynamic coarsening experiments, many dislocations were introduced by the deformation and the diffusivity was enhanced by pipe diffusion.

The dynamic coarsening rates in Ti-6Al-4V at 955 °C were reported to be 29.0 and 50.2 $\mu m^3/h$ at strain rates of 0.0001 and 0.001 s^{-1}, respectively, by Semiatin et al. [2]. These rates are lower than that of the post-dynamic coarsening rate (65.5 $\mu m^3/h$) after compression at a strain rate of 0.01 s^{-1} at 940 °C. The primary reason for this is the higher dislocation density associated with the higher strain rate. Furthermore, the publications of Ardell [21] and Brailsford and Wynblatt [22] indicate that the increase in volume fraction of the alpha phase contributes significantly to the increase in the post-dynamic coarsening rate as the increased fraction decreased the mean separation between particles. Dynamic transformation (alpha to beta) is accompanied by dynamic coarsening and thus the dynamic coarsening rate is reduced by the decrease in volume fraction of the alpha phase. However, the reverse transformation (beta to alpha) during isothermal holding following deformation gives rise to an increase in the post-dynamic

coarsening rate. In addition, the irregular shape of alpha phase in Fig. 6.1 (especially in long holding time) is indicative of the occurrence of coalescence of the alpha phases [23]. This accelerated the coarsening behavior and was one of the reasons why the measured post-dynamic coarsening rate was obviously greater than that in the static.

A dilatometer equipped with a compression module was employed to determine the kinetics of reverse transformation. The test material for the experiments was Ti-6Al-4V with a composition (in weight percent) of 6.53 aluminum, 4.10 vanadium, 0.17 iron, 0.17 oxygen, 0.03 carbon, 0.03 nitrogen, the balance being titanium. The as-received material was characterized by an equiaxed microstructure and was machined into compression cylinders with heights of 10.0 mm and diameters of 5.0 mm. Hot compression tests were performed in a high-resolution TA DIL 805A/D dilatometer (TA instruments, New Castle, DE, USA) with a length resolution of 50 nm to follow the reverse transformation after compression.

The samples were heated at 2°C/s to the compression temperature and then held for 900 seconds prior to deformation. Molybdenum sheets were applied to the end surfaces of the samples for lubrication purposes. A vacuum atmosphere was used to minimize oxidation during deformation and holding. The compression tests were carried out at a constant speed of 0.05 mm/s with a reduction of 4mm at both 930°C and 970°C. After compression, the samples were held isothermally for 2000s and their length changes with time were measured by the dilatometer, see Fig. 6.4. All the test samples were cooled using helium gas at 25°C/s.

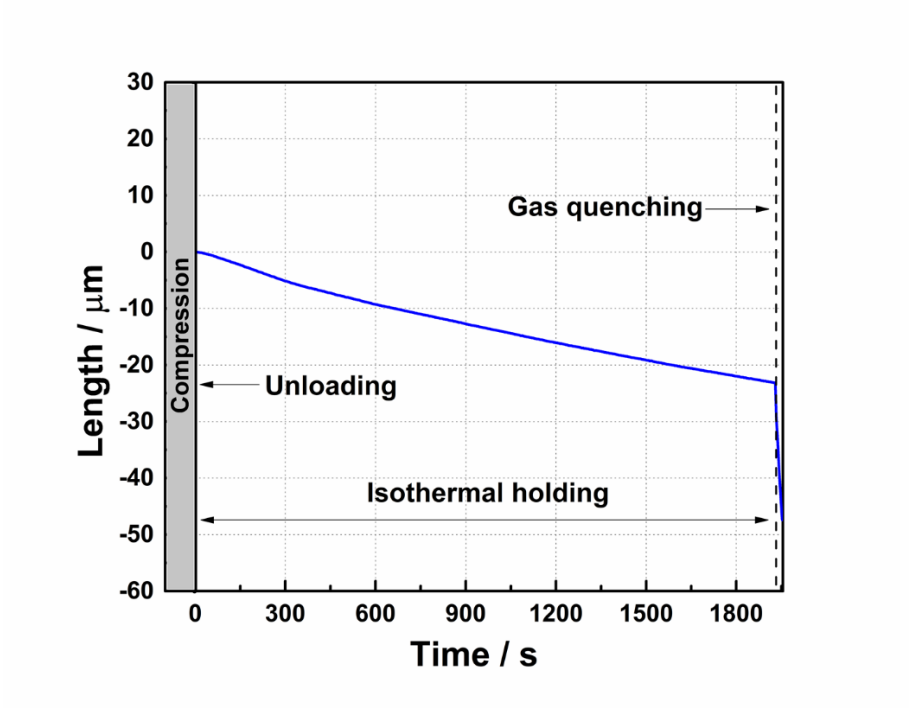

Fig. 6.4 Experimental schedule and length change of sample during isothermal holding after compression at 970 °C.

In Fig. 6.4, the length changes during isothermal holding following compression are depicted by the blue curves, which exhibit gradual contraction during isothermal holding and then drastic decreases in length on gas quenching. The length contraction during isothermal holding is ascribed here to reverse transformation (beta to alpha). The Johnson–Mehl–Avrami equation [24, 25] was employed here to describe the kinetics of the reverse transformation.

$$f = 1 - \exp(-kt^n) \qquad (6-4)$$

Here *f* is the volume fraction of the transformation product, *t* denotes the transformation time, *k* refers to the transformation rate constant, and *n* is the Avrami index, which is in turn related to the nucleation and growth mechanisms. Based on the dilatometer measurements, the volume fraction change is expressed by [26, 27]:

$$f = (L - L_0)/(L_f - L_0) \qquad (6-5)$$

where L_0 is the initial specimen length, L_f is the final length, and L is the instantaneous length. Eq. (6-4) can be converted into: $ln(ln(1/(1-f))) = n\,ln\,t + ln\,k$. When *ln(ln(1/(1-y)))* is plotted against *ln t*, the slope of the line refers to the Avrami exponent *n* and the intercept corresponds to *ln k*. Based on this approach, the results at 930 °C and 970 °C are displayed in Fig. 6.5. There are two stages in the reverse transformation. In the initial stage, the value of n is relatively low, 0.69 at 930 °C and 0.67 at 970 °C. In the second stage, the value of n increases to 1.49 at 930 °C and 1.29 at 970 °C.

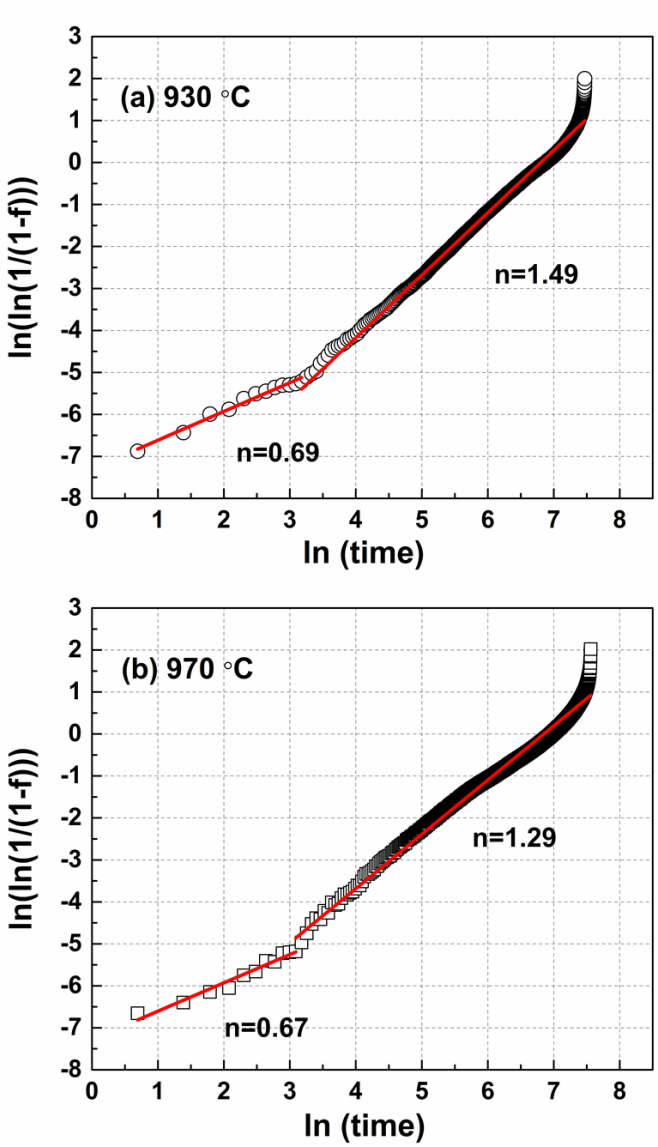

Fig. 6.5 Dependence of ln(ln(1/(1-f))) on ln (t) for Ti-6Al-4V at (a) 930 °C and (b) 970 °C.

Research by Harper [28] and Cottrell and Bilby [29] has indicated that the precipitated fraction is proportional to $t^{2/3}$ for stress-assisted precipitation on dislocations. Later Ham [30] and Bullough and Newman [31] found that such kinetics of nucleation along dislocations only take place in the early stages of annealing after deformation. A similar summary by Christian [32] led to the conclusion that n=2/3 is indicative of transformation on dislocations during the initial stages of holding. It can be therefore concluded that the mechanism of the first stage (n=0.69 and 0.67) in Figs. 6.4 (a) and (b) pertains to transformation on dislocations.

Malinov et al. [33] found that the transformation from beta to alpha in Ti-6Al-4V and Ti–6Al–2Sn–4Zr–2Mo-0.08Si during static annealing is homogeneous and that grain boundary nucleation and the growth of alpha occurred when n was 1.35 and 1.48. Later they obtained similar values of n of around 1.42 in Ti-8Al-1Mo-1V and concluded that the transformation mechanism was same as in Ti-6Al-4V and Ti–6Al–2Sn–4Zr–2Mo-0.08S [34]. In the meantime, lower values of n such as 1.1 and 1.01 have been considered to correspond to alpha formation at grain boundaries [33, 34].

The work by Malinov et al. [35] suggested that still lower values of n (i.e. 0.40 and 0.36) in β21s signify that the mechanism is the slow diffusion-controlled growth of fine alpha plates. This was later confirmed by Naveen el al. [36] in Ti15-3. Compared with the tests by Malinov et al [33, 34], the undercooling in Fig. 6.4 was negligible and numerous defects were introduced by the deformation, which makes homogeneous nucleation difficult to take place. The present results suggest that the second stage of the reverse transformation (n=1.29 and 1.49) in Figs. 6.5 (a) and (b) involves the growth of the alpha structure.

6.4 Conclusions

In summary, both post-dynamic coarsening and reverse transformation occurred during isothermal holding following the deformation of samples of Ti-6Al-4V. The kinetics of post-dynamic coarsening were one order of magnitude faster than during static coarsening and this mechanism appears to be controlled by bulk diffusion, i.e. vanadium diffusion through the beta matrix. The reverse transformation took place in two stages: the first stage was transformation along dislocations; the second stage involved the growth of the alpha structure.

References

[1] S.L. Semiatin, B. Kirby, G. Salishchev, Coarsening behavior of an alpha-beta titanium alloy, Metallurgical and Materials Transactions A 35(9) (2004) 2809-2819.

[2] S.L. Semiatin, M. Corbett, P. Fagin, G. Salishchev, C. Lee, Dynamic-coarsening behavior of an α/β titanium alloy, Metallurgical and Materials Transactions A 37(4) (2006) 1125-1136.

[3] C.H. Park, B. Lee, S.L. Semiatin, C.S. Lee, Low-temperature superplasticity and coarsening behavior of Ti–6Al–2Sn–4Zr–2Mo–0.1 Si, Materials Science and Engineering: A 527(20) (2010) 5203-5211.

[4] G. Sargent, A. Zane, P. Fagin, A. Ghosh, S.L. Semiatin, Low-temperature coarsening and plastic flow behavior of an alpha/beta titanium billet material with an ultrafine microstructure, Metallurgical and Materials Transactions A 39(12) (2008) 2949.

[5] S. Zherebtsov, E. Kudryavtsev, G. Salishchev, B. Straumal, S.L. Semiatin, Microstructure evolution and mechanical behavior of ultrafine Ti6Al4V during low-temperature superplastic deformation, Acta Materialia 121 (2016) 152-163.

[6] A. Dutta, N. Birla, Stress induced hydrogen diffusion in a α+β titanium alloy during superplastic deformation, Scripta Metallurgica 21(8) (1987) 1051-1054.

[7] L. Jing, R. Fu, Y. Wang, L. Qiu, B. Yan, Discontinuous yielding behavior and microstructure evolution during hot deformation of TC11 alloy, Materials Science and Engineering: A 704 (2017) 434-439.

[8] B. Guo, S.L. Semiatin, J. Liang, B. Sun, J.J. Jonas, Opposing and Driving Forces Associated with the Dynamic Transformation of Ti-6Al-4V, Metallurgical and Materials Transactions A 49(5) (2018) 1450-1454.

[9] B. Guo, S.L. Semiatin, J.J. Jonas, S. Yue, Dynamic transformation of Ti–6Al–4V during torsion in the two-phase region, Journal of Materials Science 53 (2018) 9305-9315.

[10] B. Guo, C. Aranas, A. Foul, X. Ji, A. Fall, M. Jahazi, J.J. Jonas, Effect of multipass deformation at elevated temperatures on the flow behavior and microstructural evolution in Ti-6Al-4V, Materials Science and Engineering: A 729 (2018) 119-124.

[11] J. Koike, Y. Shimoyama, I. Ohnuma, T. Okamura, R. Kainuma, K. Ishida, K. Maruyama, Stress-induced phase transformation during superplastic deformation in two-phase Ti–Al–Fe alloy, Acta Materialia 48(9) (2000) 2059-2069.

[12] B. Guo, C. Aranas, B. Sun, X. Ji, J.J. Jonas, Reverse Transformation Behavior of Ti-6Al-4V After Deformation in the Two-Phase Region, Metallurgical and Materials Transactions A 49(1) (2018) 22-27.

[13] S. Xiao, P. Haasen, HREM investigation of homogeneous decomposition in a Ni-12 at.% A1 Alloy, Acta Metallurgica et Materialia 39(4) (1991) 651-659.

[14] I. Lifshitz, IM Lifshitz and VV Slyozov, J. Phys. Chem. Solids 19, 35 (1961), J. Phys. Chem. Solids 19 (1961) 35.

[15] W. Sun, M. Militzer, J. Jonas, Diffusion-controlled growth and, Metallurgical Transactions A 23(11) (1992) 3013-3023.

[16] O. Senkov, M. Myshlyaev, Grain growth in a superplastic Zn-22% Al alloy, Acta Metallurgica 34(1) (1986) 97-106.

[17] K. Russell, F. Froes, Compound dispersoid stability on grain boundaries, Scripta Metallurgica 22(4) (1988) 495-499.

[18] H. Calderon, P. Voorhees, J. Murray, G. Kostorz, Ostwald ripening in concentrated alloys, Acta Metallurgica et Materialia 42(3) (1994) 991-1000.

[19] P.W. Voorhees, M. Glicksman, Solution to the multi-particle diffusion problem with applications to Ostwald ripening—II. Computer simulations, Acta Metallurgica 32(11) (1984) 2013-2030.

[20] I. Weiss, J. Jonas, Interaction between recrystallization and precipitation during the high temperature deformation of HSLA steels, Metallurgical Transactions A 10(7) (1979) 831-840.

[21] A. Ardell, The effect of volume fraction on particle coarsening: theoretical considerations, Acta Metallurgica 20(1) (1972) 61-71.

[22] A. Brailsford, P. Wynblatt, The dependence of Ostwald ripening kinetics on particle volume fraction, Acta Metallurgica 27(3) (1979) 489-497.

[23] R. MacKay, M. Nathal, γ’ coarsening in high volume fraction nickel-base alloys, Acta Metallurgica et Materialia 38(6) (1990) 993-1005.

[24] M. Avrami, Granulation, phase change, and microstructure kinetics of phase change. III, The Journal of Chemical Physics 9(2) (1941) 177-184.

[25] W. Johnson, WA Johnson and RF Mehl, Trans. Am. Inst. Min., Metall. Pet. Eng. 135, 416 (1939), Trans. Am. Inst. Min., Metall. Pet. Eng. 135 (1939) 416.

[26] M.N. Ahmadabadi, S. Farjami, Transformation kinetics of unalloyed and high Mn austempered ductile iron, Materials Science and Technology 19(5) (2003) 645-649.

[27] E. Mittemeijer, A. Van Gent, P. Van der Schaaf, Analysis of transformation kinetics by nonisothermal dilatometry, Metallurgical Transactions A 17(8) (1986) 1441-1445.

[28] S. Harper, Precipitation of carbon and nitrogen in cold-worked alpha-iron, Physical Review 83(4) (1951) 709.

[29] A.H. Cottrell, B. Bilby, Dislocation theory of yielding and strain ageing of iron, Proceedings of the Physical Society. Section A 62(1) (1949) 49.

[30] F.S. Ham, Stress‐assisted precipitation on dislocations, Journal of Applied Physics 30(6) (1959) 915-926.

[31] R. Bullough, R.C. Newman, The growth of impurity atmospheres round dislocations, Proc. R. Soc. Lond. A 266(1325) (1962) 198-208.

[32] J.W. Christian, The Theory of Transformation in Metals and Alloys: Equilibrium and General Kinetic Theory, 2nd Edition, Pergamon, Oxford (1975) 525–548.

[33] S. Malinov, P. Markovsky, W. Sha, Z. Guo, Resistivity study and computer modelling of the isothermal transformation kinetics of Ti–6Al–4V and Ti–6Al–2Sn–4Zr–2Mo–0.08 Si alloys, Journal of Alloys and Compounds 314(1-2) (2001) 181-192.

[34] S. Malinov, P. Markovsky, W. Sha, Resistivity study and computer modelling of the isothermal transformation kinetics of Ti–8Al–1Mo–1V alloy, Journal of Alloys and Compounds 333(1-2) (2002) 122-132.

[35] S. Malinov, W. Sha, P. Markovsky, Experimental study and computer modelling of the β⇒ α+β phase transformation in β21s alloy at isothermal conditions, Journal of Alloys and Compounds 348(1-2) (2003) 110-118.

[36] M. Naveen, R. Santhosh, M. Geetha, M.N. Rao, Experimental study and computer modelling of the β⟶α+β phase transformation in Ti15-3 alloy under isothermal conditions, Journal of Alloys and Compounds 616 (2014) 607-613.

Chapter 7

Role of Dynamic Transformation in the Flow Behavior During the Hot Working of Two-Phase Titanium Alloys

In this chapter, two initial microstructures of Ti-6Al-4V alloy were used during compression tests at elevated temperatures. The dynamic transformation was found in the two microstructures at different strain rates. Self-consistent modeling was employed to reveal the role of dynamic transformation in the flow softening in titanium alloys. The remaining softening/hardening sources such as texture and coarsening were discussed as well. The approach was extended to other titanium alloys (IMI 834) so as to unveil the effects of transformation on flow behavior.

- **Baoqi Guo** *, S. L. Semiatin, John J. Jonas. Role of dynamic transformation in the flow behavior during the hot working of two-phase titanium alloys. To be submitted. 2018.

Abstract:

The role of dynamic transformation in flow stress during the deformation of two-phase titanium alloys was evaluated using isothermal compression and self-consistent modeling. Dynamic transformation took place in both the equiaxed and lamellar microstructures at temperatures ranging from 815 °C to 950 °C. There was more flow softening in the lamellar than in the equiaxed microstructure. However, the extent of dynamic transformation and the associated flow softening were similar in the two microstructures. The softening proportion from texture evolution was analogous to that from dynamic transformation in the lamellar microstructure. Dynamic transformation served as the main source of flow softening in the equiaxed microstructure particularly at low strain rates, while its contribution to the flow softening in the lamellar microstructure was evidently reduced. An appropriate strain rate for observing dynamic transformation lay in the range from 0.01 s^{-1} to 0.001 s^{-1} based on the balance between inhibiting adiabatic heating and increasing driving forces. This approach was further applied on an IMI 834 alloy and its behavior was similar to that for Ti-6Al-4V.

7.1 Introduction

In the 1980s, Dutta and Birla [1] reported that the beta volume fraction increased appreciably when their Ti-6.3Al-2.7Mo-1.7Zr alloy was deformed at 850 °C. Later Prada et al. [2] observed that the beta phase fraction was increased by continuous straining at 815 °C in a Ni modified Ti-6Al-4V alloy. Similar work on Ti-6Al-4V was undertaken by Yang et al. [3] which showed that the dynamic transformation of alpha to beta was dependent on temperatures. In later work by Koike et al. [4], the free energy of the alpha phase was considered to have been increased by 500 J/mol to by the deformation. In a similar manner, an increase in the beta phase fraction in TiBw/Ti-6Al-4V composites was observed by Lu et al. [5] during tensile testing.

Dynamic transformation has also been reported in lamellar microstructure during hot deformation. Chen et al. [6] showed that the dynamic transformation in a Ti-6Al-4V alloy took place between adjacent lamellae of the colony microstructure during the hot tensile testing. In tests by Matsumoto et al. [7], beta precipitation was observed in a Ti-6Al-4V with an initial martensitic microstructure and served as an additional stress accommodation mechanism. The dynamic transformation can be activated by various types of deformation such as tension, compression and torsion. In the work by Zong et al. [8], it was shown that alpha phase in a TC11 alloy can be transformed into beta phase by compression at 900 °C. Later Jing et al. [9] observed discontinuous yielding in TC11 during hot compression and attributed this to the dynamic transformation. Such softening during torsion testing was also observed by the present authors [10] during torsion to a strain of 2.0 at a strain rate of 0.01 s^{-1} at temperatures ranging from 880 to 980 °C.

More recently, Jonas et al. [11] reported a noticeable increase in the beta phase fraction when an IMI 834 alloy was compressed at 975 and 1000 °C. Wang et al. [12] noted the presence of more beta phase when a near alpha titanium alloy TA15 was deformed. In a similar manner, the excellent superplastic elongation of Ti-6Al-4V in work by Zhang et al. [13] was partially ascribed to the dynamic transformation taking place during tensile testing at 700 and 800 °C. Matsumoto et al. [14] suggested that the beta phase increase by deformation in equiaxed microstructure contributed to the accommodation of stress concentration at grain boundaries. However, the

contribution of dynamic transformation to the flow stress at elevated temperatures has still not been illuminated.

Numerous works have been done regarding the modeling of the flow behavior of titanium alloys. For example, the dislocation-density based model was investigated by Babu and Lindgren [15]; their results showed that the simulated stresses between 800-950 °C were higher than the measured especially at the greater strain regime; note that dynamic transformation can occur readily within this temperature range due to the low energy barriers. Self-consistent model [16] and crystal plasticity [17] constitutive models developed by Fan et al. indicated that measured flow stresses were lower than the simulated ones as well. These discrepancies can be attributed to the dynamic transformation as a softening mechanism. The effect of the transformation on flow behavior has been omitted in previous works irrespective of its significance in the flow stress modeling. In the present work, the role of dynamic transformation is analyzed using self-consistent modeling and the significance of dynamic transformation in the flow behavior is illustrated. Other factors affecting the flow stress including texture evolution, dynamic coarsening and morphological changes are discussed here as well.

7.2 Experiment

The present compression tests were performed on a Ti-6Al-4V alloy with the transus temperature about 1015°C. The material was composed of 6.54% aluminum, 4.14% vanadium, 0.18% iron, 0.17% oxygen, 0.03% carbon, 0.03% nitrogen (in weight percent), the balance being titanium. The as-received material was characterized by an equiaxed microstructure. The as-received material was heat treated at 1060 °C for 15 min and then water quenched in order to produce a lamellar microstructure. Samples with these two microstructures (equiaxed and lamellar) were machined into compression cylinders with heights of 9.6mm and diameters of 6.4mm. The tests were conducted on a servohydraulic MTS compression machine with a radiation furnace and an argon gas atmosphere.

The samples were heated at 2°C/s to the deformation temperature (815, 850, 900, 955 °C) and then held for 15 min prior to deformation [18]. The samples were compressed to logarithmic strains of 0.4 and 0.7 at strain rates of 0.01 and 0.001 s^{-1}, respectively. All the samples after the

compression were water quenched to preserve the microstructures. Each compression test was repeated at least twice to ensure the reproducibility of the flow curves and microstructures. Strain-rate jump tests were performed to measure the strain rate sensitivity in three strain rate ranges (i.e. 0.1-0.5, 0.01-0.05 and 0.001-0.005 s^{-1}). For example, the initial strain rate of 0.1 increased to 0.5 at a strain of 0.1. Then it decreased back to 0.1 after reaching a strain of 0.2. Such jump test was repeated to a total strain of 0.8.

Samples were cut along the axial direction and prepared using standard metallographic techniques. Colloidal silica suspension was employed in the final polishing using a vibratory polisher. EBSD was carried out using an accelerattion voltage of 15 kV and a working distance of 15 mm. The HKL Channel 5 softeware was employed for data acquisition and analysis. The microstructures were examined using backscattered electron imaging (BSEI) in a scanning electron microscope (SEM). The microstructures pertain to the centers of the samples to avoid the dead zones at the ends. In each sample, at least three EBSD pictures were taken to determine the Taylor factor based on the average value. The volume fractions of the alpha phase were evaluated on the basis of five micrographs for each sample. These fractions were determined using the ImageJ software. The alpha particle radius was estimated using the average alpha particle size (A_α) according to the circle equivalent area method [19]. Five BSEI photographs were taken in each condition to ensure that at least 600 alpha particles were sampled.

7.3 Results

The microstructures of Ti-6Al-4V samples with an initial equiaxed microstructure deformed at a strain rate of 0.001 s^{-1} to strains of 0.4 and 0.7 are displayed in **Fig. 7.1** (a), (b) and (c) at 900 °C and in **Fig. 7.1** (d), (e) and (f) at 955 °C. Dynamic transformation was observed to take place during straining and the alpha phase fraction was observed to decrease by around 6-9% in the equiaxed microstructure, as listed in **Table. 7.1.** Dynamic coarsening was observed to take place particularly at the higher temperatures. The irregular shapes of the alpha particles signified that alpha phases coalescence took place during deformation. In **Table 7.1**, the diameter of alpha particles at 900 °C was 3.59 µm and increased to 4.72 µm and 5.67 µm by compression to a strain of 0.7 at strain rates of 0.01 s^{-1} and 0.001 s^{-1}, respectively. This diameter was further increased

from 3.62 µm prior to deformation to 4.79 µm at a strain rate of 0.01 s^{-1} and to 6.84 µm at a strain rate of 0.001 s^{-1} at 955 °C. The impact of dynamic coarsening on the flow stress is discussed in section 4.4. The microstructures of Ti-6Al-4V samples with an initial lamellar microstructure deformed at a strain rate of 0.001 s^{-1} to strains of 0.4 and 0.7 are displayed in **Fig. 7.2** (a), (b) and (c) at 900 °C and **Fig. 7.2** (d), (e) and (f) at 955 °C. Spheroidization of the alpha phase is evident, accompanied by flow softening of the lamellar microstructure.

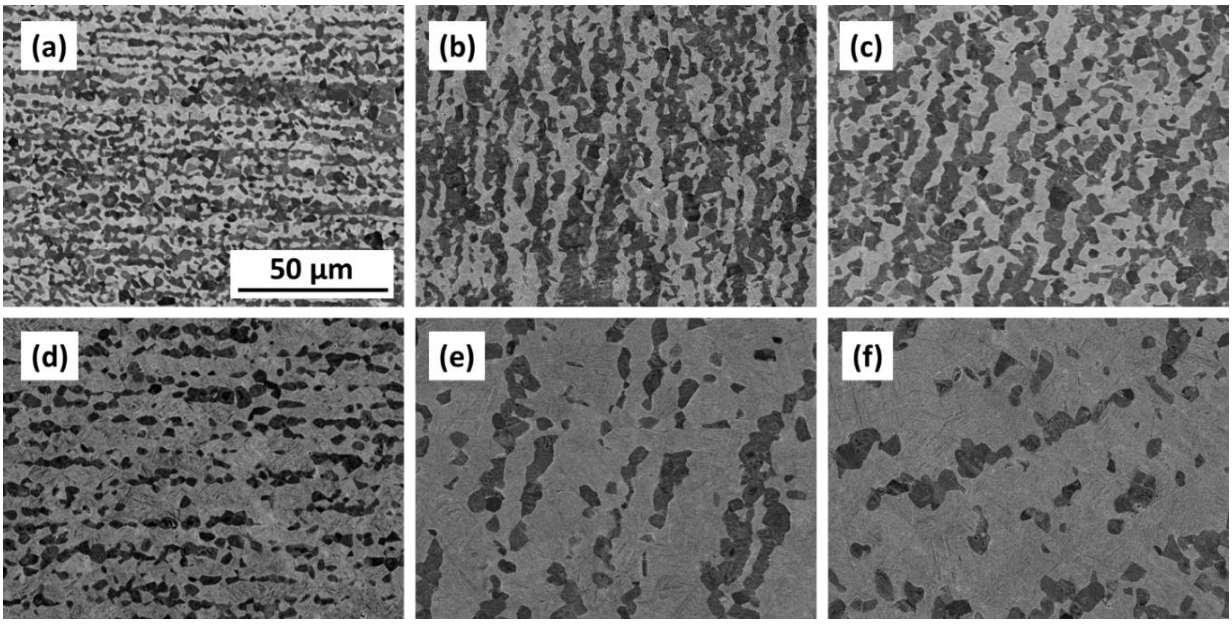

Fig. 7.1 SEM-BSE micrographs of Ti-6Al-4V samples with an initial equiaxed microstructure deformed at a strain rate of 0.001 s^{-1} to strains of (a) 0, (b) 0.4 and (c) 0.7 at 900 °C and to strains of (a) 0, (b) 0.4 and (c) 0.7 at 955 °C. The beta/transformed beta is white and the alpha appears dark.

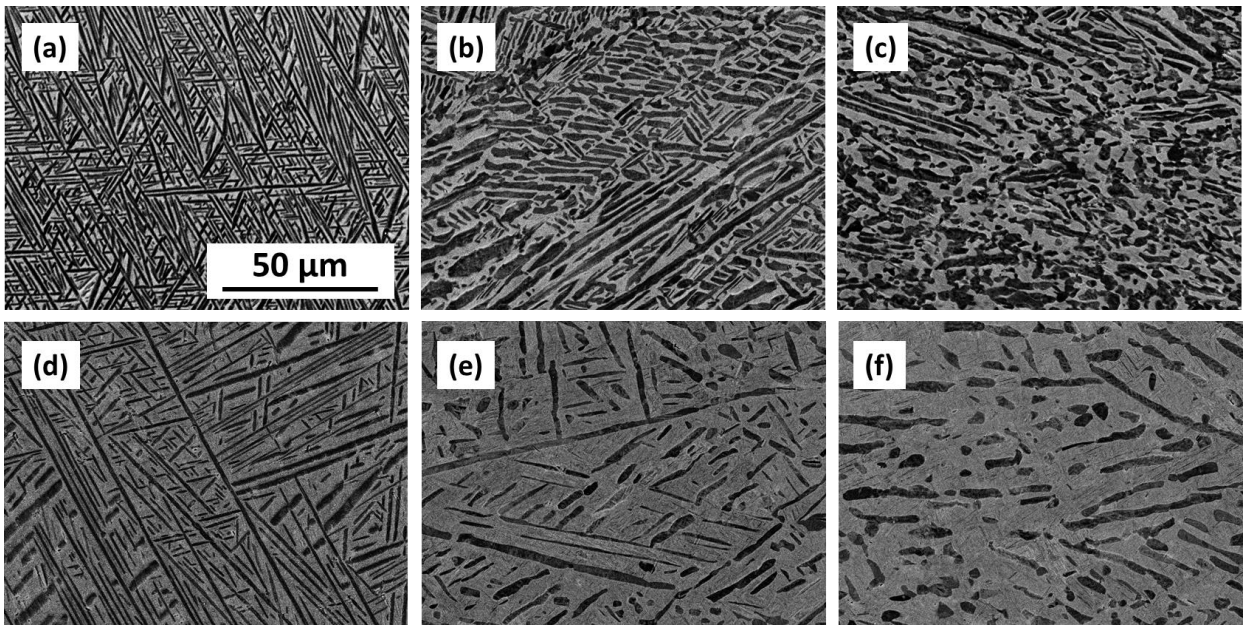

Fig. 7.2 SEM-BSE micrographs of Ti-6Al-4V samples with an initial lamellar microstructure deformed at a strain rate of 0.001 s^{-1} to strains of (a) 0, (b) 0.4 and (c) 0.7 at 900 °C and to strains of (a) 0, (b) 0.4 and (c) 0.7 at 955 °C.

Table 7.1 Diameters and phase fractions of the alpha phase in the equiaxed microstructure and the measured stress as well as the predicted stress in the absence of dynamic coarsening.

Temperature (°C)	Strain rate (s^{-1})	Strain	Alpha fraction	Diameter (µm)	Measured stress (MPa)	Predicted stress (no coarsening) (MPa)
900	0.0	0.0	0.53	3.59	--	--
	0.01	0.7	0.47	4.72	57.5	55.7
	0.001	0.7	0.45	5.68	21.1	15.2
955	0.0	0.0	0.28	3.62	--	--
	0.01	0.7	0.20	4.79	32.4	31.5
	0.001	0.7	0.19	6.84	18.6	12.7

The strain rate sensitivity depended on the temperature and strain rate range in equiaxed microstructure, as shown in **Fig. 7.3**(a). At 900 °C and 955 °C and strain rate range of 0.001-0.005 s^{-1}, the index was greater than 0.4, as shown by the dotted line, indicating that the deformation was superplastic. These values ranged from 0.15 to 0.30 at strain rates of 0.01 and 0.1 s^{-1}. In the

lamellar microstructure, the strain rate sensitivity increased with strain shown in **Fig. 7.3**(b). At strains lower than 0.2, the values of the index were less than 0.3 and these increased to 0.3 and even 0.4 during deformation to a strain of 0.7, particularly at 900 °C at 0.001 s^{-1}. This signified a transition from power-law creep to superplastic flow.

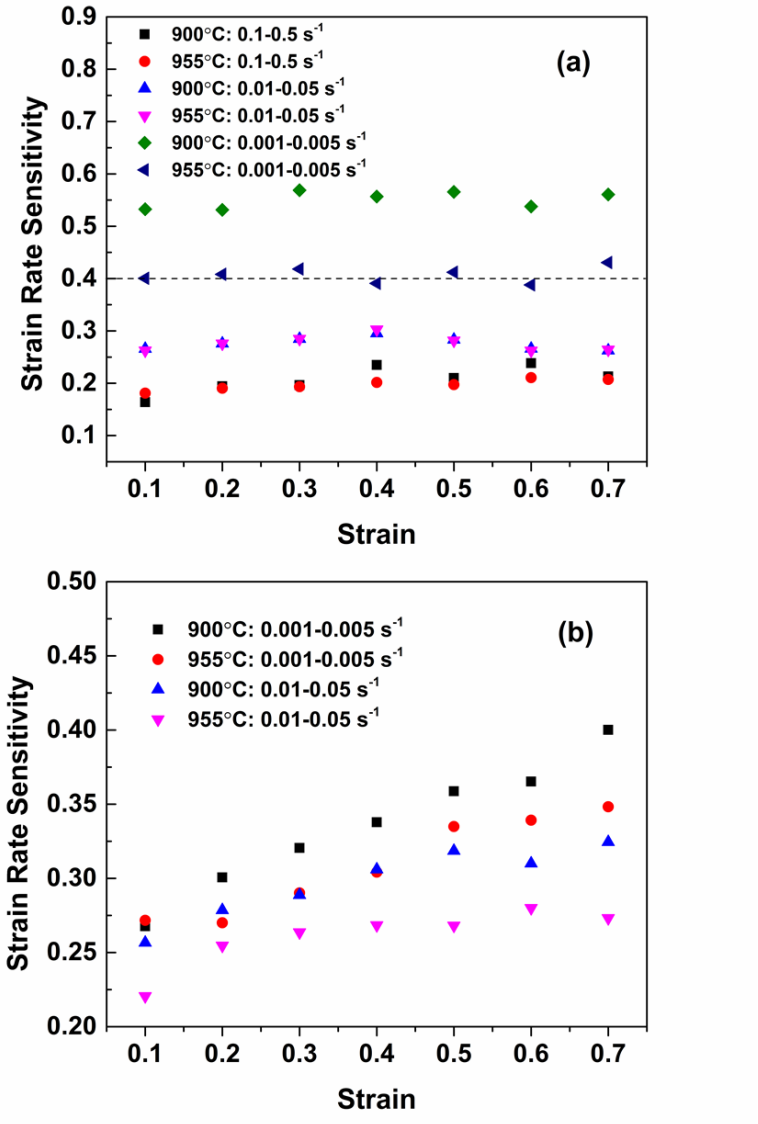

Fig. 7.3 Dependence of strain rate sensitivity on temperature and strain rate for two initial microstructures: (a) equiaxed and (b) lamellar.

Texture evolution in the equiaxed microstructure as a result of deformation is illustrated in **Fig. 7.4**(a) and (b), respectively. Here only the texture of alpha phase was shown since the

directionality of beta phase has little effect on the flow stress. The white matrix represents the transformed beta. The $\{10\bar{1}0\}$ prism plane was approximately perpendicular to the loading direction (LD) in the undeformed sample with the equiaxed microstructure at 900 °C. This texture component was characterized by a rotation of around 45° from the X direction (LD) after hot deformation. In the lamellar microstructure, the texture prior to deformation illustrated in **Fig. 7.5**(a) was composed partly of basal poles by around 45 °C rotated from the LD. The component was rotated by around 45°C to the transverse direction by the deformation, as shown in **Fig. 7.5**(b). These components are similar to those observed in previous works with similar microstructures [20].

The evaluation of the Taylor factor in the alpha phase is indicative of the softening/hardening produced by the deformation. The distribution of this parameter was included in the EBSD figures as shown by the column graphs. The average value of the Taylor factor remained approximately unchanged by deformation at 900 °C, i.e. 2.91 and 2.86 at a strain rate of 0.001 s^{-1} in the equiaxed microstructure. The same trend was observed at the higher strain rate of 0.01 s^{-1}. Hence, its effects on the flow stress are negligible here. However, the average value decreased from 3.00 to 2.64 after deformation at a strain rate of 0.001 s^{-1} in the lamellar microstructure at 900 °C, as shown in **Fig. 7.5**. Similarly, the Taylor factor in the lamellar microstructure decreased from 3.00 to 2.76 during straining at a strain rate of 0.01 s^{-1} at both 900 and 955 °C. Its impact on the flow stress is discussed in section 7.4.2.

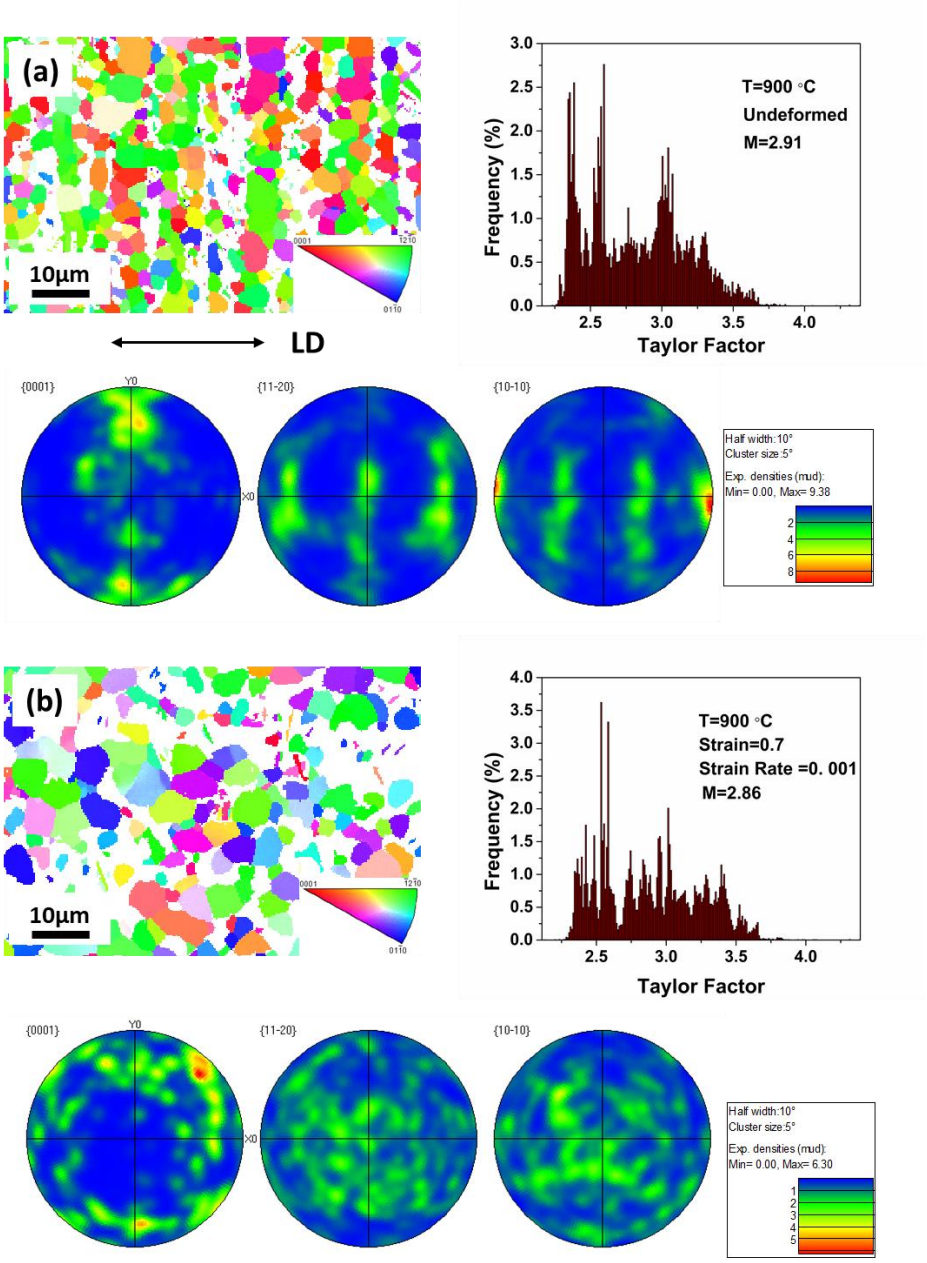

Fig. 7.4 Texture evolution and Taylor factor distribution in Ti-6Al-4V with initial equiaxed microstructure of (a) undeformed sample at 900 °C and (b) deformed to a strain of 0.7 at a strain rate of 0.001 s^{-1} at 900 °C. The loading direction (LD) and transverse direction (TD) are parallel to the X and Y directions, respectively.

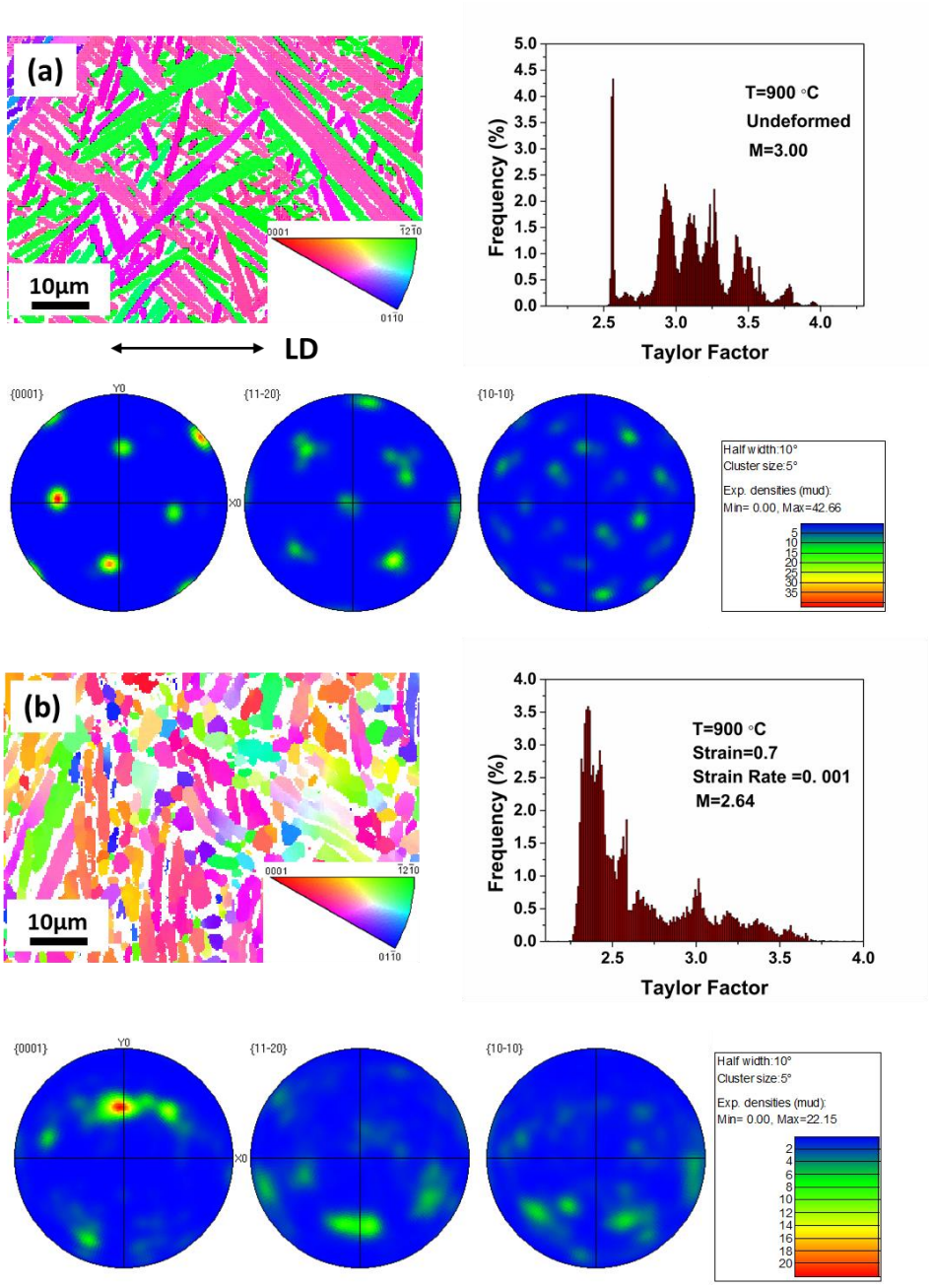

Fig. 7.5 Texture evolution and Taylor factor distribution in Ti-6Al-4V with initial lamellar microstructure of (a) undeformed sample at 900 °C and (b) deformed to a strain of 0.7 at a strain rate of 0.001 s^{-1} at 900 °C.

7.4 Discussion

Dynamic recovery acted as a source of flow softening and demonstrated a steady state flow stress in both single-phase alpha and beta titanium alloys at elevated temperatures [21, 22]. The

occurrence of dynamic recrystallization was dependent on temperature and strain rate based on the double differentiation approach to the determination of dynamic softening phenomena [23] and such correlation was not found in Ti-6Al-4V [24]. This is also consistent with the present results that dynamic coarsening rather than recrystallization was observed at the elevated temperatures. These dynamic phenomena generated substructures associated with dislocation evolution and indeed produced a minor effect on the flow softening in titanium alloys.

Another source of flow softening is the adiabatic heating during deformation and the temperature increase (ΔT) is evaluated by the equation: $\Delta T = 0.95\eta/\rho C_{\mathrm{p}} \int \sigma d\varepsilon$, where η is the adiabatic correction factor (0, 0.25 and 0.75 for strain rates of 0.001, 0.01 and 0.1, respectively), σ and ε denote the stress and strain, respectively, ρ the density of Ti-6Al-4V and C_p the specific heat [18]. The ΔT during the compression to a strain of 0.7 at a strain rate of 0.1 s^{-1} is around 25 °C, 17 °C and 9 °C at 850 °C, 900 °C, 955 °C, respectively. It is reduced to around 3 °C in the temperature range from 850 °C to 955 °C with the strain rate decreasing to 0.01 s^{-1}. Here the amount of adiabatic heating associated with 3 °C is negligible as it is readily dissipated at the elevated temperatures. According to the approach by Semiatin and Lahoti [25], the flow softening caused by adiabatic heating can be estimated using the relation between flow stress and instantaneous temperature at different strains. Based on this method, the flow softening fraction associated with adiabatic heating during compression to a strain of 0.7 at a strain rate of 0.1 s^{-1} was 17%, 15% and 12% at the temperatures of 850 °C, 900 °C and 955 °C, respectively. Similar tests on the Ti-6Al-4V also suggested that the heating related softening by the compression to a strain of 0.5 was 0%, 10% and 17% at the strain rates of 0.001 s^{-1}, 0.1 s^{-1} and 10 s^{-1}, respectively [24]. Hence, the deformation heating is a significant source of flow softening at a relatively high strain rate such as 0.1 s^{-1}. The temperature rise caused by adiabatic heating at high strain rates can produce the phase transformation from alpha to beta, which might be confounded with the dynamic transformation induced by stress. The appropriate strain rate range for the observation of stress-induced transformation should be around 0.01 s^{-1} or lower than this value.

7.4.1 Effect of dynamic transformation on the flow behavior

7.4.1.1. Self-consistent modeling

The relation between flow behavior and dynamic transformation is established through developing the self-consistent model. This model is derived from the approach on linearly elastic solids [26] and further applied in linearly viscous incompressible cases. The constitutive equation is expressed by:

$$\sigma_{\mathrm{i}} = k_{\mathrm{i}}^{\mathrm{L}} \dot{\varepsilon}_{\mathrm{i}} \tag{7-1}$$

Where σ_{i} is the flow stress and $\dot{\varepsilon}_{\mathrm{i}}$ strain rate, $k_{\mathrm{i}}^{\mathrm{L}}$ refers to the viscosity parameter of component *i* (alpha and beta phase in present alloy). The viscosity of aggregate $k_{\alpha+\beta}^{\mathrm{L}}$ is described by:

$$k_{\alpha+\beta}^{\mathrm{L}}/k_{\alpha}^{\mathrm{L}} = (1/6)\left\{3 - 2\rho + 5(1-f)(\rho-1) + \sqrt{[3 - 2\rho + 5(1-f)(\rho-1)]^2 + 24\rho}\right\} \tag{7-2}$$

Here f represents the volume fraction of alpha phase, and ρ is defined as $k_{\beta}^{\mathrm{L}}/k_{\alpha}^{\mathrm{L}}$. Later the approach is further developed in the power-law viscoplastic system [27], shown as follows.

$$\sigma_{\mathrm{i}} = k_{\mathrm{i}} \dot{\varepsilon}_{\mathrm{i}}^{\mathrm{m_i}} \tag{7-3}$$

Here m_i is the strain rate sensitivity and its values are approximately the same in the alpha and beta phases based on the work by Kim et al. [28]. The values of m index were taken from the measurement in **Fig. 7.3**. It is further applied to the calculation of entire viscosity-like parameter of $k_{\alpha+\beta}$.

$$k_{\alpha+\beta}/k_{\alpha} = \min_{\rho \geq 0}\left\{(k_{\alpha+\beta}^{\mathrm{L}}/k_{\alpha}^{\mathrm{L}})^{(m+1)/2} \cdot \left[f + (1-f)\rho^{(m+1)/(m-1)}(k_{\beta}/k_{\alpha})^{2/(1-m)}\right]^{(1-m)/2}\right\} \tag{7-4}$$

Where $k_{\alpha+\beta}/k_{\alpha}$ is obtained when the right part in braces reaches minimum with $\rho \geq 0$. The $k_{\alpha+\beta}^{\mathrm{L}}/k_{\alpha}^{\mathrm{L}}$ is substituted by Eq. (7-2) and then Eq. (7-4) is expressed by a function of ρ, f, k_{β}/k_{α} and m. Among these parameters, the values of f, k_{β}/k_{α} and m are constants or material properties [29].

The $k_{\alpha+\beta}/k_{\alpha}$ is dependent on the phase fractions due to the remarkable difference in stress ratio of alpha/beta and is related to the kinetics of dynamic transformation. Flow softening caused by dynamic transformation is defined by the index $\Delta\sigma_{\mathrm{dt}}$:

$$\Delta\sigma_{\mathrm{dt}} = \frac{(k_{\alpha+\beta}/k_{\alpha})_{\varepsilon} - (k_{\alpha+\beta}/k_{\alpha})_{\mathrm{p}}}{(k_{\alpha+\beta}/k_{\alpha})_{\mathrm{p}}} \qquad (7-5)$$

Here $(k_{\alpha+\beta}/k_{\alpha})_{\varepsilon}$ denotes the value of $k_{\alpha+\beta}/k_{\alpha}$ corresponding to the deformation to a certain strain (0, 0.4 and 0.7) and $(k_{\alpha+\beta}/k_{\alpha})_{\mathrm{p}}$ is the value of the strength ratio at the peak stress. It is assumed that the initiation of dynamic transformation lies in the peak stress according to previous work [30] and the k_{α} is constant when the model is used to evaluate the effect of transformation on flow stress. The measured flow softening index $\Delta\sigma_{\mathrm{m}}$ is expressed by:

$$\Delta\sigma_{\mathrm{m}} = (\sigma_{\mathrm{p}} - \sigma_{\mathrm{ss}})/\sigma_{\mathrm{p}} \qquad (7\text{-}6)$$

Where σ_{p} and σ_{ss} represent the peak and steady-state flow stresses (ε=0.7), respectively.

The alpha phase fraction and $k_{\alpha+\beta}/k_{\alpha}$ were plotted versus strain in **Fig. 7.6**. The alpha phase fraction in the equiaxed microstructures at 900 °C was decreased from 53% to 47% and 45% after the compression to the strains of 0, 0.4 and 0.7 at a strain rate of 0.001 s^{-1}, respectively. The continuous flow softening by dynamic transformation was described by the decrease in $k_{\alpha+\beta}/k_{\alpha}$ during straining from 0 to 0.7. The softening fractions by the transformation ($\Delta\sigma_{\mathrm{dt}}$) were marked by the arrows in the graph. For instance, the flow softening fraction increased from 10.7% to 13.8% with straining from 0.4 to 0.7 at 900 °C. These values were analogous to those at the higher temperatures (12.5% and 15.9% at 950 °C at the strains of 0.4 and 0.7, respectively). The trend of flow softening was consistent with that of the alpha phase fraction.

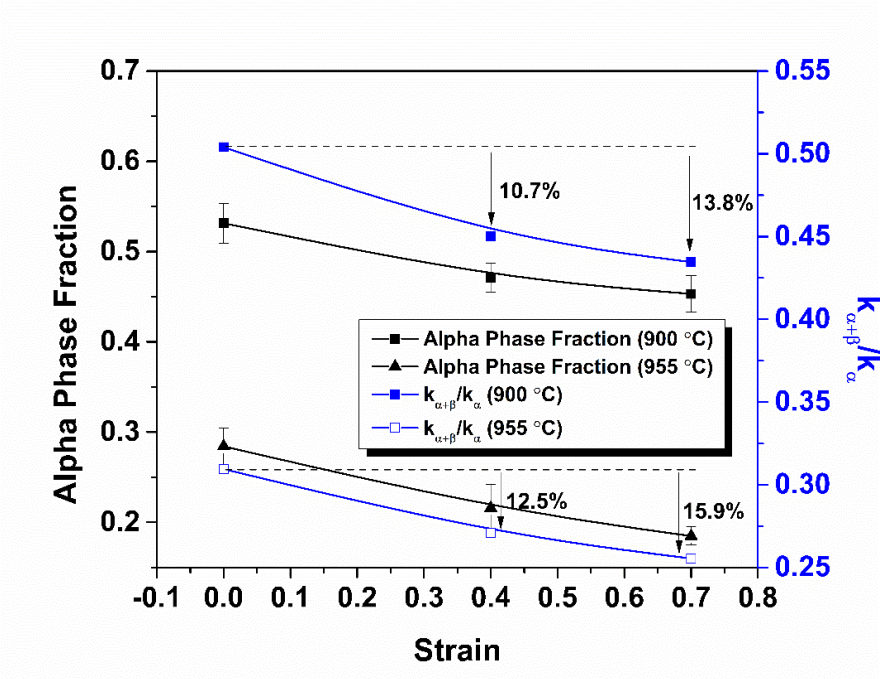

Fig. 7.6 Dependence of beta phase fraction and viscosity coefficient $k_{\alpha+\beta}/k_\alpha$ on the strain at (a) 900 °C and (b) 955 °C at a strain rate of 0.001 s^{-1} in the equiaxed microstructure.

In order to validate the approach, the constitutive relations for alpha and beta phases were used for the evaluation of flow stress and softening in titanium alloys. According to the work by Oikawa and Oomori [31], the flow stress of alpha phase is expressed by: $\sigma_\alpha^{4.6} = K_\alpha(Al)\{exp(273000/RT)\}\dot{\varepsilon}$, where R denotes the gas constant, T is the absolute temperature and phase strength parameter K_α is described by: log K_α = 0.37 *Al*-3.375. In a similar manner, the constitutive equation for beta phase is derived from the work by Oikawa et al. [32]: $\sigma_\beta^{4.2} = K_\beta(V)\{exp(160000/RT)\}\dot{\varepsilon}$, where beta phase strength parameter is expressed by log K_β(V)= 3.387 log V_{eq} - 1.769, and the V_{eq} is described by: (V + 0.27Al + 0Sn + 2Mo + 0.3Zr + Cr) [33]. As discussed by previous works [4, 30], the alloy contents in two phases were varied due to the dynamic transformation and here the compositional variations during straining were considered in the flow stress evaluation, i.e. the changes of K_α and K_β. The contents of aluminum and vanadium in alpha phases were approximately unchanged with temperatures according to the measurements by Semiatin et al. [34] and the compositional variations in beta phases were derived from the equation based on mass balance:

$$C_{\mathrm{m}} = (C_0 - f_\alpha C_\alpha)/(1 - f_\alpha) \qquad (7-7)$$

Where C_0 and f_α represent the overall alloy composition and the alpha phase fraction, respectively, C_{m} represents the alloy concentration of the matrix beta, C_α denotes the equilibrium alloy concentration in alpha phase. By applying **Eq.** (7-2)-(7-5) and **Eq.** (7-7) as well as the Law of Mixtures, the aggregate flow stresses were obtained through the flow stress of alpha and beta phases. The strain rates in alpha and beta phases were derived from the self-consistent model [29]. Then the flow softening fraction based on phase transformation and compositional variation in the equiaxed microstructure are shown in **Table 7.2**. The flow softening fractions derived from the constitutive equations were approximately consistent with those from the self-consistent model. It was found that the composition variation associated with dynamic transformation was not negligible in the flow stress modeling. For example, the flow softening fraction based on constitutive equations decreased from 0.094 to 0.062, 0.073 to 0.053 at 900 °C at the strain rates of 0.1 and 0.01 s^{-1}, respectively, if the compositions of two phases are assumed to be constant during hot deformation.

Table 7.2 Comparison of flow softening fractions derived from dynamic transformation based on self-consistent model and constitutive equations.

Temperature (°C)	Method	Strain rate (s^{-1})		
		0.1	0.01	0.001
900	Self-Consistent Model	0.096	0.093	0.138
	Constitutive Equations	0.094	0.073	0.111
955	Self-Consistent Model	0.106	0.134	0.159
	Constitutive Equations	0.110	0.133	0.150

The effect of dynamic transformation alone on flow stress is determined by the properties of the alpha and beta phases such as their strength or hardness ratios. These parameters between the two phases were approximately unchanged when the samples were deformed at the identical condition irrespective of different morphologies. It is assumed that the flow softening fraction

produced by per transformation fraction (alpha to beta) is same in both equiaxed and lamellar microstructures.

7.4.1.2. Flow softening associated with dynamic transformation

The measured flow softening $\Delta\sigma_{\mathrm{m}}$ and dynamic transformation softening $\Delta\sigma_{\mathrm{dt}}$ in both equiaxed and lamellar microstructures at various temperatures and strain rates are listed in **Table 7.3** and **Table 7.4**. The measured flow softening $\Delta\sigma_{\mathrm{m}}$ in the lamellar microstructure was greater than that in the equiaxed microstructure at the same strain rate and temperature. This was attributed to more sources of softening during the deformation of the lamellar microstructure such as the noticeable texture evolution, dynamic spheroidization and morphological variation. The higher magnitude of flow stress in the lamellar microstructure also contributed to the greater measured softening fraction.

In the equiaxed microstructure, the measured flow softening index increased with the strain rate in **Table 7.3**, which was caused by less dynamic coarsening and more adiabatic heating at the higher strain rates. However, the measured index $\Delta\sigma_m$ was independent on the strain rate in the lamellar microstructure. For example, it only decreased slightly from 43.4% to 40.7% as the strain rate increased from 0.01 s^{-1} to 0.001 s^{-1} at 850 °C shown in **Table 7.4**. This difference indicated that the hardening of dynamic coarsening on the flow stress were more remarkable in equiaxed microstructure than that in the lamellar microstructure. The measured index in lamellar microstructure was approximately stable at 815 and 900 °C at a strain rate of 0.01 s^{-1}, i.e. 43%, and this value decreased to 36% at 955 °C. Similar changes were observed at the lower strain rate of 0.001 s^{-1}. These trends were derived from the texture softening especially at the lower temperatures with more alpha phases. Similar variations were not found in the equiaxed microstructure due to the different softening/hardening mechanisms.

The dynamic transformation softening index $\Delta\sigma_{\mathrm{dt}}$ was approximately the same in both the equiaxed and lamellar microstructures with the identical deformation condition. It seemed that the effects of initial microstructure on the transformation softening is minor, although their influence on the magnitude of flow stress is significant. Note that the dynamic transformation softening index was comparable to the measured flow softening index at 850 °C at a strain rate

of 0.001 s^{-1} in the equiaxed microstructure. The former even exceeded the latter at 900 °C and 955 °C. This revealed that an evident flow hardening behavior existed here and became more dominant at the higher temperatures, i.e. dynamic coarsening of alpha phase.

The proportion of transformation softening in the measured softening can be depicted by the ratio of $\Delta\sigma_{\mathrm{dt}}/\Delta\sigma_{\mathrm{m}}$. In the equiaxed microstructure, the dynamic transformation proportion accounted for 24.4% at 815 °C, 58.2% at 900 °C and 74.6% at 955 °C of the corresponding measured softening at strain rate of 0.01 s^{-1}, suggesting that dynamic transformation became a primary softening mechanism at higher temperatures. Furthermore, this ratio increased noticeably by decreasing strain rate and this signified the dominant role of dynamic transformation in softening especially at lower strain rates. By contrast, the ratio of $\Delta\sigma_{\mathrm{dt}}/\Delta\sigma_{\mathrm{m}}$ was decreased in the lamellar microstructure and the value ranged from 22.4% to 38.7% at a strain rate of 0.01 s^{-1} and from 12.4% to 38.8% at a lower strain rate of 0.001 s^{-1}. The decrease in the $\Delta\sigma_{\mathrm{dt}}/\Delta\sigma_{\mathrm{m}}$ from the lamellar microstructure to the equiaxed was indicative of more sources of softening in the former. For example, dynamic spheriodization occurred in the lamellar microstructure at a relatively high strain such as 0.5 [24, 35] and this phenomenon was observed in the present tests such as at the strain of 0.7 in **Fig. 7.2**. The kinking or bending of the lamellar morphology can produce flow softening as well. Note that the kinking of alpha platelets can be found at the strain of 0.7 in **Fig. 7.2** as well. Similar finding was observed by Mironov et al. [36] and Miller et al. [37] and the kinking was associated with the evolution of shear bands and flow softening. These pertained to the morphological evolution in the lamellar microstructure and were marked as one of the softening sources in **Fig. 7.9**.

Table 7.3 Flow softening index derived from the measurement ($\Delta\sigma_m$) and dynamic transformation prediction ($\Delta\sigma_{dt}$) of Ti-6Al-4V samples with an initial equiaxed microstructure deformed to a strain of 0.7 at different strain rates and temperatures.

Temperature/°C	Strain rate=0.1 (s^{-1})		Strain rate=0.01 (s^{-1})		Strain rate=0.001 (s^{-1})	
	Measurement	Dynamic Transformation	Measurement	Dynamic Transformation	Measurement	Dynamic Transformation
815	--	--	0.228	0.056	0.080	0.043
850	0.255	0.057	0.185	0.049	0.075	0.078
900	0.246	0.096	0.159	0.093	0.125	0.138
955	0.228	0.106	0.179	0.134	0.100	0.159

Table 7.4 Flow softening index of the measurement ($\Delta\sigma_m$) and dynamic transformation prediction ($\Delta\sigma_{dt}$) of Ti-6Al-4V samples with an initial lamellar microstructure deformed to a strain of 0.7 at different strain rates and temperatures.

Temperature/°C	Strain rate=0.01 (s^{-1})		Strain rate=0.001 (s^{-1})	
	Measurement	Dynamic Transformation	Measurement	Dynamic Transformation
850	0.434	0.097	0.407	0.050
900	0.431	0.088	0.418	0.175
955	0.360	0.140	0.359	0.139

The dynamic transformation softening $\Delta\sigma_{dt}$ increased with temperature in both equiaxed and lamellar microstructures at the two strain rates, which can be rationalized by the thermodynamics associated with the transformation. The main energy barrier of the dynamic transformation was Gibbs free energy which was evaluated using the work by present authors [30]. The required Gibbs energy for dynamic transformation was plotted versus temperature with various amounts of transformation (alpha to beta) in **Fig. 7.7**. The values of the Gibbs energy decreased with temperature above 850 °C irrespective of the different amounts of transformation. This trend was not observed at 815 °C with limited amounts of transformation. In the present temperature range and transformation fraction (around 8%), the transformation can take place readily at the higher temperatures due to the lower energy barrier indicated by

the green area in **Fig. 7.7**. This was supported by the previous works by Prada et al. [2] and Guo et al. [10] that the fractional alpha involved in the transformation increased with temperature.

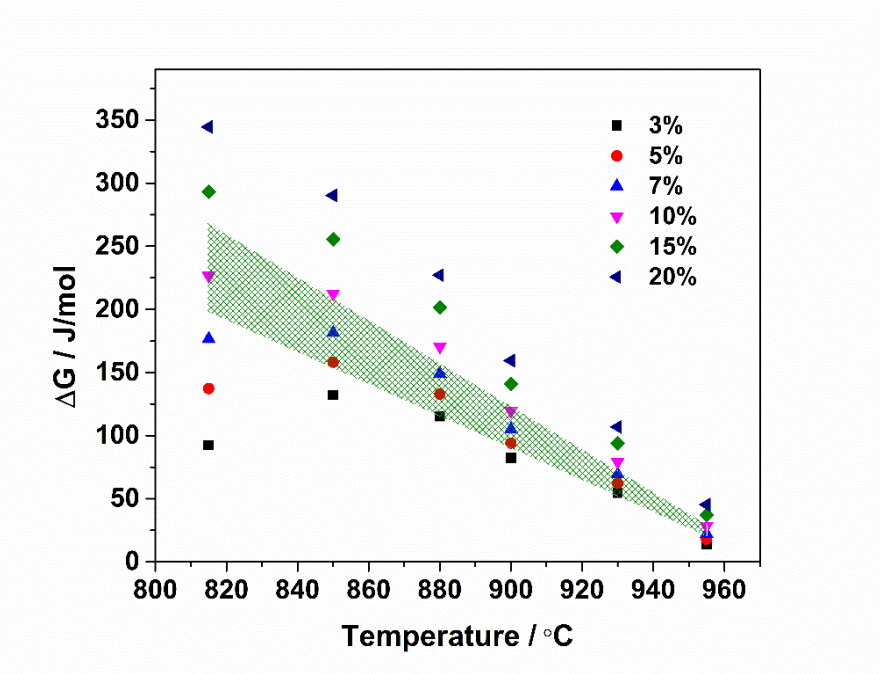

Fig. 7.7 Dependence of the Gibbs energy on temperature with various amounts of dynamic transformation (alpha to beta) ranging from 3% to 20%.

The works by the present authors [30, 38] showed that the driving force (σ_d) for dynamic transformation is described by the flow softening and is defined as: $\sigma_{\mathrm{d}} = \sigma_{\mathrm{critical-alpha}} - \sigma_{\mathrm{yield-beta}}$, where $\sigma_{\mathrm{critical-alpha}}$ denotes the critical stress that activates the dynamic transformation in the alpha phase and usually substituted by its peak stress, and $\sigma_{yield-beta}$ refers to the yield stress of the beta phase. The driving force σ_{d} is increased by the increased stress magnitude at higher strain rates. However, the greater strain rates may lead to the aforementioned adiabatic heating. Thus, a moderate strain rate range of 0.01 s^{-1}-0.001 s^{-1} is proposed here for the study of dynamic transformation by inhibiting the deformation heating and promoting the occurrence of the transformation.

7.4.2. Effect of texture evolution on flow stress

The texture variation of titanium alloys can provide flow softening/hardening especially in the alpha phase. The flow softening/hardening associated with texture evolution can be evaluated via the strength factor in self-consistent model and the Law of Mixtures.

$$\sigma_{\mathrm{mix}} = f_{\alpha} \cdot \sigma_{\alpha} + f_{\beta} \cdot \sigma_{\beta} = f_{\alpha} \cdot \sigma_{\alpha} + f_{\beta} \cdot k_{\beta}/k_{\alpha} \cdot \sigma_{\alpha} \quad (7\text{-}8)$$

Here σ_{α} and σ_{β} denote the stress of alpha and beta phase, respectively, the overall stress is described by the Law of Mixtures using alpha (f_{α}) and beta phase (f_{β}) fractions and strength factors k_{β}/k_{α}. The k_{α} is decreased by the texture softening in the alpha phase. The effect of texture on strength of beta phase is negligible and the k_{β} is assumed to be constant at a fixed temperature in terms of texture evolution. Hence, the overall stress response to the texture evolution of alpha is estimated by the variation of k_{α}, which was associated with the Taylor factor variations. The effect of texture on the flow stress in a polycrystal can be described by: $\sigma = M\ \tau_{\mathrm{crss}}$, where σ denotes the flow stress, *M* the average Taylor factor (a function of texture) and τ_{crss} the critical resolved shear stress (constant) [39].

In the present work, the stress variation of alpha with texture was evaluated using the Taylor factor in the lamellar microstructure. In the compression to a strain of 0.7 at a strain rate of 0.001 s^{-1} at 900 °C, the Taylor factor varied from 3.00 to 2.64 and the strength factor of alpha phase (k_{α}) was decreased by 12%. By inserting this lower k_{α} into **Eq. (7-8)**, the macroscopic stress response to the texture was assessed and it exhibited a 10.3% overall flow softening associated with the texture at the temperature. The approach was applied to other temperatures and the softening by the texture was 11.8% and 8.1% at 815 °C and 955 °C, respectively. In a same manner, the flow softening fraction derived from texture at a higher strain rate of 0.01 s^{-1} was 6.6% and 5.0% at 900 and 955 °C, respectively. The effect of texture on flow stress tends to be evident at the lower temperatures. Similar work [40] showed that the average value of Taylor factor in the Ti-6Al-4V with a lamellar microstructure decreased from 5.1 to 3.7 deformed to a strain of 0.7 at a strain rate of 0.1 s^{-1} at 900 °C. The minor influence of texture on flow stress in equiaxed microstructure was related to the negligible variation in Taylor factor. This was analogous to the

work where the average values of Taylor factor were 2.83, 2.88 and 2.84 with the strain ranging from 0.1 to 0.3 in TA15 titanium alloy with equiaxed microstructure [41].

7.4.3 Influence of dynamic coarsening on flow stress

The loss of Hall-Petch effect strengthening is one of sources of flow softening. This behavior was valid at high strain rates and was not observed at low strain rates. For example, the work by Semiatin and Bieler [18] showed that the peak stresses of Ti-6Al-4V at 815 °C and 900 °C were increased with the inverse spare root of alpha platelet thickness at the strain rates of 0.1, 1.0 and 10.0 s^{-1} in the lamellar microstructure. However, the peak stress was approximately unchanged at lower strain rates of 0.01 and 0.001 s^{-1}. This suggested that the flow stresses with lamellar microstructure were independent of alpha platelet thickness in the present tests and Hall-Petch was unable to account for the flow behavior here.

The dynamic coarsening was the primary source of flow hardening at low strain rates and it was controlled by bulk diffusion and can occur more readily during the longer deformation time. The coarsening behavior gave rise to the loss of grain boundaries which acted as the sources of deformation at elevated temperatures. As described in **Fig. 7.3**, the deformation mechanism transitioned from pow-law creep to superplastic deformation via grain boundary sliding when the value of strain rate sensitivity increased from 0.2 at the strain rates of 0.1 and 0.01 to 0.4 at a strain rate of 0.001 s^{-1} at these temperatures. The relation between superplastic flow behavior and grain size associated with dynamic coarsening was described by the Bird-Mukherjee-Dorn generalized constitutive relation [42]:

$$\dot{\varepsilon} = \left(\frac{\mathrm{A}DGb}{\mathrm{k}T}\right)\left(\frac{\sigma}{G}\right)^{\mathrm{n}}\left(\frac{b}{d}\right)^{\mathrm{p}} \qquad (7-9)$$

Here A denotes a constant, D is a diffusion parameter, G is the shear modulus, b is the length of the Burgers vector, k is Boltzmann's constant, σ is the flow stress, d is the grain diameter of alpha particle based on the Gifkins model of superplastic deformation [43], n is the stress exponent and its value is equal to the inverse of strain rate sensitivity (m), p is the grain size exponent. This constitutive relation is further depicted by the normalized form $\sigma/\sigma_0 = (d/d_0)^{p/n}$, which indicated that the superplastic flow stress is determined by the diameter of grain size of alpha particles.

The ratio of p/n is derived from the d(ln(σ))/d(ln(d)) and the data on the flow stress and grain size from the work by Ghosh and Hamilton [44] was used. Results showed that the ratio was 0.7 and 1.0 at 927 °C at the strain rates of 0.001 s^{-1} and 0.0002 s^{-1}, respectively. Similar findings by Paton and Hamilton [45] showed that the ratio of p/n at 927 °C was 0.1 and 0.6 at the strain rates of 0.008 s^{-1} and 0.0008 s^{-1}, respectively. In the present work, the ratios of 0.1 ($\dot{\varepsilon}$=0.01 s^{-1}) and 0.7 ($\dot{\varepsilon}$=0.001 s^{-1}) were used to determine effects of coarsening on flow stress at 900 and 955 °C. By applying this correlation and coefficients, the flow stress at a strain rate of 0.001 s^{-1} was increased by 0.39 and 0.46 times due to the dynamic coarsening at 900 °C and 955 °C, respectively. As shown in **Table 7.1**, the predicted stress in the absence of dynamic coarsening was 15.2 MPa (measured stress=21.1 MPa) at 900 °C and 12.7 MPa (measured stress=18.6 MPa) at 955 °C deformed to a strain of 0.7 at a strain rate of 0.001 s^{-1}. By increasing the strain rate to 0.01 s^{-1}, the flow stress (ε=0.7) was decreased from 57.5 MPa to 55.7 MPa at 900 °C and from 32.4 MPa to 31.5 MPa at 955 °C via eliminating dynamic coarsening. By comparison, it can be found that the effect of dynamic coarsening on flow hardening was greater at the lower strain rate. The flow hardening by dynamic coarsening at relatively high strain rates (0.1 and 0.01 s^{-1}) was negligible at elevated temperatures.

The roles of each factor in the flow behavior at elevated temperatures were plotted in the stress-strain curves to illustrate the softening/hardening mechanism in the hot deformation. The thick lines (black) denote the measured flow stress and the flow softening/hardening derived from each behavior was indicated by the thin lines (gray) and arrows. **Fig. 7.8**(a) and (b) described the flow stress of the equiaxed microstructures at a strain rate of 0.1 s^{-1}, in which dynamic transformation and adiabatic heating served as the primary softening mechanisms. At a lower strain rate of 0.01 s^{-1} in **Fig. 7.8**(c) and (d), the transformation also acted as the major softening source and the softening associated with adiabatic heating was around 4% and not marked in the figure here. Further decreasing the strain rate to 0.001 s^{-1}, dynamic coarsening was dominant in the flow hardening as indicated by the gray lines in **Fig. 7.8**(e) and (f), suggesting the predicted flow curves in the absence of dynamic coarsening; the predicted flow stresses were substantially reduced at the strain rate of 0.001 s^{-1} compared with the measured stresses and these two values tended to be same at the higher strain rate of 0.01 s^{-1} in **Fig. 7.8**(c) and (d). In the lamellar

microstructure, the softening proportions by transformation and texture were comparable at different strain rates and temperatures in **Fig. 7.9**; the morphological evolution was predominant in the flow softening and outweighed the contribution from either transformation or texture. As aforementioned, the morphological effects involved the kinking and spheroidization of lamellar alpha phases according to the present observation.

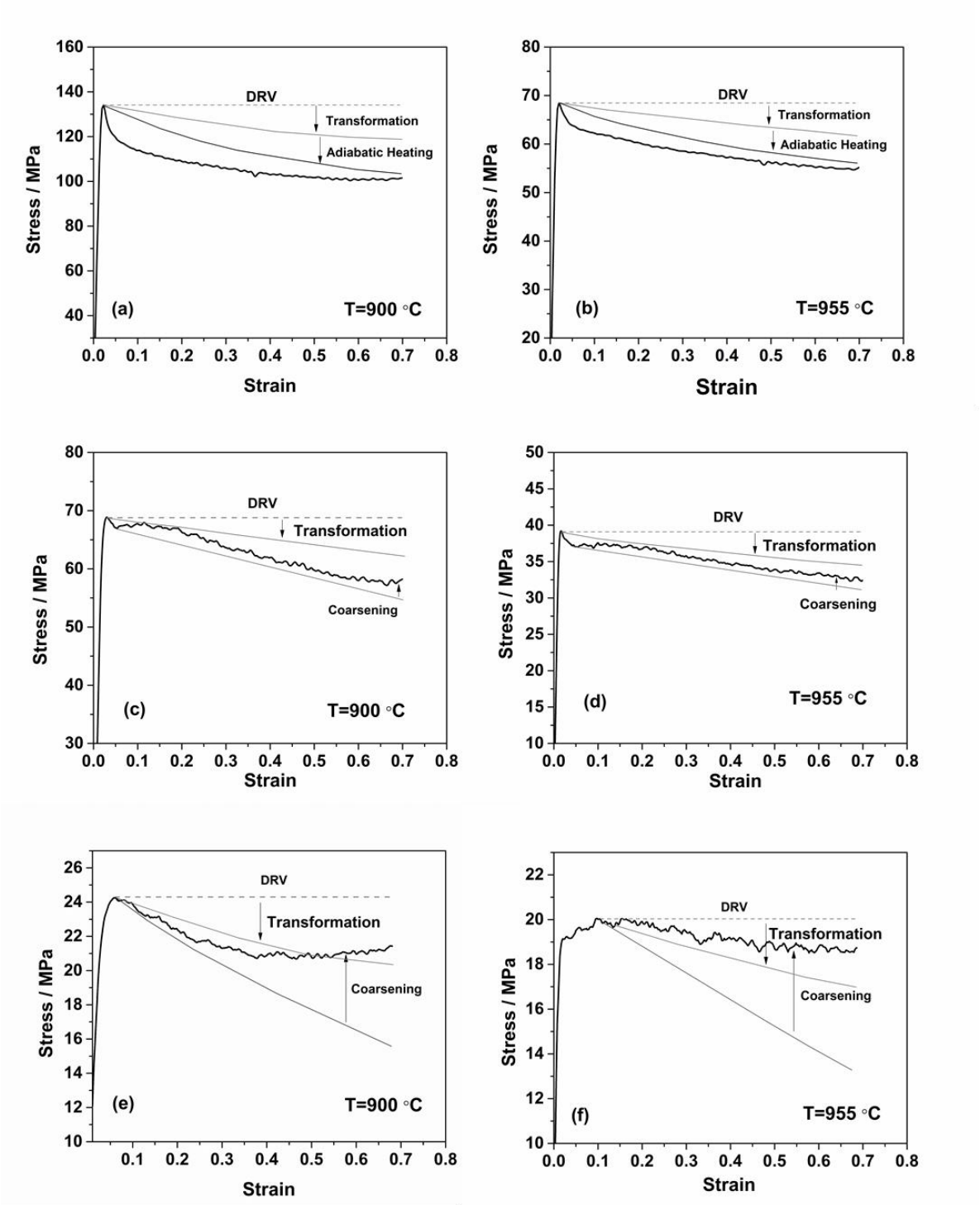

Fig. 7.8 Stress-strain curves and flow hardening/softening components of the Ti-6Al-4V samples with initial equiaxed microstructures deformed at strain rates of (a) (b) 0.1 s^{-1}, (c) (d) 0.01 s^{-1} and (e) (f) 0.001 s^{-1}. The test temperatures are marked on each figure.

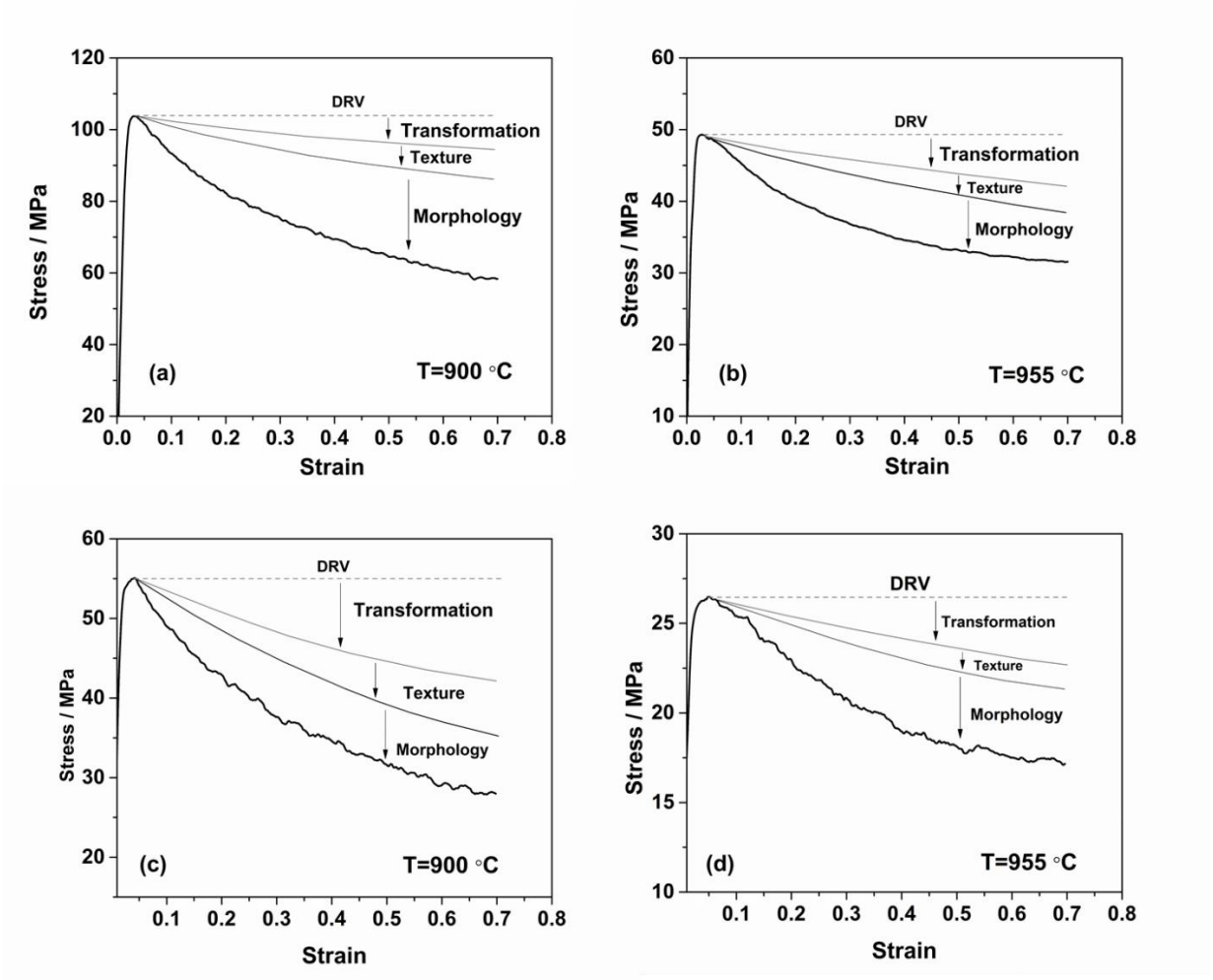

Fig. 7.9 Stress-strain curves and flow softening components of Ti-6Al-4V samples with initial lamellar microstructures at strain rates of (a) (b) 0.01 s^{-1}, (c) (d) 0.001 s^{-1}. The test temperatures are marked on each picture.

7.4.4 Effect of dynamic transformation on flow stress in other titanium alloys.

The dynamic transformation in IMI 834 alloy was discussed here in terms of its effects on the flow softening. The present method based on self-consistent model was extended to the softening prediction of the IMI 834 alloy. The dynamic transformation in IMI 834 alloy with an initial equiaxed microstructure was observed by Jonas et al. [11]. They found that the beta phase fraction was increased from 49% to 72% at 975 °C, from 68% to 89% at 1000 °C, 71% to 92% at 1025 °C during the isothermal compression at strain rate of 0.01 s^{-1} to a strain of 1.0. The alpha phase fraction was decreased by around 20% at each temperature. However, the fraction was

only 10% in Ti-6Al-4V alloy in a similar deformation condition as shown in **Fig. 7.6**. This was possibly related to the difference in the composition of titanium alloys. For instance, the kinetics of the transformation was deteriorated by the higher content of vanadium in Ti-6Al-4V due to its sluggish diffusion rate. Additionally, the strain applied in their work was also greater than that in **Fig. 7.6**.

Based on **Eq. (7-2)**-**Eq. (7-5)**, the predicted flow softening index by dynamic transformation ($\Delta\sigma_{dt}$) was obtained. The strain rate sensitivity here was 0.25 in the present deformation condition. The ratio of k_α/k_β in IMI 834 was 3.12, 3.15, 3.20 at 975, 1000 and 1025 °C, respectively [33]. The flow softening indices from both measurement and prediction by dynamic transformation at three temperatures were listed in **Table 7.5**. The measured flow softening index ranged from 25.0% to 27.4% and the softening index by dynamic transformation varied from 22.6% to 23.5%. These two indices are both greater than those in Ti-6Al-4V alloy in a comparable deformation condition through comparing **Table 7.3** with **Table 7.5**. Since the proportion of beta phase produced by hot compression in IMI 834 was around one time higher than in Ti-6Al-4V, more softening was generated in the dynamic transformation softening as well as the measured softening.

The dynamic transformation softening in IMI 834 alloy was slightly lower than the total measured softening. This signified that the dynamic transformation served as the primary source of flow softening in IMI 834 alloy and other factors such as texture or coarsening had little effects on the flow stress here.

Table 7.5 Flow softening index derived from the measurement and dynamic transformation prediction of IMI 834 samples deformed to a strain of 1.0 at a strain rate of 0.01 s^{-1}.

Temperature / °C	**Softening**	
	Measured	Dynamic Transformation
975	0.274	0.226
1000	0.250	0.235
1025	0.267	0.233

The dynamic transformation behavior can be affected by the deformation method (compression/tensile test). The developed approach in the present work was applied to tensile

tests for the estimate of flow softening from dynamic transformation. For instance, the tensile tests carried out by Yang et al. [3] exhibited a noticeable increase in beta phase fraction in Ti-6Al-4V and the softening index by dynamic transformation was 28% with strain ranging from 0.4 to 0.8 at 850 °C at a strain rate of 0.0001 s^{-1}. Similar tensile experiment by Prada et al. [2] indicated that the softening index by dynamic transformation was 13% with strain varying from 0.4 to 0.8 at 815 °C at a strain rate of 0.0002 s^{-1}. However, this index in the present compression test was only 4.3% at 815 °C and 7.8% at 850 °C with similar microstructures and strain rates. This discrepancy can be derived from the different deformation modes. Similar results by Miller et al. [37] also showed that the extent of flow softening was greater in the tension deformation than in the compression test. More softening in the equiaxed microstructure is expected at low strain rates such as 0.001 s^{-1} when the flow hardening by dynamic coarsening is eliminated in **Fig. 7.8**(e) and (f). However, dynamic transformation accounts for less than 50% of the overall softening and the remaining softening sources in **Fig. 7.8**(c)(d) and (e)(f) are still unknown and need further investigations.

7.5 Conclusions

The role of dynamic transformation in the equiaxed and lamellar microstructures was compared at different strain and strain rates based on the isothermal compression and self-consistent modelling analyses. An approach was proposed to evaluate the flow softening from dynamic transformation. The conclusions were made as follows:

(1) Dynamic transformation from alpha to beta was observed in both equiaxed and lamellar microstructures of the Ti-6Al-4V alloy. The amount of transformation and fractional flow softening derived from the transformation were approximately equal in the two initial microstructures. However, the measured flow softening in the equiaxed microstructure was greater than in the lamellar microstructure.

(2) Dynamic transformation acted as the primary source of flow softening in the equiaxed microstructure especially at low strain rates, while its contribution to the flow softening in the lamellar microstructure was substantially diminished. The greater softening in the lamellar

structure was ascribed to the texture softening, morphological variations and the limited amounts of dynamic coarsening.

(3) The texture softening in the lamellar microstructure accounted for 10% of the flow softening at 900 °C and this proportion decreased with temperature. The contribution of texture to the softening in the equiaxed microstructure was negligible. Dynamic coarsening was a primary source of flow hardening in the equiaxed microstructure particularly at the low strain rate of 0.001 s^{-1}.

(4) Adiabatic heating at the high strain rate may confound heating-induced with stress-induced transformation. The lower strain rates decreased the driving force for the transformation and impeded the reaction. Hence, an appropriate strain rate for observing dynamic transformation lies in the range from 0.01 s^{-1} to 0.001 s^{-1}.

(5) Dynamic transformation accounted for the majority of the flow softening in the IMI 834 alloy during compression to a strain of 0.7 at a strain rate of 0.01 s^{-1}. This was analogous to the softening observed in the Ti-6Al-4V alloy under the same test conditions.

References

[1] A. Dutta, N. Birla, Stress induced hydrogen diffusion in a α+β titanium alloy during superplastic deformation, Scripta metallurgica 21(8) (1987) 1051-1054.

[2] B.H. Prada, J. Mukhopadhyay, A.K. Mukherjee, Effect of strain and temperature in a superplastic Ni-modified Ti–6Al–4V Alloy, Materials Transactions, JIM 31(3) (1990) 200-206.

[3] G. Gurewitz, Mechanical behavior and microstructural evolution during superplastic deformation of Ti–6Al–4V, Materials Transactions, JIM 32(5) (1991) 465-472.

[4] J. Koike, Y. Shimoyama, I. Ohnuma, T. Okamura, R. Kainuma, K. Ishida, K. Maruyama, Stress-induced phase transformation during superplastic deformation in two-phase Ti–Al–Fe alloy, Acta materialia 48(9) (2000) 2059-2069.

[5] C. Lu, L. Huang, L. Geng, B. Kaveendran, Z. Zheng, J. Zhang, Mechanisms behind the superplastic behavior of as-extruded TiBw/Ti6Al4V composites with a network architecture, Materials Characterization 104 (2015) 139-148.

[6] S. Chen, J. Huang, D. Cheng, H. Zhang, X. Zhao, Superplastic deformation mechanism and mechanical behavior of a laser-welded Ti–6Al–4V alloy joint, Materials Science and Engineering: A 541 (2012) 110-119.

[7] H. Matsumoto, T. Nishihara, Y. Iwagaki, T. Shiraishi, Y. Ono, A. Chiba, Microstructural evolution and deformation mode under high-temperature-tensile-deformation of the Ti-6Al-4V alloy with the metastable α' martensite starting microstructure, Materials Science and Engineering: A 661 (2016) 68-78.

[8] Y. Zong, D. Shan, M. Xu, Y. Lv, Flow softening and microstructural evolution of TC11 titanium alloy during hot deformation, Journal of materials processing technology 209(4) (2009) 1988-1994.

[9] L. Jing, R. Fu, Y. Wang, L. Qiu, B. Yan, Discontinuous yielding behavior and microstructure evolution during hot deformation of TC11 alloy, Materials Science and Engineering: A 704 (2017) 434-439.

[10] B. Guo, S.L. Semiatin, J.J. Jonas, S. Yue, Dynamic transformation of Ti–6Al–4V during torsion in the two-phase region, Journal of Materials Science 53 (2018) 9305-9315.

[11] J.J. Jonas, C. Aranas Jr, A. Fall, M. Jahazi, Transformation softening in three titanium alloys, Materials & Design 113 (2017) 305-310.

[12] K. Wang, G. Liu, W. Tao, J. Zhao, K. Huang, Study on the mixed dynamic recrystallization mechanism during the globularization process of laser-welded TA15 Ti-alloy joint under hot tensile deformation, Materials Characterization 126 (2017) 57-63.

[13] T. Zhang, Y. Liu, D.G. Sanders, B. Liu, W. Zhang, C. Zhou, Development of fine-grain size titanium 6Al–4V alloy sheet material for low temperature superplastic forming, Materials Science and Engineering: A 608 (2014) 265-272.

[14] H. Matsumoto, V. Velay, A. Chiba, Flow behavior and microstructure in Ti–6Al–4V alloy with an ultrafine-grained α-single phase microstructure during low-temperature-high-strain-rate superplasticity, Materials & Design 66 (2015) 611-617.

[15] B. Babu, L.-E. Lindgren, Dislocation density based model for plastic deformation and globularization of Ti-6Al-4V, International Journal of Plasticity 50 (2013) 94-108.

[16] X. Fan, H. Yang, Internal-state-variable based self-consistent constitutive modeling for hot working of two-phase titanium alloys coupling microstructure evolution, International Journal of Plasticity 27(11) (2011) 1833-1852.

[17] X. Fan, X. Jiang, X. Zeng, Y. Shi, P. Gao, M. Zhan, Modeling the anisotropy of hot plastic deformation of two-phase titanium alloys with a colony microstructure, International Journal of Plasticity 104 (2018) 173-195.

[18] S.L. Semiatin, T. Bieler, The effect of alpha platelet thickness on plastic flow during hot working of Ti–6Al–4V with a transformed microstructure, Acta materialia 49(17) (2001) 3565-3573.

[19] S.L. Semiatin, B. Kirby, G. Salishchev, Coarsening behavior of an alpha-beta titanium alloy, Metallurgical and Materials Transactions A 35(9) (2004) 2809-2819.

[20] S.L. Semiatin, T. Bieler, Effect of texture and slip mode on the anisotropy of plastic flow and flow softening during hot working of Ti-6Al-4V, Metallurgical and Materials Transactions A 32(7) (2001) 1787-1799.

[21] I. Weiss, S.L. Semiatin, Thermomechanical processing of alpha titanium alloys—an overview, Materials Science and Engineering: A 263(2) (1999) 243-256.

[22] I. Weiss, S.L. Semiatin, Thermomechanical processing of beta titanium alloys—an overview, Materials Science and Engineering: A 243(1-2) (1998) 46-65.

[23] E. Poliak, J. Jonas, A one-parameter approach to determining the critical conditions for the initiation of dynamic recrystallization, Acta Materialia 44(1) (1996) 127-136.

[24] S.L. Semiatin, V. Seetharaman, I. Weiss, Flow behavior and globularization kinetics during hot working of Ti–6Al–4V with a colony alpha microstructure, Materials Science and Engineering: A 263(2) (1999) 257-271.

[25] S. Semiatin, G. Lahoti, Deformation and unstable flow in hot forging of Ti-6Ai-2Sn-4Zr-2Mo-0.1 Si, Metallurgical Transactions A 12(10) (1981) 1705-1717.

[26] R. Hill, A self-consistent mechanics of composite materials, Journal of the Mechanics and Physics of Solids 13(4) (1965) 213-222.

[27] P. Suquet, Overall potentials and extremal surfaces of power law or ideally plastic composites, Journal of the Mechanics and Physics of Solids 41(6) (1993) 981-1002.

[28] J.H. Kim, S. Semiatin, Y.H. Lee, C.S. Lee, A self-consistent approach for modeling the flow behavior of the alpha and beta phases in Ti-6Al-4V, Metallurgical and Materials Transactions A 42(7) (2011) 1805-1814.

[29] S.L. Semiatin, F. Montheillet, G. Shen, J.J. Jonas, Self-consistent modeling of the flow behavior of wrought alpha/beta titanium alloys under isothermal and nonisothermal hot-working conditions, Metallurgical and Materials Transactions A 33(8) (2002) 2719-2727.

[30] B. Guo, S.L. Semiatin, J. Liang, B. Sun, J.J. Jonas, Opposing and Driving Forces Associated with the Dynamic Transformation of Ti-6Al-4V, Metallurgical and Materials Transactions A 49(5) (2018) 1450-1454.

[31] H. Oikawa, T. Oomori, Steady state deformation characteristics of α-Ti Al solid solutions, Materials Science and Engineering: A 104 (1988) 125-130.

[32] H. Oikawa, K. Nishimura, M. Cui, High-temperature deformation of polycrystalline beta titanium, Scripta metallurgica 19(7) (1985) 825-828.

[33] P. Vo, M. Jahazi, S. Yue, P. Bocher, Flow stress prediction during hot working of near-α titanium alloys, Materials Science and Engineering: A 447(1-2) (2007) 99-110.

[34] S.L. Semiatin, S. Knisley, P. Fagin, D. Barker, F. Zhang, Microstructure evolution during alpha-beta heat treatment of Ti-6Al-4V, Metallurgical and Materials Transactions A 34(10) (2003) 2377-2386.

[35] S. Zherebtsov, M. Murzinova, G. Salishchev, S. Semiatin, Spheroidization of the lamellar microstructure in Ti–6Al–4V alloy during warm deformation and annealing, Acta Materialia 59(10) (2011) 4138-4150.

[36] S. Mironov, M. Murzinova, S. Zherebtsov, G. Salishchev, S. Semiatin, Microstructure evolution during warm working of Ti–6Al–4V with a colony-α microstructure, Acta Materialia 57(8) (2009) 2470-2481.

[37] R. Miller, T. Bieler, S. Semiatin, Flow softening during hot working of Ti-6Al-4V with a lamellar colony microstructure, Scripta materialia 40(12) (1999) 1387-1394.

[38] J.J. Jonas, C. Ghosh, Role of mechanical activation in the dynamic transformation of austenite, Acta Materialia 61(16) (2013) 6125-6131.

[39] H. Mecking, U. Kocks, C. Hartig, Taylor factors in materials with many deformation modes, Scripta materialia 35(4) (1996).

[40] C.H. Park, J.H. Kim, Y.-T. Hyun, J.-T. Yeom, N. Reddy, The origins of flow softening during high-temperature deformation of a Ti–6Al–4V alloy with a lamellar microstructure, Journal of Alloys and Compounds 582 (2014) 126-129.

[41] G. Liu, K. Wang, B. He, M. Huang, S. Yuan, Mechanism of saturated flow stress during hot tensile deformation of a TA15 Ti alloy, Materials & Design 86 (2015) 146-151.

[42] J. Bird, A. Mukherjee, J. Dorn, Quantitative relation between properties and microstructure, Israel Universities Press, Jerusalem, 255 (1969).

[43] R.C. Gifkins, Grain-boundary sliding and its accommodation during creep and superplasticity, Metallurgical transactions a 7(8) (1976) 1225-1232.

[44] A. Ghosh, C. Hamilton, Mechanical behavior and hardening characteristics of a superplastic Ti-6AI-4V alloy, Metallurgical transactions A 10(6) (1979) 699-706.

[45] N. Paton, C. Hamilton, Microstructural influences on superplasticity in Ti-6AI-4V, Metallurgical Transactions A 10(2) (1979) 241-250.

Chapter 8

Effect of Multipass Deformation at Elevated Temperatures on the Flow Behavior and Microstructural Evolution in Ti-6Al-4V

In this chapter, the effects of dynamic transformation on flow stress were further studied in Ti-6Al-4V during multipass deformation. The torsion tests were carried out for the simulation of multipass deformation with various interpass times. Dynamic and reverse transformation were observed during the deformation and the interpass holding time, respectively. In the meanwhile, coarsening took place as well in the process and served as the flow hardening mechanism.

- This chapter has been published: **Baoqi Guo** *, Clodualdo Aranas Jr., Anes Foul, Xiankun Ji, Ameth Fall, Mohammad Jahazi, John J. Jonas. Effect of multipass deformation at elevated temperatures on the flow behavior and microstructural evolution in Ti-6Al-4V. Materials Science and Engineering: A, 2018, 729: 119-124.

Abstract

Simulated multipass deformation experiments were carried out via torsion testing on a Ti-6Al-4V alloy in the two-phase region under both isothermal and continuous cooling conditions. Flow softening was observed during the isothermal multipass deformation tests as indicated by the evolution of the mean flow stress (MFS). The MFS values increased with interpass time from 2s to 32s. Using BSE-SEM characterization techniques, dynamic phase transformation (alpha to beta) and coarsening of the alpha phase took place. The quantitative results indicate that the alpha phase transforms into beta during straining, but it retransforms statically into alpha by amounts that increase with interpass time. The flow softening observed is the net result of softening by dynamic transformation and hardening by reverse transformation.

8.1 Introduction

Research by Murty et al. [1] has shown that the multipass hot rolling of Ti-6Al-4V improves mechanical properties such as the yield strength and ultimate tensile strength due to the associated microstructural and texture changes. In the two-pass isothermal compression tests carried out by Fan et al. [2] on a near-alpha titanium alloy, the net flow softening was shown to be dependent on the interpass time. Isothermal multipass rolling tests were performed between 700°C and 950°C on Ti-6Al-4V by Nayan et al. [3], in which they determined the dependence of the beta phase fraction on rolling temperature. Zherebtsov et al. [4] produced a microstructure of homogenous submicrocrystalline Ti-6Al-4V by using multistep isothermal forging under superplastic conditions. Similar multistep isothermal forging tests were conducted on Ti-6Al-4V by Salishchev et al. [5] to study the microstructural characteristics.

One-pass compression tests during cooling by Fan et al. [6] showed that the change in phase fraction during deformation generated a difference of 53.4% between calculated and experimental flow stresses. The evolution of an initial lamellar into an equiaxed structure during non-isothermal multiforging has been described by Kim et al. [7]. Salem et al. [8] investigated the effects of different temperatures and heating schedules during the multipass rolling of Ti-6Al-4V on the microstructure and texture development. More systematic investigations of texture evolution and globularization in Ti-6Al-4V have also been reported [9, 10].

Most of these studies focused on the morphological evolution of the phases and on texture evolution, while relevant data with respect to dynamic phase transformation and coarsening [11-15] are mostly lacking. Furthermore, the relations between the flow behavior and interpass time as well as microstructural evolution in the multi deformation of the Ti-6Al-4V are unknown. In the present work, seven-pass torsion testing was adopted to mimic multipass deformation under both isothermal and continuous cooling conditions. The relation between the flow behavior and the microstructural evolution was then established by quantifying the volume fraction and dimensions of the alpha phase.

8.2 Experimental procedure

8.2.1 Thermomechanical Schedule

The present material contained 6.54 % aluminum, 4.14 % vanadium, 0.18 % iron, 0.17 % oxygen, 0.03 % carbon, 0.03 % nitrogen (all in weight percent), the balance being titanium. The transus temperature of this alloy was estimated to be about 1015°C by means of differential thermal analysis (DTA). The as-received material was equiaxed and was machined into torsion samples with diameters of 6.3 mm and gauge lengths of 22.2 mm. Two routes of multipass torsion were employed here, i.e. testing under (i) isothermal and (ii) continuous cooling conditions. The tests were performed on a servohydraulic MTS torsion machine equipped with a horizontal radiation furnace and a temperature controller. The torque-twist curves were converted into stress-strain curves using the Fields and Backofen formulae [16]. A thermocouple was welded to the center of each sample to allow the deformation temperature to be tracked with accuracy. An argon protective atmosphere was used to reduce oxidation during torsion.

For the isothermal tests, the samples were heated at 2°C/s to the deformation temperature of 940°C and then held for 15 min prior to deformation to reach equilibrium. They were deformed monotonically to true strains of 0.4 at a strain rate of 0.05 s^{-1} during each pass and were water quenched. Interpass times of 2s, 8s, 16s and 32s were employed to determine their effects on the flow stress and microstructure. Samples were water quenched after the 1^{st}, 4^{th}, and 7^{th} passes, as shown in Fig. 8.1(a).

In the continuous cooling tests, the same heating rates, deformation temperatures, holding times and strains and strain rates were employed as in isothermal testing, as shown in Fig. 8.1(b). The samples were cooled at 1°C/s during testing and interpass times of 2s and 8s were used. After testing, the samples were quenched with water.

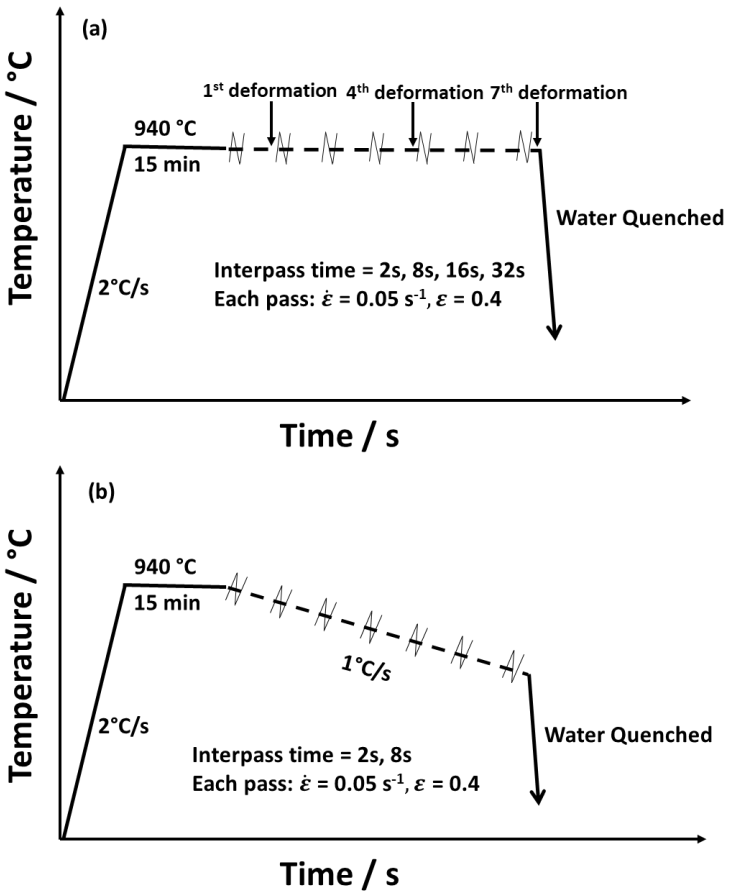

Fig. 8.1 Schematic representations of the multipass torsion tests carried out under (a) isothermal and (b) continuous cooling conditions at 1 °C/s. Strains of 0.4 were applied at a strain rate of 0.05 s^{-1}. Samples were water quenched after the indicated passes to preserve the respective microstructures.

8.2.2 Metallography

Samples were cut transversely for microstructural examination and mounted using a phenolic mounting resin. SiC papers from 400 to 1200 grit were used for grinding. Polishing was carried out with 3 µm and 1 µm diamond suspensions and a colloidal silica suspension was employed for final polishing. The microstructures were examined using backscattered electron imaging (BSEI) in a scanning electron microscope (SEM). In the BSEI micrograghs, the beta/transformed beta is white and alpha appears dark. The volume fractions of the alpha phase were evaluated on the basis of five micrographs for each sample. These fractions were determined using the ImageJ software. The alpha particle radius was derived from the average alpha particle size (A_α)

according to the circle equivalent area method. Here the average alpha particle size (A_α) was estimated using the equation $A_\alpha = f_\alpha A/N$, where A is the total area of the micrograph, N is the number of alpha particles and f_α denotes the volume fraction of the alpha phase [13]. Particles with "dog-leg" morphologies were treated as being 1.5 particles in quantity. The BSEI photographs were taken at different magnifications to ensure that at least 600 alpha particles were sampled.

8.3 Results and Discussion

8.3.1 Flow behavior during multipass torsion

The stress-strain curves determined by means of 7-pass torsion testing at 940°C at a strain rate of 0.05 s^{-1} are displayed in Fig. 8.2. Here, the effects of 2s, 8s, 16s and 32s interpass times are shown. There is evident flow softening in all the interpass time tests, especially when the interpass time is short.

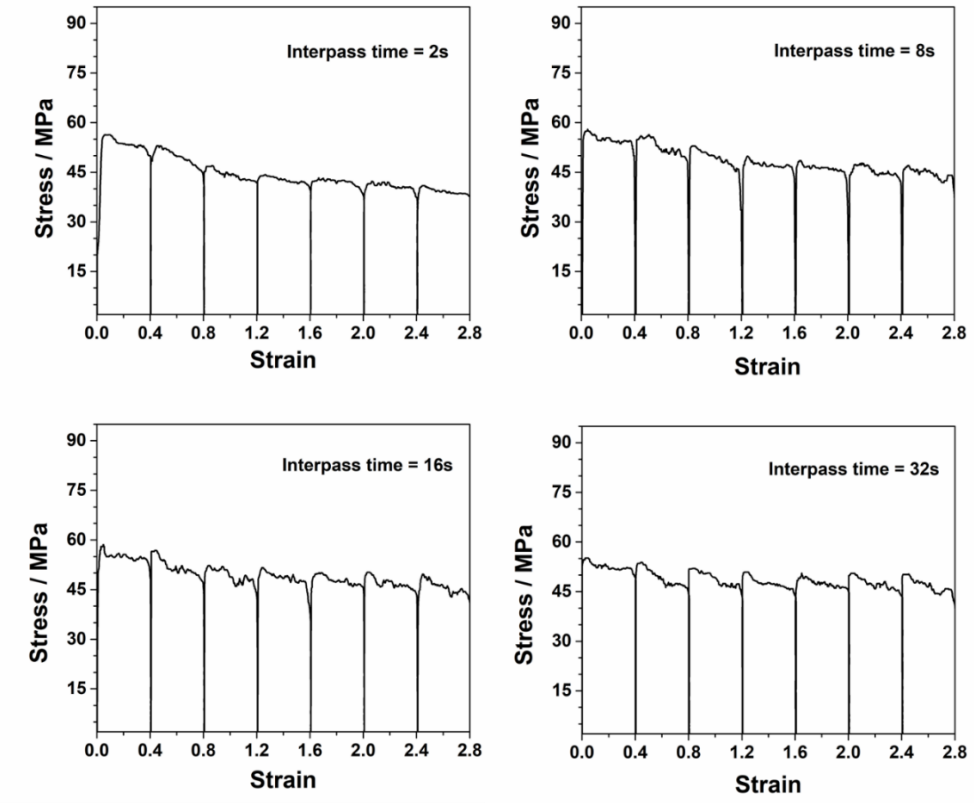

Fig. 8.2 Stress-strain curves recorded during the seven-pass torsion tests of Fig. 8.1(a) show a lesser amount of softening with increasing interpass time.

The stress-strain curves associated with cooling at 1°C/s are shown in Fig. 8.3. When the interpass time is 2s, the flow curves exhibit initial softening followed by work hardening as the strain is increased. When the interpass time is increased from 2s to 8s, there is progressively more strain hardening. The temperature at the endpoint of each pass is indicated at the top of Fig. 8.3. When the interpass time is 2s, the temperature decreased from 940°C to 872°C during cooling. It dropped from 940°C to 835°C when the interpass time was 8s.

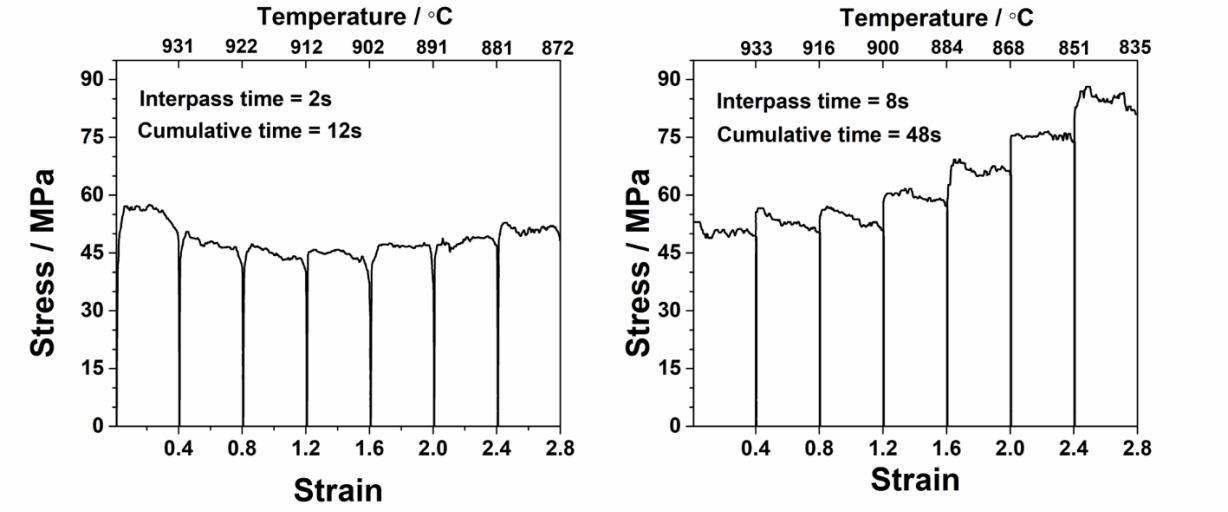

Fig. 8.3 Stress-strain curves associated with seven-pass torsion tests carried out under the conditions of continuous cooling in Fig. 8.1(b) show a decreasing flow stress with shorter interpass time and increasing stress with longer interpass time. The endpoint temperature of each pass is indicated at the top of each figure.

8.3.2 Mean flow stress

The mean flow stress (MFS) was employed here to provide insight into the microstructural evolution. It is defined here as [17]:

$$MFS = \frac{1}{\varepsilon_b - \varepsilon_a} \int_{\varepsilon_a}^{\varepsilon_b} \sigma d\varepsilon \qquad (8-1)$$

Here ε_a and ε_b denote the strains associated with the beginning and end of the strain interval, ε is the true strain and σ is the flow stress. The MFS curves associated with interpass times of 2s, 8s, 16s and 32s are displayed in Fig. 8.4. The MFS values decrease with pass number (i.e. strain)

indicating that flow softening takes place during strain accumulation. It is of interest that shorter interpass times give rise to more flow softening.

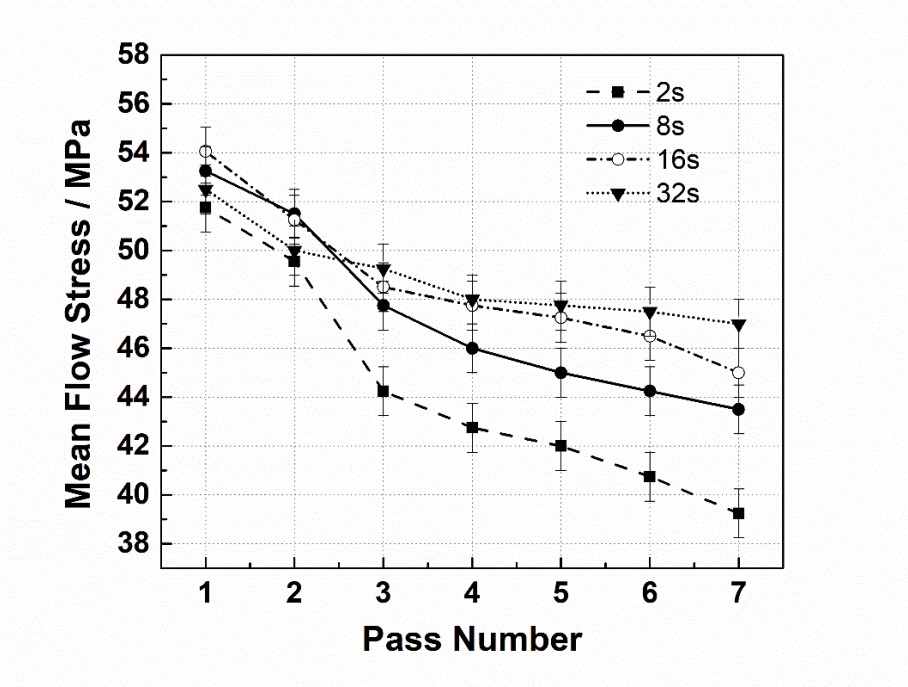

Fig. 8.4 Dependence of the mean flow stress on pass number as derived from the isothermal flow curves of Fig. 8.2.

8.3.3 Microstructural evolution

The microstructures associated with interpass times of 2s, 8s, 16s and 32s are presented in Fig. 8.5. It can be seen that the alpha phase coarsens while the material is being subjected to seven passes using various interpass times. Evident decreases in alpha phase fraction took place when short interpass times such as 2s were employed. The alpha phase fraction and alpha particle radius are quantified by Fig. 8.6. The alpha phase fractions of the undeformed samples are the equilibrium values associated with long-time annealing of the Ti-6Al-4V at 940°C. After undergoing the seven-pass torsions tests, the alpha phase fraction was decreased with different interpass times, i.e. the occurrence of dynamic transformation (from alpha to beta). The transformation has been shown to take place displacively during hot deformation on both titanium and steel. Shear stress imposed on the habit plane acts as the driving force, which makes the reaction initiate and develop rapidly [17, 18].

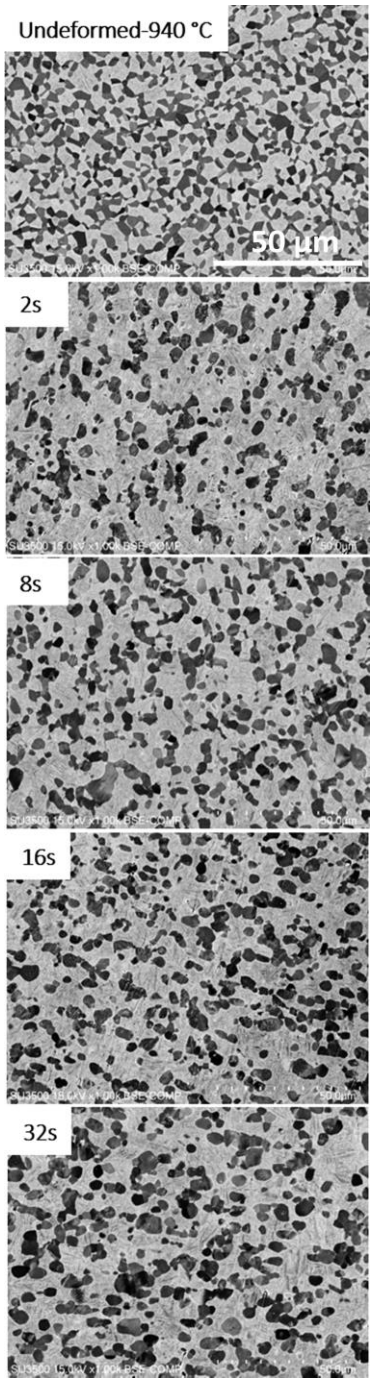

Fig. 8.5 SEM-BSE microstructures produced by the seven-pass torsion tests (ε = 2.8) of Fig. 8.1(a) associated with interpass times of 0s, 2s, 8s, 16s and 32s.

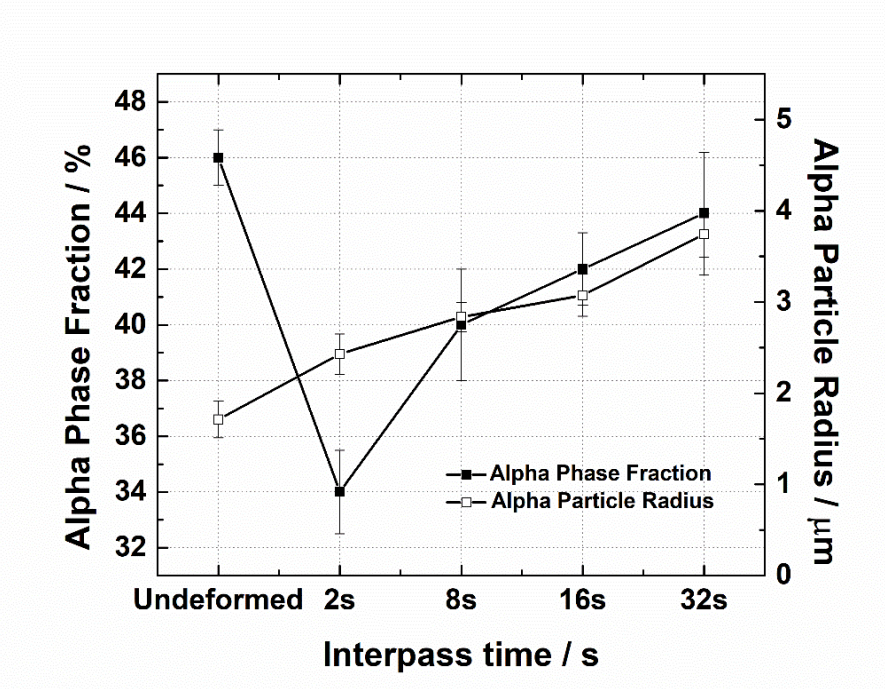

Fig. 8.6 Dependence of the alpha phase fraction and alpha particle radius on interpass time as derived from the microstructures of Fig. 8.5 with seven passes (ε = 2.8).

The results indicate that torsion tests with longer interpass times generate less beta while undergoing the same amounts of strain. For example, the alpha phase fraction decreased from 46% to 34% after deformation with interpass time of 2s while it only dropped from 46% to 44% after increasing the interpass time to 32s. The difference is attributed to the occurrence of reverse transformation from beta to alpha during holding. This reaction has been shown to occur after unloading in a diffusional and sluggish way and the amount of reverse transformation is therefore dependent on time [19]. Due to the different kinetics between the dynamic and reverse transformation, the amount of beta produced by the former during each pass deformation is more than that consumed by the latter during interpass time. This contributes to a net decrease in alpha phase fraction after seven-pass deformation irrespective of various interpass times.

The microstructural changes with respect to an undeformed sample is shown for samples subjected to one-pass, four-pass and seven-pass simulations in Fig. 8.7. Here it can be seen that the alpha phase fraction decreases with pass number (i.e. strain accumulation). The alpha particle radii associated with interpass times of 2s and 32s are plotted against pass number in Fig. 8.8. It

is evident that the radius increases with pass number, indicating that dynamic coarsening is taking place. Such dynamic coarsening has been shown to be controlled by the bulk diffusion of solutes through the beta matrix and is enhanced by straining [13, 20]. The alpha particle radius also increases with interpass time. For instance, it is around 2.41 μm and 2.43 μm after 4th and 7th passes when the interpass time is 2s. These increase to 2.96 μm and 3.74 μm when the interpass time is increased to 32s. This indicates that static coarsening takes place in the holding times between multiple passes. Such static behavior is diffusion controlled [21] and is much slower than the dynamic coarsening associated with the enhanced pipe diffusion when deformation is taking place.

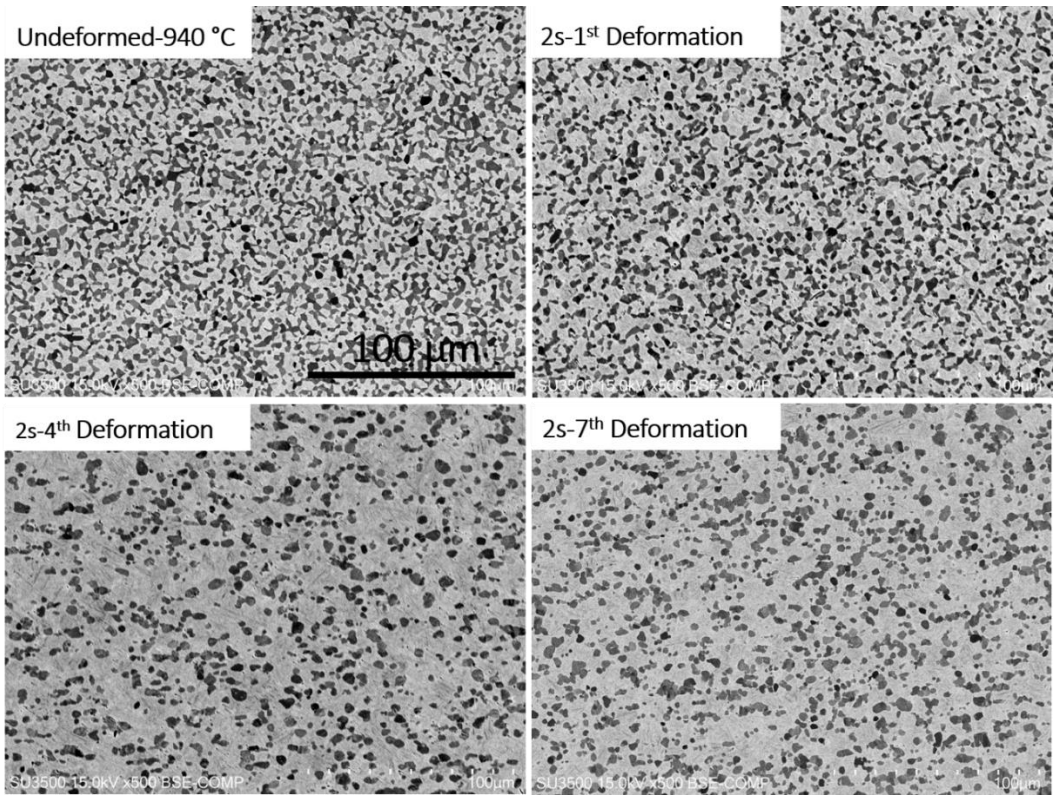

Fig. 8.7 SEM-BSE microstructures produced by testing using an interpass time of 2s. The samples were water quenched after the (b) 1st pass, (c) 4th pass and (d) 7th pass.

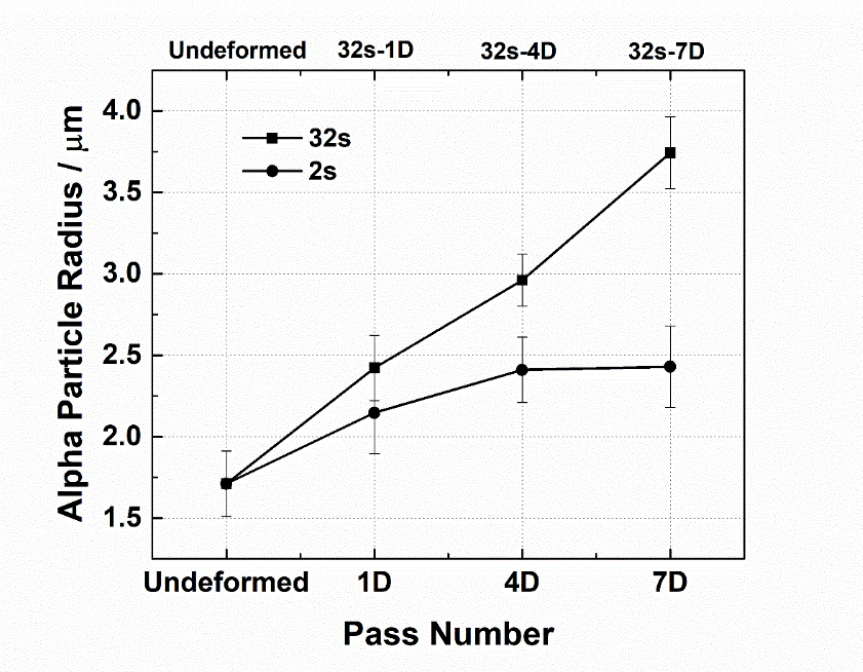

Fig. 8.8 Dependence of the alpha particle radius on deformation pass during isothermal torsion at 940 °C. Interpass times of 2s and 32s were employed.

The microstructural evolution occurring during the seven-pass torsion testing of Fig. 8.1(b) is displayed in Fig. 8.9. Here the marked coarsening of the alpha phase and the increase in its volume fraction can be seen. The alpha phase fractions and particle radii were measured and are plotted in Fig. 8.10. As indicated by the broken lines, the alpha particle radius increases with interpass time under both isothermal and cooling conditions. For the same interpass time, the alpha radii deformed under cooling conditions are higher than those associated with isothermal straining. This shows that coarsening is not only promoted by employing longer interpass times but by the deformation during cooling. The alpha phase fractions produced by deformation under these two conditions are represented by the solid lines. The alpha phase fraction increased during cooling, especially when longer interpass times were employed.

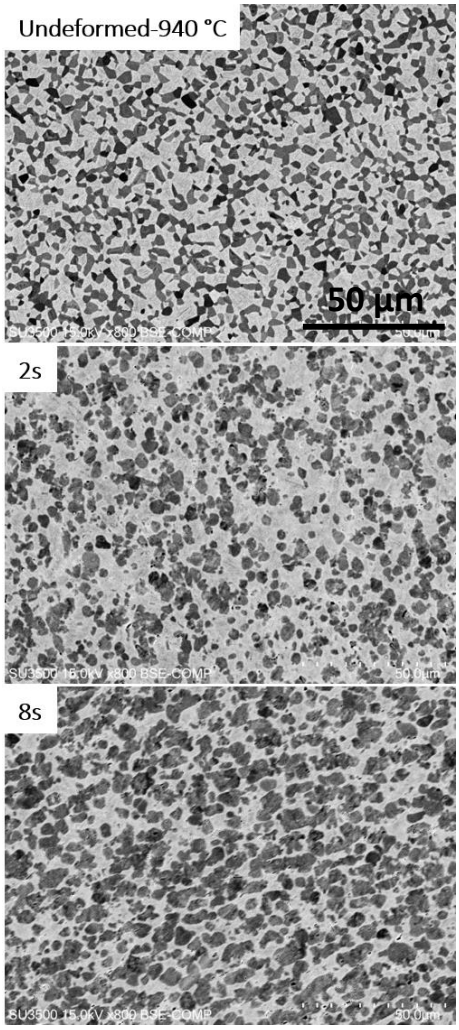

Fig. 8.9 SEM-BSE microstructures produced by means of seven-pass torsion tests carried out under continuous cooling conditions (1°C/s). Heat treatment at 940°C and testing using interpass times of 2s and 8s.

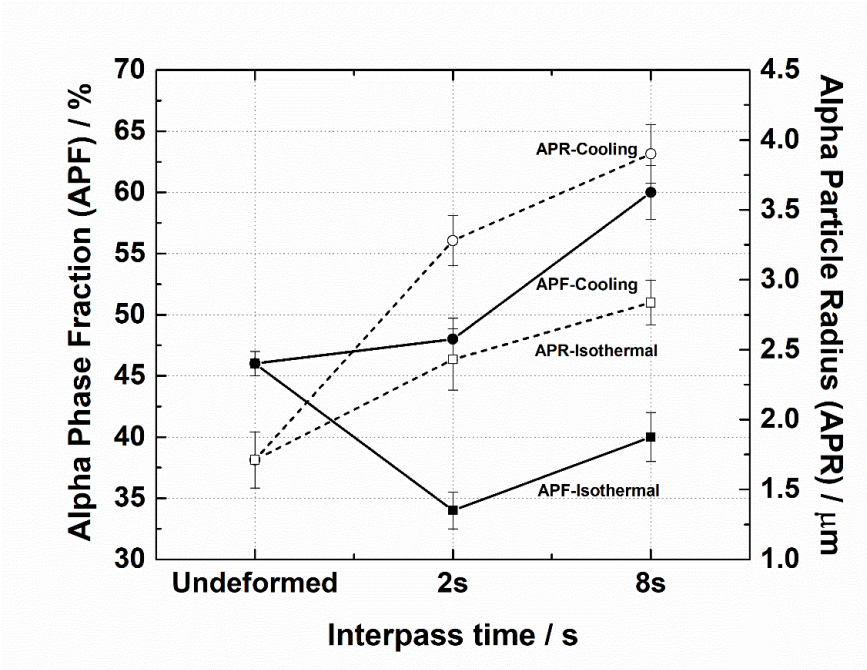

Fig. 8.10 Dependence of the alpha phase fraction (solid lines) and alpha particle radius (dashed lines) on interpass time in both isothermal and cooling conditions. The alpha phase fraction and alpha particle radius increase more rapidly with longer interpass annealing times than short times.

8.3.4 Relation between flow behavior and microstructural evolution

In the present study, flow softening was observed during the multipass torsion tests that were performed. Concurrently, dynamic transformation (alpha to beta) and coarsening of the alpha phase also took place. Such dynamic transformation produces flow softening in titanium alloys, as the harder alpha is transformed into the softer beta phase when deformation is performed within the two-phase region [15]. By contrast, the reverse transformation from beta to alpha took place during isothermal holding after each deformation, generating flow hardening. This is because more alpha phase is produced when the interpass time is long, so that the amount of softening decreases with interpass time.

Ghosh and Hamilton [22] observed that the flow stress in Ti-6Al-4V increased with the alpha grain size and that the coarsening behavior contributed to the strain hardening produced during hot deformation. Later Semiatin et al. [13] also showed that dynamic coarsening produced flow hardening when Ti-6Al-4V was deformed at elevated temperatures. In the present experiments,

coarsening of the alpha phase was promoted when the interpass time was lengthened, as indicated in Fig. 8.6. Thus both the grain size as well as the flow stress level increase when longer interpass times are employed, as shown in Fig. 8.2 and Fig. 8.6. The flow hardening observed in multipass torsion during continuous cooling can thus be attributed to the decrease in temperature as well as to the increase in alpha phase fraction.

The flow softening derived from dynamic transformation and the flow hardening by coarsening and reverse transformation should be considered in the modeling of flow behavior during multi-deformation in the future. The relationship between interpass time and flow stress discussed in the present work provides a basis for optimizing the manufacture of titanium alloys during multi-pass rolling.

8.4 Conclusions

(1) Flow softening is produced during the isothermal multipass deformation of Ti-6Al-4V, as indicated by the mean flow stress. Values of the latter increase when the interpass time is increased from 2s to 32s, i.e. longer interpass times cause less flow softening.

(2) Dynamic transformation and coarsening of the alpha phase take place during multipass deformation experiments. The results indicate that the alpha phase is transformed into beta during straining and the net amount of alpha phase consumed by straining decreases with interpass time due to the occurrence of reverse transformation.

(3) Flow softening during isothermal multipass deformation is the net result of softening by dynamic transformation and hardening by reverse transformation. The flow hardening during the cooling is due to the decrease in temperature and the increase in the alpha phase fraction.

References

[1] S.N. Murty, N. Nayan, P. Kumar, P.R. Narayanan, S. Sharma, K.M. George, Microstructure–texture–mechanical properties relationship in multi-pass warm rolled Ti–6Al–4V Alloy, Materials Science and Engineering: A 589 (2014) 174-181.

[2] X. Fan, H. Yang, P. Gao, Deformation behavior and microstructure evolution in multistage hot working of TA15 titanium alloy: on the role of recrystallization, Journal of Materials Science 46(18) (2011) 6018-6028.

[3] N. Nayan, G. Singh, T.A. Prabhu, S.N. Murty, U. Ramamurty, Cryogenic Mechanical Properties of Warm Multi-Pass Caliber-Rolled Fine-Grained Titanium Alloys: Ti-6Al-4V (Normal and ELI Grades) and VT14, Metallurgical and Materials Transactions A 49(1) (2018) 128-146.

[4] S. Zherebtsov, G. Salishchev, R. Galeyev, O. Valiakhmetov, S.Y. Mironov, S. L. Semiatin, Production of submicrocrystalline structure in large-scale Ti–6Al–4V billet by warm severe deformation processing, Scripta Materialia 51(12) (2004) 1147-1151.

[5] G. Salishchev, R. Galeyev, O. Valiakhmetov, R. Safiullin, R.Y. Lutfullin, O.N. Senkov, F. Froes, O. Kaibyshev, Development of Ti–6Al–4V sheet with low temperature superplastic properties, Journal of Materials Processing Technology 116(2-3) (2001) 265-268.

[6] X. Fan, M. Meng, P. Gao, M. Zhan, Coupled effects of deformation and cooling on the evolution of primary and secondary alpha of two-phase Ti-alloys, Materials Science and Engineering: A 710 (2018) 271-279.

[7] J.Y. Kim, K.-T. Park, I.O. Shim, S.H. Hong, Globularization behavior of ELI grade Ti-6Al-4V alloy during non-isothermal multi-step forging, Materials Transactions 49(1) (2008) 215-223.

[8] A. Salem, M. Glavicic, S. L. Semiatin, The effect of preheat temperature and inter-pass reheating on microstructure and texture evolution during hot rolling of Ti–6Al–4V, Materials Science and Engineering: A 496(1-2) (2008) 169-176.

[9] G. Obasi, S. Birosca, D.L. Prakash, J.Q. Da Fonseca, M. Preuss, The influence of rolling temperature on texture evolution and variant selection during $\alpha \rightarrow \beta \rightarrow \alpha$ phase transformation in Ti–6Al–4V, Acta Materialia 60(17) (2012) 6013-6024.

[10] J.L. Warwick, N.G. Jones, I. Bantounas, M. Preuss, D. Dye, In situ observation of texture and microstructure evolution during rolling and globularization of Ti–6Al–4V, Acta Materialia 61(5) (2013) 1603-1615.

[11] B. Guo, S. L. Semiatin, J. Liang, B. Sun, J.J. Jonas, Opposing and Driving Forces Associated with the Dynamic Transformation of Ti-6Al-4V, Metallurgical and Materials Transactions A 49(5) (2018) 1450-1454.

[12] J. Koike, Y. Shimoyama, I. Ohnuma, T. Okamura, R. Kainuma, K. Ishida, K. Maruyama, Stress-induced phase transformation during superplastic deformation in two-phase Ti–Al–Fe alloy, Acta Materialia 48(9) (2000) 2059-2069.

[13] S. L. Semiatin, M. Corbett, P. Fagin, G. Salishchev, C. Lee, Dynamic-coarsening behavior of an α/β titanium alloy, Metallurgical and Materials Transactions A 37(4) (2006) 1125-1136.

[14] C.H. Park, B. Lee, S. L. Semiatin, C.S. Lee, Low-temperature superplasticity and coarsening behavior of Ti–6Al–2Sn–4Zr–2Mo–0.1 Si, Materials Science and Engineering: A 527(20) (2010) 5203-5211.

[15] J.J. Jonas, C. Aranas Jr, A. Fall, M. Jahazi, Transformation softening in three titanium alloys, Materials & Design 113 (2017) 305-310.

[16] D. Fields, W. Backofen, Determination of strain hardening characteristics by torsion testing, Proc. ASTM, 1957, pp. 1259-1272.

[17] C. Ghosh, C. Aranas Jr, J.J. Jonas, Dynamic transformation of deformed austenite at temperatures above the Ae_3, Progress in Materials Science 82 (2016) 151-233.

[18] J.J. Jonas, C. Ghosh, Role of mechanical activation in the dynamic transformation of austenite, Acta Materialia 61(16) (2013) 6125-6131.

[19] B. Guo, C. Aranas, B. Sun, X. Ji, J.J. Jonas, Reverse Transformation Behavior of Ti-6Al-4V After Deformation in the Two-Phase Region, Metallurgical and Materials Transactions A 49(1) (2018) 22-27.

[20] G. Sargent, A. Zane, P. Fagin, A. Ghosh, S. L. Semiatin, Low-temperature coarsening and plastic flow behavior of an alpha/beta titanium billet material with an ultrafine microstructure, Metallurgical and Materials Transactions A 39(12) (2008) 2949.

[21] S. L. Semiatin, B. Kirby, G. Salishchev, Coarsening behavior of an alpha-beta titanium alloy, Metallurgical and Materials Transactions A 35(9) (2004) 2809-2819.

[22] A. Ghosh, C. Hamilton, Mechanical behavior and hardening characteristics of a superplastic Ti-6AI-4V alloy, Metallurgical Transactions A 10(6) (1979) 699-706.

Chapter 9 Conclusions

The objective of the present work is to investigate the dynamic and reverse transformation in Ti-6Al-4V alloy. Specifically, the characterization of dynamic transformation in Ti-6Al-4V was described in Chapter 3 using torsion tests. The driving force and energy barriers of the transformation were analyzed in Chapter 4. Metallographic measurements and kinetics of reverse transformation were discussed in Chapter 5 and 6. The role of dynamic and reverse transformation in flow behavior was illustrated in Chapter 7 and 8. The corresponding conclusions are summarized as follows.

(1) The dynamic transformation of Ti-6Al-4V was studied by means of torsion tests carried out in the two-phase region. Dynamic transformation takes place at 880°C, 940°C, 960°C, 980°C and 1000°C. Under these conditions, the beta phase fraction increases with strain and also slightly with strain rate. The percentage of primary alpha transformed into beta during deformation increases with temperature in the two-phase region since the energy barrier opposing dynamic transformation decreases as the temperature approaches the transus. The critical stresses required to initiate dynamic transformation are less than the peak stresses at the temperatures employed here, which makes it thermodynamically possible for the transformation to occur.

(2) The driving force and energy barriers of dynamic transformation were calculated. Results indicated that dislocations are the main source of stored energy and the excess-vacancy energy is negligible for Ti-6Al-4V. The stored energy is lower than the opposing force inhibiting dynamic transformation. By contrast, the driving force derived from the net softening associated with dynamic transformation is much higher than the opposing force and acts as the source of for initiating the transformation. Dynamic transformation consumes 4-18% of the mechanical deformation work, the rest of which is distributed between heatings and stored energy. Hot deformation can reduce the transus temperature and produce a metastable state.

(3) The reverse transformation in Ti-6Al-4V was observed during holding after unloading at 940°C, 970°C and 1000°C through microstructural evolution. This transformation is diffusion controlled, the extent of which depends on holding time. The time-temperature-reverse transformation (TTRT) curves associated with the reverse transformation were derived, which indicate that the

rates of reverse transformation are similar at different temperatures when the holding time is short (18s) but is dependent on temperature at longer holding times, i.e. 180s and 1800s. The driving force for reverse transformation is much higher than the work of accommodation at the present three temperatures, which makes it possible for the reverse transformation to occur.

(4) The kinetics of the reverse transformation were further studied via dilatometer equipped with compression apparatus. The results showed that both post-dynamic coarsening and reverse transformation occurred during isothermal holding after compression. The kinetics of post-dynamic coarsening were one order of magnitude faster than during static coarsening and this mechanism appears to be controlled by bulk diffusion, i.e. vanadium diffusion through the beta matrix. The reverse transformation took place in two stages: the first stage was transformation along dislocations; the second stage involved the growth of the alpha structure.

(5) The role of dynamic transformation in flow behavior was illustrated by compression and modeling. The transformation from alpha to beta was observed in both globular and colony microstructures of Ti-6Al-4V alloy. The amount of transformation and fractional flow softening derived from the transformation were approximately independent of the initial microstructures. However, the measured flow softening in the globular microstructure was greater than in the colony microstructure. Dynamic transformation acted as the primary source of flow softening in globular microstructure especially at low strain rates, while its contribution on the flow softening in colony microstructure was substantially diminished. The texture softening in the colony microstructure accounted for 12% of flow softening at 900 °C and this proportion decreased with temperature. The adiabatic heating at the high strain rate may confound heating-induced with stress-induced transformation. The lower strain rates decreased the driving force for the transformation and impeded the reaction. Hence, the reasonable strain rates for observing dynamic transformation approximately are in the range: 0.01 s^{-1} - 0.001 s^{-1}.

(6) The role of dynamic and reverse transformation was further studied in multipass deformation using torsion tests. Flow softening is produced during the isothermal multipass deformation of Ti-6Al-4V, as indicated by the mean flow stress. Values of the latter increase as the interpass time is increased from 2s to 32s, i.e. longer interpass times cause less flow softening. Dynamic

transformation and coarsening of the alpha phase take place during multipass deformation experiments. The results indicate that the alpha phase is transformed into beta during straining and the net amount of alpha phase consumed by straining decreases with interpass time due to the occurrence of reverse transformation. Flow softening during isothermal multipass deformation is the net result of softening by dynamic transformation and hardening by reverse transformation.

Chapter 10 Contributions to Original Knowledge

The contributions to original knowledge consist of four sections and are summarized as follows:

(1) The occurrence of dynamic transformation in Ti-6Al-4V has been reported in tensile and compression tests by previous workers. This phenomenon was observed in torsion tests for the first time in the present work. The source of the driving force for the transformation was unknown in the past and is addressed by the thermodynamic calculation in Chapter 4. The critical stress for the initiation of dynamic transformation is obtained in Chapter 3 as well.

(2) The reverse transformation has rarely been studied by earlier workers. The present work fills this gap in Chapter 5. Furthermore, the kinetics of the reverse transformation were elucidated using the compression dilatometer for the first time in Chapter 6. The mechanism of the reverse transformation is introduced.

(3) The occurrence of transformation was not considered during the previous works on flow modeling in both steel and titanium alloys. Hence, this omission is corrected in the present work in Chapter 7. The effects of dynamic transformation on the flow stress are characterized with two initial microstructures and the self-consistent model is employed to demonstrate the contribution to flow softening for the first time.

(4) Here, for the first time, the occurrence of dynamic and reverse transformation during multipass torsion tests is described in Chapter 8 with various interpass times. This provides useful guidance for the rolling of titanium alloys in manufacturing.

Appendix

Determination of the critical stress for the initiation of dynamic transformation in commercially pure titanium

Abstract

The dynamic transformation of alpha to beta is shown to take place in titanium at temperatures below the beta transus. The driving force for this transformation is the net softening associated with the formation of the lower flow stress beta phase. The obstacle to the transformation consists of the free energy difference between the phases as well as the work of dilatation during the phase change. Here the critical condition for transformation is defined as the moment when the driving force becomes equal to the obstacle energy. This approach is supported by data obtained from compression tests.

*This paper has been published: Clodualdo Aranas Jr., Anes Foul, **Baoqi Guo**, Ameth Fall, Mohammad Jahazi and John J. Jonas. Determination of the critical stress for the initiation of dynamic transformation in commercially pure titanium. Scripta Materialia, 2017, 133: 83-85.

Dynamic transformation of α → β titanium at temperatures below the β-transus in commercially pure titanium

Abstract

Hot compression tests were carried out on commercially pure titanium grade 2 at temperatures below the β-transus (915 °C). At temperatures of 840, 860, 880, and 900 °C, the β volume fraction increased by 30%, 32%, 36%, and 55%, respectively. The minimum temperature at which dynamic transformation could be induced was 765 °C. The driving force for transformation given by the net softening associated with the formation of the lower flow stress beta phase was calculated to fall in the range between 200 and 500 J/mol.

*This paper has been published: Anes Foul, Clodualdo Aranas Jr., **Baoqi Guo**, John J. Jonas. Dynamic transformation of α→β titanium at temperatures below the β-transus in commercially pure titanium. Materials Science and Engineering: A, 2018, 722: 156-159.

Deformation-induced phase transformation in Zircaloy-4 below the beta transus

Abstract

Dynamic transformation is shown to take place in steels and titanium alloys at temperatures above and below the beta transus, respectively. Here the hard phase transforms into a softer phase during deformation. This unusual metallurgical phenomenon has previously been explained in terms of transformation softening (Ghosh et al., 2016). In the present work, compression tests were performed on samples of Zircaloy-4 at temperatures below the beta transus. The microstructures and microhardness measurements indicate that alpha transforms displacively into beta during deformation at temperatures down to about 75 °C below the transus.

*This paper has been published: Clodualdo Aranas Jr., **Baoqi Guo**, Samuel Rodrigues, Joonphil Choi, Sanghoon Kim, Binhan Sun, John J. Jonas. Deformation-induced phase transformation in Zircaloy-4 below the beta transus. Materials Letters, 2018, 220: 229-233.